APPLICATION OF BURNUP CREDIT TO PRESERVE SPENT FUEL STORAGE SPACE

by
Ally Mathye
(1510456)

Dissertation
Submitted in fulfilment of the requirements for the degree
Master of Science
in
Physics
School of Physics
Faculty of Science
University of the Witwatersrand, Johannesburg, South Africa

Supervisor: Professor Iyabo Usman
Co-supervisor: Dr Mosebetsi Leotlela

February 2025

DECLARATION

I declare that this dissertation is my own, unaided work. It is being submitted for the Degree of Master of Science at the University of the Witwatersrand, Johannesburg. It has not been submitted before for any degree or examination at any other University.

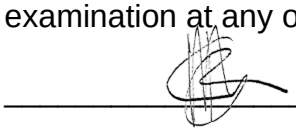

(Signature of candidate)

11 day of February 2025 at Sunninghill

ABSTRACT

This study delves into the complexities of burnup credit, exploring area savings (ΔA) achieved by taking credit for different nuclide groups compared to fresh fuel and their implications on reactivity within Spent Nuclear Fuel (SNF) cask storage. The project investigated the benefit of burnup credit using a structured 2 x 2 spent fuel storage matrix for the SNF casks, conducting a thorough analysis of the effective multiplication factor (k_{eff}) at different areas occupied by the SNF casks utilizing the SCALE code, a robust nuclear analysis software suite. Fresh fuel served as a k_{eff} benchmark, with major actinides exhibiting modest reactivity and space savings, while actinides plus principal fission products highlighted substantial space savings alongside the highest reactivity savings. This analysis provides crucial insights for optimizing SNF storage capacity using burnup credit to achieve area savings in cask storage. The research underscores the pivotal role of burnup credit in enhancing efficiency and safety in SNF cask storage, offering valuable perspectives for advancing nuclear fuel management practices.

In Memory of My Late Father

John ‘Boyi’ Mathye

1948 – 2021

And

My Grandfather

July Maswanganyi

ACKNOWLEDGMENTS

I am profoundly grateful to God for His unwavering wisdom, guidance, and support throughout this research journey, providing the strength and inspiration needed to persevere.

A heartfelt appreciation goes to my manager, Mr. Mmeli Fipaza, for his generous allocation of time and resources that enabled the successful completion of this research. His understanding and support have been pivotal in navigating the challenges of this endeavour.

I extend my sincere thanks to my colleague, Thulani Kubeka, for his invaluable input and assistance, especially during moments when complex numerical aspects demanded additional clarity. His collaboration significantly enriched the research process.

Special recognition is reserved for my supervisor, Dr. M. Leotlela. In our earlier days as colleagues, he introduced me to the complexities of the SCALE code. I express deep gratitude for his extensive knowledge, insightful guidance, and patience during the learning process. Dr. Leotlela's mentorship, particularly when we were colleagues, laid a solid foundation for the successful execution of this research.

To supervisor, Professor I. Usman, thank you for your exceptional guidance, support, and mentorship throughout this research project. Her dedication to excellence and her consistent efforts in offering constructive feedback and encouragement have been instrumental in the successful completion of this work. I am profoundly grateful for the opportunity to learn from Professor Usman's wealth of knowledge and experience, and I am deeply appreciative of their ongoing support. Thank you for your exceptional contributions to this research endeavour.

To my family: your patience and encouragement, especially on weekends, were indispensable as I dedicated time to this endeavour. A special acknowledgment goes to my partner, Ms. N. Mgimeti, whose steadfast support and understanding have been the pillars that sustained me. I

express my deep appreciation to my children, Nhluvuko, Nobuhle, Nhlalala, and Nhlulo Mathye, for their resilience and understanding during times when my attention was focused on the research. Their love and encouragement were a constant source of motivation.

These acknowledgments are a testament to the collective efforts that have shaped this research. I am thankful for the support and mentorship provided by Mr. Fipaza and Dr. Leotlela, which have been instrumental in the realization of this study.

CONTENTS PAGE

DECLARATION ii
ABSTRACT iii
ACKNOWLEDGMENTS v
LIST OF FIGURES x
LIST OF TABLES xii
ACRONYMS xiii
Chapter 1 : Introduction 1
1.1. Aims and objectives. 2
1.2. Hypothesis and questions 3
Chapter 2 : Fundamental Concepts 6
2.1. Nuclear reactions 6
2.1.1. Fission process and fuel depletion 7
2.1.2. Radioactive decay and nuclide build-up 10
2.2. Cross section of nuclear reactions 14
2.2.1. Cross section libraries 17
2.2.2. Radiative capture cross section of the major actinides 17
2.2.3. Radiative capture cross sections of fission products 19
2.3. Effects of fuel and moderator temperature and density on k_{eff}. 20
2.3.1. Effect of fuel temperature on k_{eff}. 20
2.3.2. Effect of fuel density on k_{eff}. 22
2.3.3. Effect of moderator temperature and density on k_{eff}. 22
2.4. Criticality and criticality safety 22
2.4.1. Effective neutron multiplication factor (six factor formula) 23
2.4.2. Boltzmann transport equation 25
2.4.2.1. Methods of solving Boltzmann transport equation 27
2.4.2.1.1. Deterministic method 27
2.4.2.1.2. Monte Carlo method 27
2.4.2.2. Tools for solving Boltzmann transport equation 28
2.4.2.2.1. Overview of SCALE code 29
2.4.2.2.1.1. KENO 30
2.4.2.2.1.2. STARBUCS 30
2.5. Fuel burnup 31

2.6. Overview of the spent nuclear fuel casks 33
2.6.1. Transportation casks 33
2.6.2. Dual-purpose casks 33
2.6.3. Dry storage casks 34
2.6.3.1. CASTOR X/28 35
2.7. Application of burnup credit on various facilities around the world 36
2.7.1. Application of burnup credit on transportation, reprocessing and disposal systems 37
2.7.2. Application of burnup credit on dry and wet SNF storages around the world 37
2.8. Regulations of SNF in South Africa 38
Chapter 3 : Methodology and Modelling 40
3.1. Modelling and simulation overview 40
3.2. Calculation techniques and design 42
3.3.1. Fuel assembly design 42
3.3.1.1. Characteristics of fresh fuel and SNF 45
3.3.1.2. Neutron axial profile of the fuel assembly 45
3.3.2. Castor x/28 cask design 46
Chapter 4 : Results and Discussions 54
4.1. Uncertainty of the results 54
4.2. Fresh fuel scenario 56
4.3. Burnup credit for different nuclide groups 59
4.3.1. Taking credit for major actinides 60
4.3.2. Actinides plus principal fission products 63
4.3.3. Actinides Plus Minor Fission Product 66
4.4. Determining storage space saving 68
4.5. Effect of fuel temperature and fuel density on k_{eff}. 70
4.5.1. Effect of fuel temperature on k_{eff}. 71
4.5.2. Fuel density 72
4.6. Effect of moderator temperature and moderator density on k_{eff}. 74
4.6.1. Moderator temperature 74
4.6.2. Moderator density 75

4.7. Summary of the results 76
Chapter 5 : Sensitivity Analysis 78
5.1. Sensitivity analysis of different nuclide groups 78
5.1.2. Sensitivity analysis of major actinides 81
5.1.3. Sensitivity analysis of actinides plus minor fission products. 82
5.1.4. Sensitivity analysis of actinides plus principal fission products. 84
5.2. Sensitivity Analysis of Important Parameters 85
5.2.1. Sensitivity Analysis of Fuel Temperature 86
5.2.2. Sensitivity analysis of fuel density 88
5.2.3. Sensitivity analysis of moderator density 89
5.2.4. Sensitivity of moderator temperature 90
5.3. Summary of Sensitivity Analysis 91
Chapter 6 : Conclusion 93
6.1. Reactivity of Different Nuclide Groups 93
6.2. Reactivity Saving Due to Taking Credit for Fuel Burnup 93
6.3. Sensitivity Analysis 94
6.4. Space Savings due to taking credit for fuel burnup. 95
6.5. Recommendations for future research 96
References 98
Appendix A: Nuclide build-up 101
Appendix B: Coordinates of Polyethylene Rods 104
Appendix C: Coordinates of the CASTOR X/28 Casks 107
Appendix D: Data for k_{eff} as a Function of Area for Different Nuclide Groups 110
Appendix E: Data for area saved when taking credit for burnup. 113

LIST OF FIGURES

Figure 2.1: Fission product yield for ^{235}U at neutron energy of 0.025 eV [6]. 8
Figure 2.2: Build-up of ^{137}Ba and decay of ^{137}Cs over a period of 100 years [9]. 12
Figure 2.3: Build-up and decay of various nuclides over a period of 12 months (see Appendix A, Table A.1). 13
Figure 2.4: Build-up and decay of various nuclides over a period of 100 years (see Appendix A, Table A.2). 14
Figure 2.5: Fission cross-section of ^{235}U, showing thermal, fast and resonance absorption regions [6]. 16
Figure 2.6: The relationship between neutron energy and the radiative capture microscopic cross section of ^{240}Pu. 18
Figure 2.7: The relationship between neutron energy and the radiative capture microscopic cross section of ^{155}Gd. 19
Figure 2.8: Effect of burnup on k_{eff} for different nuclides groups [6]. 32
Figure 2.9: A typical spent nuclear fuel cask [6]. 36
Figure 3.1: Calculation sequence for CSAS6 [15]. 40
Figure 3.2: STARBUCS running sequence [15]. 41
Figure 3.3: A 17x17 Westinghouse Fuel Assembly Showing Fuel Rod, Guide tube and Instrument Tube Arrangement [20]. 43
Figure 3.4: Axial profile of the Fuel Assembly taken at fuel burnup of 28 GWD/MTU. 46
Figure 3.5: A typical spent nuclear fuel cask [6]. 47
Figure 3.6: Castor X/28 casks installed horizontally at Koeberg Power Station [31]. 47
Figure 3.7: Castor x/28 cask generated by SCALE code in this current research project. 51
Figure 3.8: A cut through of the SNF casks arranged in 2 x 2 matrix generated by SCALE code in this research project. 52
Figure 4.1: $keff$ as a function of area occupied by the SNF casks for fresh fuel. 57

Figure 4.2: Effect of changing area on k_{eff} when taking credit for burnup of major actinides only. 60
Figure 4.3: Reactivity savings when taking credit for major actinides only. 62
Figure 4.4: Effect of area on k_{eff} when taking credit for burnup on actinides plus principal fission products. 63
Figure 4.5: Reactivity savings when taking credit for actinides plus principal fission products. 65
Figure 4.6: Effect of area on k_{eff} when taking credit for burnup on actinides + minor fission products. 66
Figure 4.7: Reactivity savings when taking credit for actinides plus minor fission products. 68
Figure 4.8: Space saved due to taking credit for major actinides, actinides plus principal fission products and actinides plus minor fission products. 69
Figure 4.9: Effect of increasing fuel temperature on k_{eff}. 72
Figure 4.10: Effect of Fuel Density on k_{eff}. 73
Figure 4.11: Effect of moderator temperature on k_{eff}. 74
Figure 4.12: Effect of Moderator Density on k_{eff}. 76
Figure 5.1: Sensitivity analysis of the fresh fuel. 80
Figure 5.2: Sensitivity analysis of major actinides 81
Figure 5.3: Sensitivity analysis of actinides plus minor fission products. 83
Figure 5.4: Sensitivity analysis of actinides plus principal fission products. 84
Figure 5.5: Sensitivity of k_{eff} as a function of fuel temperature. 87
Figure 5.6: Sensitivity of k_{eff} as a function of fuel density. 88
Figure 5.7: Sensitivity of k_{eff} as a function of moderator density. 89
Figure 5.8: Sensitivity of k_{eff} as a function of moderator temperature. 90

LIST OF TABLES

Table 2.1: Nuclide groups used in burnup credit. 31
Table 2.2: SNF dry storage casks [16]. 35
Table 3.1: Fuel Assembly Design Description 43
Table 3.2: Fuel assembly coordinates inside CASTOR X/18 cask 48
Table 3.3: Inner fuel assembly placement inside CASTOR X/28. 49
Table 4.1: Effects of Fuel and Moderator Properties on k_{eff}. 71
Table 5.1: Sensitivity of k_{eff} as a function of SNF casks area. 79
Table 5.2: Sensitivity of k_{eff} as a function of fuel and moderator temperatures and fuel and moderator densities. 86

ACRONYMS

CE	Continuous Energy
CDF	Continuous Distribution Function
CSAS5	Criticality Safety Analysis Sequence with KENO-V.a
CSAS6	Criticality Safety Analysis Sequence with KENO-VI
GeeWiz	Graphically Enhanced Editing Wizard
GNB	Gesselschaft für Nuklear-Behalter
GUI	Graphic User Interface
ICF	Isotopic Correction Factor
LANL	Los Alamos National Laboratory
MC	Monte Carlo
MCNP	Monte Carlo N-Particle
MG	Multigroup
NEFCD	Nuclear Energy and Fuel Cycle Division
ORNL	Oak Ridge National Laboratory
PWR	Pressurised Water Reactor
RSICC	Radiation Safety Information Computational Center
SCALE	Standardized Computer Analyses for Licensing Evaluations
SNF	Spent Nuclear Fuel
STARBUCS	Standardized Analysis of Reactivity for Burnup Credit using SCALE.
UK	United Kingdom
USA	United States of America

Chapter 1 : Introduction

Spent fuel storage spaces, such as fuel pool storage, are becoming limited at many nuclear power plants commissioned in the 1980s [1]. The primary purpose of storing spent nuclear fuel is to prevent overheating, which could lead to the release of radionuclides into the environment. Additionally, it is crucial to store spent fuel to prevent criticality accidents, ensuring the safety of both the facility and the surrounding area. To address this, the nuclear operator must explore cost-effective and readily available solutions to maintain spent fuel storage capacity. While spent fuel casks are an option, they are more expensive compared to the economic advantages of burnup credit, which can be implemented immediately (pending regulatory approval) without additional cost.

This project provides a comparative analysis of storage space preservation by incorporating burnup credit, as compared to the 'fresh fuel scenario' approach. Several studies have shown that the 'fresh fuel scenario' is a conservative and restrictive method, often resulting in the use of more storage space than necessary under the guise of safety [2, 3, 4, 5]. However, these studies primarily focused on the change in multiplication factor (Δk_{eff}) between fresh fuel and the effective multiplication factor (k_{eff}) achieved by accounting for burnup credit [2].

This project provides a comparative analysis of storage space optimization by accounting for burnup credit in contrast to the ‘fresh fuel scenario’ approach. Numerous studies have indicated that the ‘fresh fuel scenario’ is a conservative and overly conservative, often leading to the use of excessive storage space under the guise of safety, beyond what is necessary [2, 3, 4, 5]. However, these cited studies only indicated the change in multiplication factor (Δk_{eff}) between fresh fuel and the effective multiplication factor (k_{eff}) obtained as a result of taking credit for burnup [2].

Hence, the novelty of this research project is to demonstrate the economic benefit of taking credit for burnup using scientific methods or techniques based on saved or recovered spent fuel storage space in the form of change in area (*ΔA*) which would have been lost if fresh fuel scenario was used or credit for burnup was not considered. The nuclide sets used in this analysis are the following:

- Major Actinides only
- Actinides + minor fission products
- Actinides + principal fission products

It is essential to highlight that both Δk_{eff} and ΔA for each of the aforementioned nuclides will be computed with respect to the fresh fuel scenario.

1.1. Aims and objectives.

Nuclear fuel storage infrastructure are designed to guarantee that k_{eff}, which serves as an indication of reactivity, remains below 0.95 under all circumstances, including accident conditions [6]. The objective of this research is to perform a criticality safety analysis of the SNF casks to confirm their safety under all conditions, considering a storage pattern that incorporates fuel burn-up credit. These aims were achieved with the following objectives:

- Analysis of the fresh fuel scenario.
- Spatial configuration of casks in the spent fuel storage facility
- Comparison of k_{eff} values for fresh fuel versus those of the major actinides only, actinides plus minor fission products, and actinides plus principal fission products.
- Calculate Δk_{eff} of fresh fuel and taking burnup credit of the nuclide sets; and
- Determine storage savings of the SNF casks after taking credit for burnup.

In the fresh fuel scenario analysis, it is assumed that the fuel has not experienced any previous irradiation. Consequently, the analysis excludes other nuclides present in the fuel. This simplification is made with the understanding that the absence of prior irradiation means there are no fission products and actinides in the fresh fuel that could absorb neutrons. Accordingly, the fresh fuel scenario is expected to yield a higher k_{eff} since there are no neutron-absorbing elements present, allowing for a more straightforward evaluation of the intrinsic reactivity of the fresh fuel.

1.2. Hypothesis and questions

The assertion that utilizing the 'fresh fuel' scenario for spent fuel storage is excessively conservative and could potentially result in space limitations aligns with the acknowledged challenges confronted by nuclear plants operating over prolonged periods. The conservative approach, prioritizing safety, often results in a tendency to use more storage space than strictly necessary. Consequently, this can lead to situations where nuclear plants, operational for over 40 years, encounter challenges related to the depletion of spent fuel storage space before decommissioning.

To address the issue of storage space optimization and to recover the storage space that would have been lost if fresh fuel scenario was used, the 'burnup credit' approach is proposed. This approach involves taking credit for burnup in the analysis, aiming to achieve a more efficient utilization of storage space. By incorporating burnup credit, the strategy is to store spent fuel closer together than the 'fresh fuel' scenario would allow, while still adhering to nuclear safety principles by ensuring that the k_{eff} remains below the critical threshold [6].

The critical question at the heart of this research is whether taking credit for burnup in the analysis of SNF casks can indeed result in storage savings. This question underscores the need for a comprehensive examination of the potential benefits and safety implications associated with implementing burnup credit in the storage of the SNF casks. It reflects a careful balance

between optimizing storage space and maintaining rigorous safety standards within the nuclear industry.

1.3. Overview of dissertation framework

Chapter 2 covers into various theorical concepts of nuclear reactor physics, including nuclear reactions (Section 2.1), cross section of nuclear reactions (Section 2.2), effects of fuel and moderator properties on k_{eff} (Section 2.3), criticality and criticality safety (Section 2.4), fuel burnup (section 2.5). The chapter also covers characteristics of SNF casks including their application in nuclear facilities around the world (Section 2.6 and 2.7). It also covers the regulation of SNF storage in South Africa (Section 2.8).

Chapter 3 delves into modelling design overview, establishing the foundation for subsequent analyses. This chapter presents an outline of the design of the fuel assembly and the CASTOR X/28 casks. This chapter provides essential input values for analysis with the SCALE code.

Chapter 4 presents the results of the research, with a primary focus on the fresh fuel scenario and burnup credit for different nuclide groups. The chapter provides detailed discussions covering major actinides, actinides plus principal fission products, and actinides plus minor fission products. Additionally, it addresses the determination of storage space savings and offers a comprehensive summary of the results. Furthermore, the chapter presents the results of k_{eff} vs. fuel and moderator temperature, as well as k_{eff} *vs.* fuel and moderator density.

Chapter 5 presents a comprehensive sensitivity analysis for different nuclide groups, assessing how changes in area (distance) affect the k_{eff} of fresh fuel, major actinides, actinides plus principal fission products, and actinides plus minor fission products. The sensitivity of k_{eff} to changes in fuel temperature as well as changes in moderator density is also presented. The results are discussed in detail, offering valuable insights for this study.

In the concluding chapter (Chapter 6), findings from the exploration of the reactivity of different nuclide groups, both reactivity saving and the space savings achieved through taking credit for burnup are consolidated. This chapter offers a comprehensive wrap-up of the study, underlining its significance and potential implications for advancing nuclear reactor safety and efficiency. It also gives recommendations for future research in this field of study.

Chapter 2 : Fundamental Concepts

Neutron transport is a complex and interdisciplinary field that combines nuclear physics, mathematical modelling, and computational methods to understand and predict the behaviour of neutrons in various nuclear environments [7]. The accurate modelling of neutron transport is crucial for the reliable and optimized performance of nuclear reactors, SNF storage casks and other applications in the field of nuclear science and technology.

In this chapter, the application of burnup credit to various SNF storage facilities around the world is presented. The chapter also gives an overview of SNF cask storage. The chapter also introduces the Boltzmann transport equation and explore its solution methods, encompassing both deterministic approaches and Monte Carlo methods. Furthermore, this chapter delves into the physical concepts of nuclear criticality safety, fuel burnup, and the cross-sections of nuclear reactions.

2.1. Nuclear reactions

A nuclear reaction is a process in which the nucleus of an atom undergoes a change due to interaction with another particle or nucleus, leading to a transformation in its composition, energy state, or structure. These interactions can result in the release or absorption of energy and the production of different elements or isotopes. There are two main types of nuclear reactions that can occur when an incident particle interacts with the nucleus: elastic and inelastic reactions [4, 5].

Elastic reactions are those in which the incident particle (e.g., neutron) and the nucleus do not change their internal structure after the interaction. The total kinetic energy and momentum are conserved, and the particles emerge from the interaction unchanged except for their energy and direction. In contrast, inelastic reactions result in a change in the internal structure of either the incident particle, the nucleus, or both. These reactions can lead

to the excitation of the nucleus, the emission of gamma rays, or the ejection of other particles.

The reactions of primary interest in reactor operations are inelastic reactions, as they play a crucial role in the behaviour and management of nuclear reactors. These reactions include nuclear fission, and radioactive decay, which are discussed in the following sections.

2.1.1. Fission process and fuel depletion

Fission is a nuclear reaction in which the nucleus of a heavy atom, such as ^{235}U and ^{239}Pu, undergo a split into smaller fragments, resulting in the release of a significant amount of energy (approximately 200 MeV) [5, 4]. This process is key to nuclear energy production, as it generates the heat necessary for power generation in nuclear reactors. As a reactor operates, fissile isotopes undergo fission chain reactions, contributing to sustained energy output [9]. Equation 2.1 shows an example of the fission reaction for ^{235}U [4, 5].

$$^{235}_{92}U + {}^{1}_{0}n \rightarrow {}^{236}_{92}U^{*} \rightarrow {}^{141}_{56}Ba + {}^{92}_{36}Kr + 3{}^{1}_{0}n + 200\ MeV \qquad (2.1)$$

Where,

$^{236}_{92}U^{*}$ is unstable and will eventually fission into fission products.

The 200 MeV of energy is the result of the kinetic energy of both fission products and neutrons, and the gamma radiation.

The fission product yield for ^{235}U is presented in Figure 2.1 [6]. This information illustrates which fission products are more likely to result from the fission of ^{235}U.

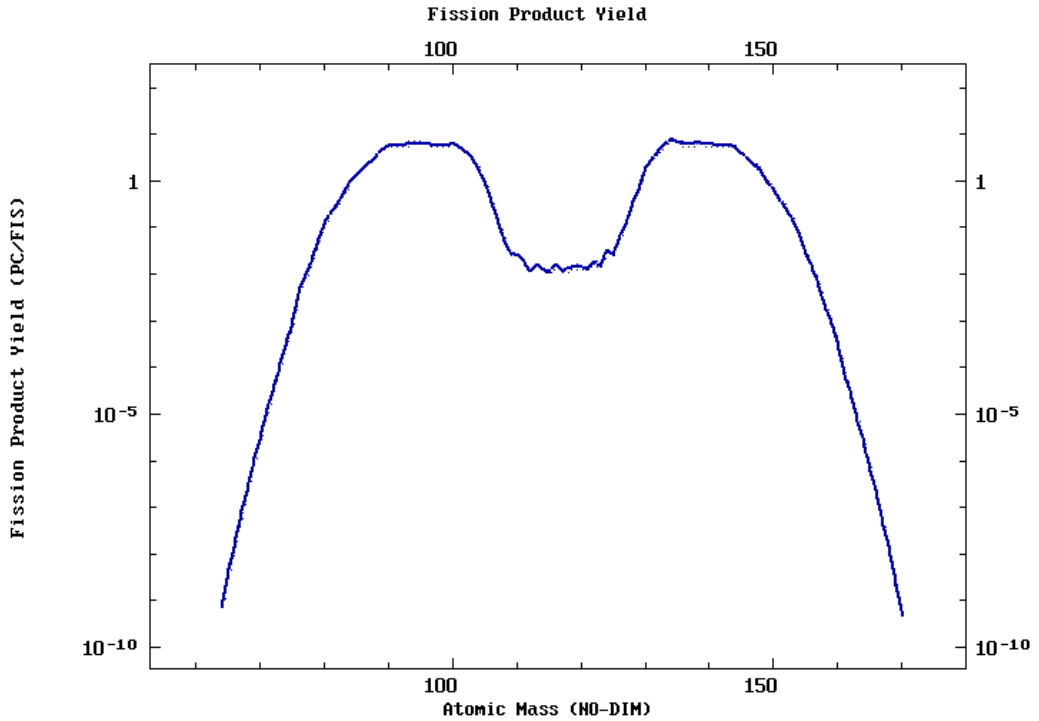

Figure 2.1: Fission product yield for ^{235}U at neutron energy of 0.025 eV [6].

In parallel to the fission process, fuel depletion, the gradual reduction in the concentration of fissile isotopes such as ^{235}U and ^{239}Pu within nuclear fuel takes place. This fuel depletion results from the consumption of these isotopes during fission reactions and during neutron capture reaction [5].

The depletion of ^{235}U begins with a neutron capture reaction, depicted in Equation 2.2, where ^{235}U captures a neutron to form ^{236}U and simultaneously emits gamma radiation. Gamma radiation is high-energy electromagnetic radiation emitted during radioactive decay or nuclear processes [5]:

$$^{235}_{92}U + ^{1}_{0}n \rightarrow \ ^{236}_{92}U + \ \gamma \qquad (2.2)$$

Furthermore, ^{236}U undergoes neutron capture to form ^{237}U, releasing gamma radiation in the process, as illustrated in Equation 2.3 [5]:

$$^{236}_{92}U + ^{1}_{0}n \rightarrow \ ^{237}_{92}U + \ \gamma \qquad (2.3)$$

Finally, ^{237}U undergoes beta-minus β^- decay. Beta decay is a process whereby a neutron is transformed into a proton (beta-minus decay), or a proton is transformed into a neutron (beta-plus decay), resulting in the emission of an electron or a positron (positive electron). The beta-minus decay of ^{237}U is shown in Equation 2.4 [5]:

$$^{237}_{92}U \rightarrow \ ^{237}_{93}Np + \beta^- \tag{2.4}$$

The depletion of ^{235}U leads to the accumulation of ^{237}Np [7]. The depletion process extends to ^{238}U, which begins with neutron capture reaction, illustrated by Equation 2.5, where ^{238}U captures a neutron to form ^{239}U and emits a gamma radiation in the process [5]:

$$^{238}_{92}U + \ ^{1}_{0}n \rightarrow \ ^{239}_{92}U + \ \gamma \tag{2.5}$$

Furthermore, ^{239}U undergoes beta-minus decay to form ^{239}Np, emitting an electron in the process, as shown in Equation 2.6 [5].

$$^{239}_{92}U \rightarrow \ ^{239}_{93}Np + \beta^- \tag{2.6}$$

Another beta-minus decay occurs as ^{239}Np transforms to form ^{239}Pu, releasing an electron in the process, as shown in Equation 2.7 [5].

$$^{239}_{93}Np \rightarrow \ ^{239}_{94}Pu + \beta^- \tag{2.7}$$

Then ^{239}Pu undergoes neutron capture to form ^{240}Pu, and subsequently, ^{240}Pu also undergoes neutron capture to form ^{241}Pu. These two reactions release gamma radiation, as illustrated in Equations 2.8 and 2.9 respectively [5]:

$$^{239}_{94}Pu + \ ^{1}_{0}n \rightarrow \ ^{240}_{94}Pu + \ \gamma \tag{2.8}$$

$$^{240}_{94}Pu + \ ^{1}_{0}n \rightarrow \ ^{241}_{94}Pu + \ \gamma \tag{2.9}$$

Finally, ^{241}Pu undergoes beta-minus decay to form ^{241}Am, releasing an electron in the process, as shown in Equation 2.10. ^{241}Pu can also undergo another neutron capture to form ^{242}Pu, as shown in Equation 2.11 [5]:

$$^{241}_{94}Pu \rightarrow \ ^{241}_{95}Am + \beta^- \tag{2.10}$$

$$^{241}_{94}Pu + ^{1}_{0}n \rightarrow ^{242}_{94}Pu + \gamma \quad (2.11)$$

Subsequently, the depletion of ^{238}U leads to the accumulation of ^{242}Am and ^{242}Pu [7].

The fissile nuclide ^{239}Pu is produced through the neutron capture of ^{238}U, eventually leading to the formation of ^{239}U, as depicted in Equation 2.12 [4, 5, 8].

$$^{238}_{92}U + ^{1}_{0}n \rightarrow ^{239}_{92}U \rightarrow ^{239}_{93}Np + \beta^{-} \rightarrow ^{239}_{94}Pu + \beta^{-} \quad (2.12)$$

Equation 2.13 shows the fission process of ^{239}Pu [4, 5, 8].

$$^{239}_{94}Pu + ^{1}_{0}n \rightarrow ^{240}_{94}Pu \rightarrow ^{140}_{54}Xe + ^{98}_{40}Zr + 2^{1}_{0}n + 200\ MeV \quad (2.13)$$

This leads to the formation of more fission products and the depletion of ^{238}U.

Understanding fission and fuel depletion is essential for optimizing SNF storage casks efficiently and addressing safety considerations in nuclear engineering.

2.1.2. Radioactive decay and nuclide build-up

The second key nuclear reaction is known as the radioactive decay reaction. This process involves an unstable atomic nucleus releasing energy through the emission of radiation, such as alpha particles, beta particles, or gamma rays, resulting in the formation of a different nuclide or a more stable configuration. An alpha particle is composed of two protons and two neutrons, resembling a ^{4}He nucleus [8].

The rate of change of nuclides due to radioactive decay and neutron capture is given in Equation 2.14 [9, 10]:

$$\frac{dN_i}{dt} = \sum_{j=1}^{M} l_{ij}\lambda_j N_j + \varphi \sum_{k=1}^{M} f_{ij}\sigma_k N_k - \lambda_i N_i - \varphi\sigma_i N_i \quad (2.14)$$

Where,

l_{ij} are branching ratios, representing the fraction of decays of species j that result in the formation of species i.

λ_j is a decay constant for species N_j, indicating the rate at which N_j decays.

N_j is a population of species j.

φ is an averaged neutron flux.

f_{ij} are branching ratios, representing the probability of a reaction involving species k that results in the formation of species i.

σ_k are cross-sections, representing the probability of a neutron-induced reaction for species k.

N_k is a population of species k.

N_i is a population of species i.

λ_i is a decay constant for N_i, indicating the rate at which N_i decays.

σ_i is a capture cross-section, representing the probability of a neutron being captured by species i.

To illustrate, Figure 2.2 and Figure 2.3 shows the build-up and radioactive decay of nuclides based on Equation 2.14. Specifically, Figure 2.2 shows the build-up of ^{137}Ba alongside the decay of ^{137}Cs. The reaction governing this process is described in Equation 2.15, where the probability of occurrence is 95% [9]:

$$^{137}_{55}Cs \rightarrow \beta^-(0.51\,MeV) + {}^{137m}_{56}Ba \rightarrow \gamma(0.66\,MeV) + {}^{137}_{56}Ba \quad (2.15)$$

The additional reaction, which occurs with a 5% probability, is described by Equation 2.16 [9]:

$$^{137}_{55}Cs \rightarrow \beta^-(1.17\,MeV) + {}^{137}_{56}Ba \quad (2.16)$$

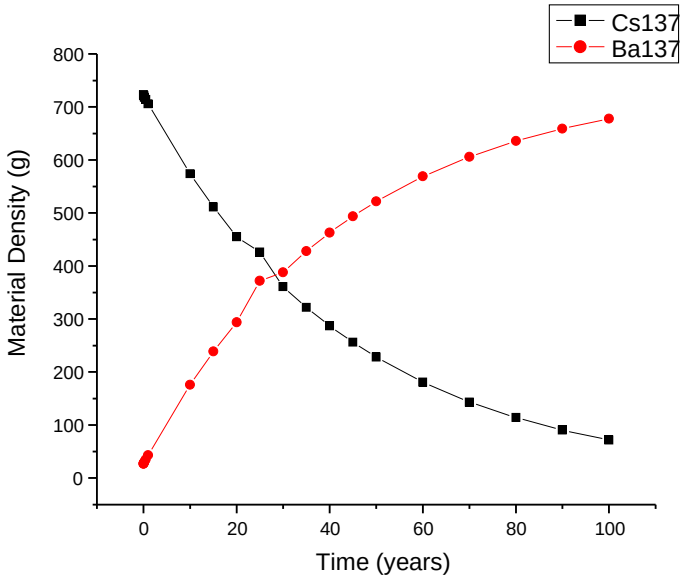

Figure 2.2: Build-up of ^{137}Ba and decay of ^{137}Cs over a period of 100 years [9].

Upon analysing Equations 2.15 and 2.16, it becomes evident that the energy released by both beta and gamma radiations is balanced (i.e., the total energy released in Equations 2.15 and 2.16 is 1.17 MeV). This energy is known as decay heat. In a reactor, decay heat is defined as the heat produced by the radioactive decay of fission products in nuclear fuel after the reactor has been shut down [4]. Understanding decay heat is crucial for managing SNF in both the fuel pool and SNF casks.

Figure 2.3 provides insight into the build-up and decay patterns of nuclides commonly found in SNF (See Appendix A). The calculations were conducted to understand what happens to the nuclide over time as they decay or build-up over a period of 12 months.

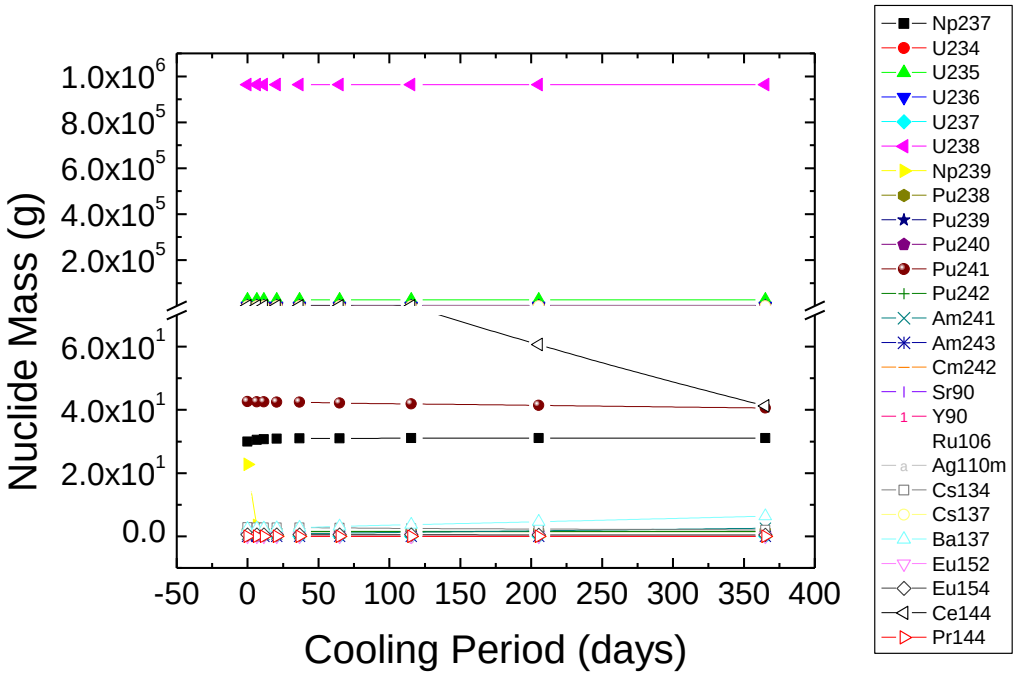

Figure 2.3: Build-up and decay of various nuclides over a period of 12 months (see Appendix A, Table A.1).

Similarly, Figure 2.4 offers insights into the build-up and decay patterns of nuclides commonly found in SNF over a period of 100 years.

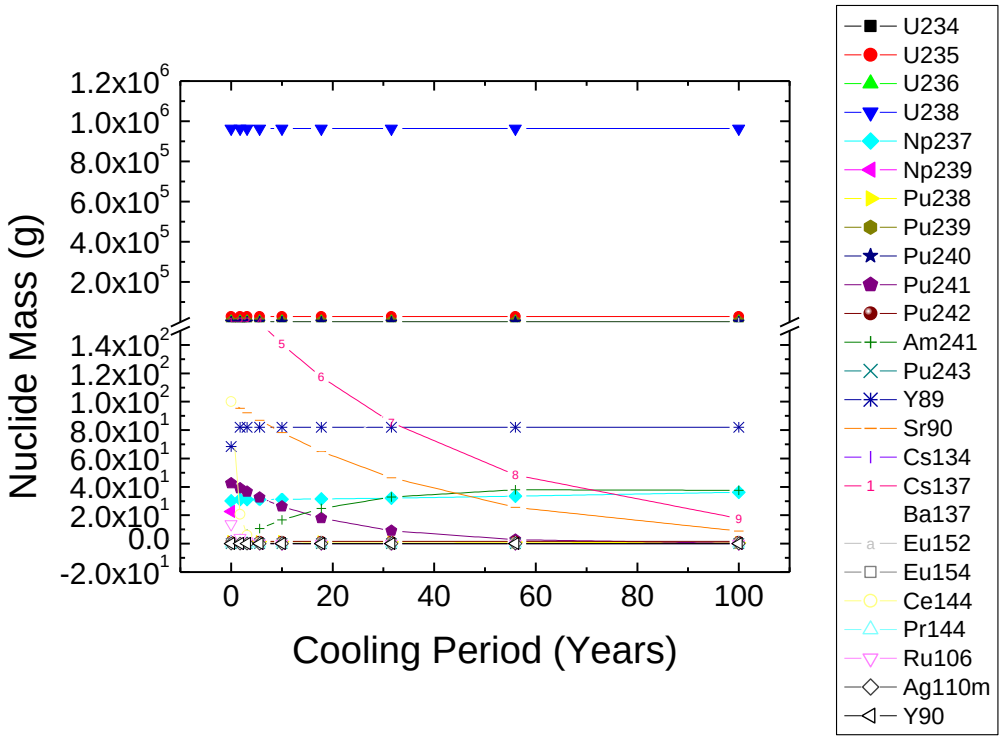

Figure 2.4: Build-up and decay of various nuclides over a period of 100 years (see Appendix A, Table A.2).

As an example, Equation 2.17 illustrates the transmutation of ^{235}U into ^{231}Pa, where ^{235}U emits an alpha particle (α) to form ^{231}Th. ^{231}Th then undergoes a beta-minus decay to form ^{231}Pa [9].

$$^{235}_{92}U \rightarrow \alpha + {}^{231}_{90}Th \rightarrow \beta^{-} + {}^{231}_{91}Pa \qquad (2.17)$$

Fission and neutron capture primarily depend on neutron cross sections. The concept of neutron cross sections is discussed in the following section.

2.2. Cross section of nuclear reactions

The microscopic cross section represents the probability of a specific reaction (such as fission) occurring when neutrons interact with an atomic nucleus. This cross section depends on the energy of the incident neutrons, and it is shown in Equation 2.18, expressed in terms of reaction rate,

neutron flux, and atom density [3, 4]. Neutron flux (ϕ) is defined as the number of neutrons passing through a unit area per unit time, typically measured in neutrons per square centimetre per second (neutrons/cm²/s). Atom density (N) is defined as the number of target nuclei per unit volume, typically measured in atoms per cubic centimetre (atoms/cm³):

$$\sigma = \frac{R}{nvN\,dx} = \frac{R}{\phi \mathrm{N}} \tag{2.18}$$

where,

R = Reaction Rate (reactions / s)

n = number of neutrons

v = neutron velocity

dx = distance covered by the neutrons

This yields units of σ in cm², introducing the concept of cross-section, often denoted in barns (1 barn = 10^{-24} cm²). In a nuclear reactor, numerous reactions occur, but three specific reactions are pivotal for criticality safety analysis. Each of these reactions is associated with its unique microscopic cross-section. These nuclear reactions include:

- Fission reaction;
- Scattering reaction; and
- Capture reaction.

For example, the fission cross section of ^{235}U, depicting the probability of a fission event, is illustrated in Figure 2.5 [6]. The figure shows three distinct neutron energy regions: thermal neutrons, the epithermal region (or resonance absorption region), and fast neutrons.

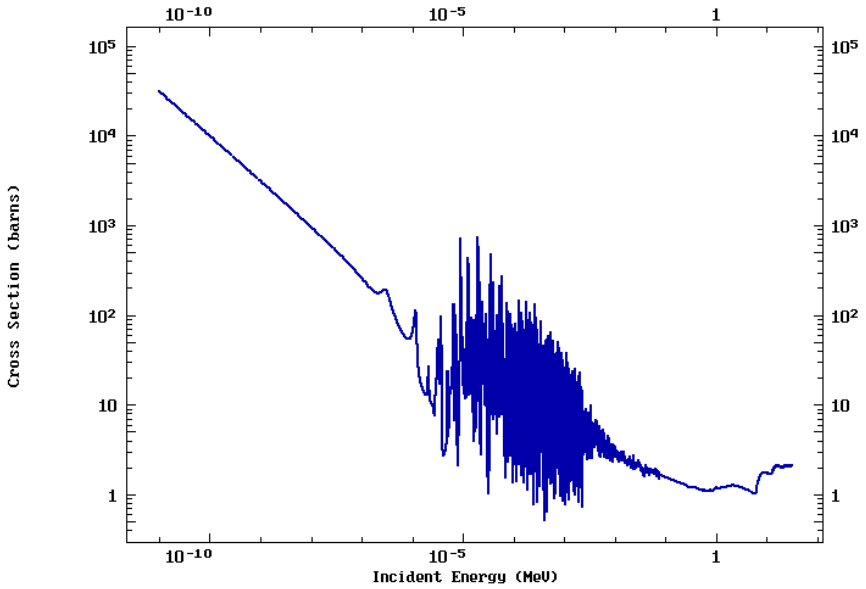

Figure 2.5: Fission cross-section of ^{235}U, showing thermal, fast and resonance absorption regions [6].

Thermal neutrons, which are slow-moving neutrons with energies around room temperature, have a significantly higher likelihood of causing fission in ^{235}U. In contrast, fast neutrons, which are high-energy neutrons with energies in the millions of electron volts (MeV), have a lower probability of inducing fission reactions in this isotope. The figure also shows a region of resonance absorption, where neutrons of specific energies are more likely to be absorbed by the ^{235}U nucleus due to energy matching with its resonance levels, resulting in fission [4].

In nuclear analysis, the macroscopic cross-section, denoted as Σ, is commonly employed and is defined in relation to the microscopic cross-section as $\sum = N\sigma$ (cm^{-1}). The macroscopic cross section is defined as measure used to describe the probability of a explicit type of interaction between neutrons and the material in a reactor. Unlike the microscopic cross section, which is concerned with individual nuclei, the macroscopic cross section considers the bulk properties of the material [3].

When taking credit for fuel burnup, the primary reaction of significance is the radiative capture reaction, where a nucleus captures a neutron and

typically emits gamma radiation. The radiative capture reaction is commonly represented as shown in Equation 2.19.

$$ {}^{1}_{0}n + {}^{A}_{Z}X \rightarrow ({}^{A+1}_{Z}X)^{*} \rightarrow {}^{A+1}_{Z}X + \gamma. \quad (2.19) $$

2.2.1. Cross section libraries

Cross section libraries are essential tools in nuclear analysis, providing detailed data on the probability of various interactions between neutrons and atomic nuclei. These libraries include information on reaction rates, such as absorption, fission, and scattering, across different energy ranges. The behaviour of nuclear materials in reactors, SNF storage casks and other applications, can be modelled accurately by using nuclear cross section libraries [10].

There are two main types of cross-section libraries: multi-group (MG) and continuous energy (CE). Multi-group libraries divide the neutron energy spectrum into discrete groups, providing averaged cross-section data for each group. This approach simplifies calculations and is commonly used in reactor physics and criticality safety analysis. Continuous energy libraries, on the other hand, offer cross-section data as continuous functions of neutron energy, allowing for more precise and detailed simulations. Both MG and CE libraries are crucial for various aspects of nuclear analysis, depending on the required level of accuracy and computational resources [10].

2.2.2. Radiative capture cross section of the major actinides

This section presents radiative capture cross sections and an illustration of major actinides cross sections. Radiative capture is crucial in SNF as it reduces the number of neutrons, thereby reducing k_{eff} of the system which leads to subcriticality.

Figure 2.6 (extracted from the ENDF library) depicts the radiative capture cross section of ^{240}Pu as an example [6]. The figure shows that the capture cross section is high for thermal neutrons (indicating a high probability of neutron capture) and low for fast neutrons. The epithermal region (resonance absorption region) lies between the thermal and fast neutron regions and is also responsible for high neutron absorption.

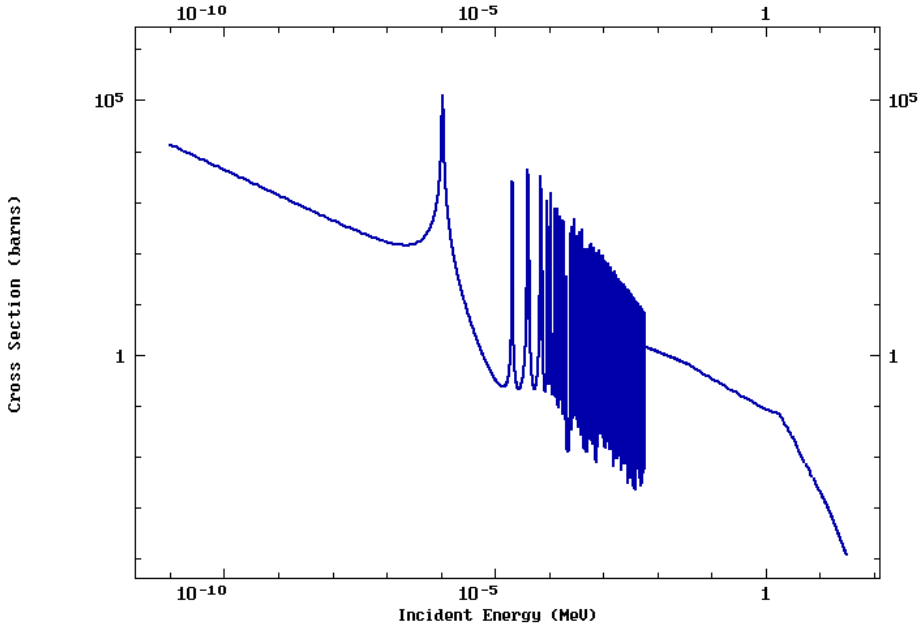

Figure 2.6: The relationship between neutron energy and the radiative capture microscopic cross section of ^{240}Pu.

This substantial cross section in the thermal region is anticipated to result in a lower k_{eff} for SNF when considering the impact of major actinides compared to fresh fuel. The high radiative capture cross section (thermal neutrons) in major actinides implies a heightened tendency to absorb neutrons, thereby influencing the overall reactivity of the system. Consequently, taking credit for major actinides in the analysis is expected to contribute to a reduction in k_{eff} for the SNF casks, a critical parameter in assessing the behaviour and safety considerations of nuclear systems.

2.2.3. Radiative capture cross sections of fission products

In this section, the radiative capture cross sections of fission products are explored, which are important when accounting for the fuel burnup of the SNF. The nuclide, ^{155}Gd, is used as an example to show that fission products have high neutron capture microscopic cross section. Figure 2.7 [6] (extracted from ENDF library) shows the radiative capture cross section of ^{155}Gd, with a high microscopic cross section for thermal neutrons. It also shows that fast neutrons have low microscopic cross section.

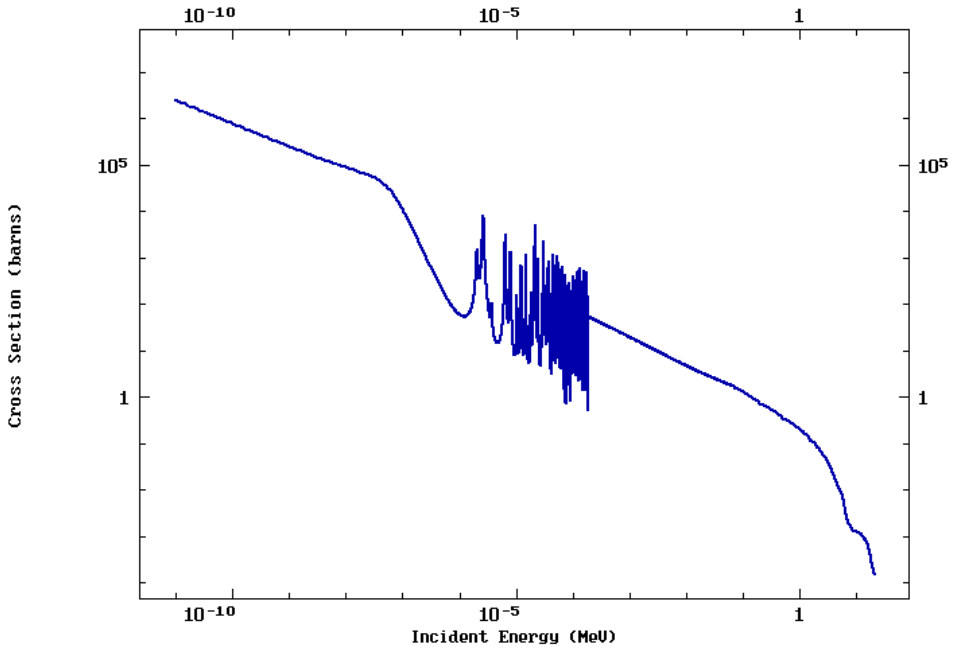

Figure 2.7: The relationship between neutron energy and the radiative capture microscopic cross section of ^{155}Gd.

The following modelling scenarios are considered:

- Fresh fuel (see Section 4.2);
- Major actinides (see Section 4.3.1);
- Actinides + principal fission products(4.3.2);
- Actinides + minor fission products (see Section 4.3.3);

The inclusion of more fission products (minor and principal fission products) will result in high neutron absorption, resulting in lower k_{eff} when compared to both fresh fuel and fuel only with major actinides.

In summary, a system that takes burnup credit for minor fission products is expected to have a higher k_{eff} compared to one that only takes principal fission products into account. This difference is caused by the presence of principal fission products in greater numbers in the SNF compared to those included in minor fission products. It is also noted that fresh fuel is expected to have a higher k_{eff} compared to when taking credit for fuel burnup.

The k_{eff} of a nuclear system is also influenced by other factors, including fuel and moderator temperatures as well as their respective densities. These parameters are examined in detail in the subsequent section.

2.3. Effects of fuel and moderator temperature and density on k_{eff}.

In this section, the impact of fuel and moderator temperature and density on $k_{eff}$is explored. Understanding their impact is crucial for optimizing reactor performance and ensuring safe operation.

2.3.1. Effect of fuel temperature on k_{eff}.

The temperature of nuclear fuel plays a significant role in determining the reactivity and k_{eff} of a nuclear system. This section explores the impact of fuel temperature on reactor performance, focusing on its influence on reactivity and k_{eff}. Reactivity in nuclear systems measures the deviation from criticality, where criticality is the balanced state of neutron production and loss. A positive reactivity indicates increased neutron multiplication, while negative reactivity signifies reduced neutron multiplication.

As the temperature of nuclear fuel increases, the thermal motion of nuclei (e.g., ^{238}U) causes their resonance peaks in neutron absorption cross-sections to broaden and flatten, a phenomenon known as Doppler broadening. This effect redistributes neutron absorption probabilities,

allowing ^{238}U to absorb neutrons in resonance energy regions more effectively. The resonance absorption will increase the overall absorption due to the broader energy range of effective capture. For commercial thermal reactors, the number of ^{238}U isotopes is much larger than the number of ^{235}U isotopes. There is therefore more absorption by ^{238}U than ^{236}U with Doppler broadening. This leads to a reduction in the k_{eff}, introducing negative reactivity feedback and contributing to reactor stability [8, 5].

The absorption of neutrons within the resonance of a specific nuclide is influenced by both neutron flux and the nuclide's macroscopic cross-section. Neutron flux refers to the density of neutrons passing through a unit area per unit time. Meanwhile, macroscopic cross-section represents the effective cross-sectional area for neutron interactions, accounting for both the microscopic cross-section and the number density of nuclei in the material [4]. This relationship is expressed in Equation 2.20 [8]:

$$F_a = \phi_{av}(E) \int \Sigma_a(E) dE \tag{2.20}$$

Where,

F_a is neutron resonance absorption rate measured in $neutrons/cm^3.sec$.

$\phi_{av}(E)$ is the average neutron flux in $neutrons/cm^2.sec$. (which depends on energy of the neutrons),

E is the energy of incident neutrons in eV.

$\Sigma_a(E)$ is the macroscopic cross section in cm^{-1}.

The integral represents the resonance area.

The average neutron flux, $\phi_{av}(E)$, depends on the temperature of the fuel. As the temperature increases, the resonance peak cross-section flattens and broadens due to Doppler broadening, leading to an increase in the flux, $\phi_{av}(E)$. From Equation 2.20, it can be concluded that the resonance absorption, F_a, for ^{238}U will also increase as the temperature rises. The overall effect of increasing fuel temperature is a reduction in the system's

reactivity, which in turn causes a decrease in the k_{eff} of the system [8, 7, 12].

2.3.2. Effect of fuel density on k_{eff}.

As fuel temperature increases, thermal expansion causes fuel density to decrease. This decrease in fuel density leads to an increase in the distance between fuel nuclei. Consequently, the mean free path of neutrons within the fuel increases. With a longer mean free path and consequently, lower macroscopic cross-section, neutrons are more likely to escape without being absorbed by fuel nuclei, resulting in reduced neutron absorption and a decrease in reactivity [8, 5, 4]. This decrease in reactivity leads to a lower k_{eff} of the system.

2.3.3. Effect of moderator temperature and density on k_{eff}.

Many factors have an influence on the moderator temperature of a nuclear reactor, with fuel temperature being one of the most significant. As fuel temperature increases, the thermal energy is transferred to the moderator, causing its temperature to rise. This rise in moderator temperature leads to thermal expansion, resulting in a decrease in moderator density. The reduction in moderator density affects neutron moderation and thermalization, influencing the overall neutron flux and reactor reactivity [4].

Specifically, the increased moderator temperature leads to more energetic collisions between neutrons and moderator nuclei, altering the neutron energy spectrum and reducing the probability of neutron capture by fissile nuclei (see Figure 2.5). As a result, reactivity could decrease, leading to a lower k_{eff} [4].

2.4. Criticality and criticality safety

The concept of criticality for fissile material involves a condition where the rate at which the number of neutrons changes in the system remains constant, typically expressed with a k_{eff} value of 1. In the realm of SNF casks, criticality safety is crucial for accident prevention and protection

against uncontrolled or controlled nuclear fission chain reactions [11]. Specifically, for the SNF casks, a system is considered safe when its k_{eff} is maintained below 0.95 [3].

Nuclear facilities handling fissile materials, including nuclear power plants and entities dealing with fresh fuel, spent fuel, and radioactive waste containing fissile material, must consistently adhere to criticality safety standards. Calculating the k_{eff} of the system is instrumental in demonstrating that SNF casks remain in a subcritical state, ensuring that safety thresholds are not breached. The achievement of subcriticality is dependent on different factors, with particular emphasis on the geometry and placement of the system, among other considerations [11]. This thorough approach is essential to uphold safety standards and prevent criticality accidents in facilities dealing with fissile materials.

In the next section, the concepts of k_{eff} and the Boltzmann Transport Equation, which are fundamental to nuclear engineering, are discussed.

2.4.1. Effective neutron multiplication factor (six factor formula)

The $k_{eff}$of a nuclear system, is a key parameter derived from solutions to the Boltzmann transport equation in nuclear reactor physics. It quantifies the balance between neutron production and losses, determining the criticality state of the reactor [4].

The k_{eff} of the system can also be mathematically determined through a six-factor formula (given in Equation 2.1). It represents the ratio of neutron production from fission in one generation to neutron absorption and leakage in the previous generation. The first four terms of Equation 2.1 are independent of the system size, signifying an infinite system, while the last two terms depend on the system size and represent neutron leakage from the system [4, 11]:

$$k_{eff} = \eta . \varepsilon . p . f . P_f . P_t \tag{2.1}$$

Where

η is the neutron reproduction factor.

ε is the fast fission factor.

p is the resonance escape probability.

f is the thermal utilization factor.

P_f is the fast non-leakage probability of the neutrons.

P_t is the thermal non-leakage probability of the neutrons.

The value of k_{eff}, is defined as follows [4]:

- $k_{eff} < 1$: subcritical.
- $k_{eff} = 1$: critical.
- $k_{eff} > 1$: supercritical.

The k_{eff} of the SNF storage casks can be determined using the above criteria to investigate the safety of the system.

The following factors can affect the behaviour of neutrons within the nuclear system (SNF casks), and therefore, can determine whether the system becomes critical, subcritical or supercritical. These factors are [4, 5, 12]:

- **Doppler broadening in SNF:** Thermal motion of fuel nuclei in SNF can lead to Doppler broadening of resonance absorption peaks in neutron cross-sections. This broadening increases the resonant absorption by ^{238}U nuclei, resulting in fewer neutrons available for fission, thereby contributing to a decrease in $k_{eff.}$
- **Neutron reflection:** The arrangement of casks has an impact on neutron reflection. Close spacing increases neutron reflection, while increased separation reduces this effect, resulting in lower k_{eff} as the separation is increased.

- **Neutron absorption:** The spacing between casks affects neutron absorption, with different materials and air contributing to absorption. Increased separation can intensify absorption effects. Higher neutron absorption leads to a decrease in the effective neutron population and a subsequent decrease in k_{eff}.

- **Neutron streaming:** Changes in the separation alter neutron streaming paths within the cask array, influencing the transport of neutrons. Altered neutron streaming paths can result in variations in neutron flux distribution, contributing to fluctuations in k_{eff}.

- **Spatial heterogeneity:** Increased separation introduces spatial heterogeneity in neutron flux across the cask array. Spatial variations affect the balance between neutron production and loss mechanisms, leading to fluctuations in k_{eff}.

- **Absorption in materials:** The materials in and around the casks contribute to neutron absorption, and changes in separation can influence the types and amounts of absorption. Variations in absorption properties can affect the overall neutron balance, influencing k_{eff}.

In summary, k_{eff} of the system serves as a crucial measure for assessing the criticality of a nuclear system and play a fundamental role in understanding and managing the behaviour of neutrons within a nuclear system.

2.4.2. Boltzmann transport equation

A critical aspect of nuclear criticality safety analysis is understanding how neutrons move through materials. This behaviour is described by the Boltzmann transport equation, which quantifies the change in neutron density over time in a closed system as the net balance between neutron sources and losses. Mathematically, this relationship is expressed in Equation 2.2 [3, 4].

$$\frac{1}{v}\frac{\partial\phi(\vec{r},E,\Omega)}{\partial t} + \nabla\left[\hat{\Omega}\phi\left(\vec{r},\mathrm{E},\hat{\Omega},\mathrm{t}\right)\right] + \Sigma_t(E)\phi\left(\vec{r},E,\hat{\Omega}\right) = \int dE' \int d\Omega' \Sigma_s(E' \rightarrow E,\Omega' \rightarrow \Omega)\phi\left(\vec{r},E',\hat{\Omega}',t\right) + S\left(\vec{r},E,\hat{\Omega},t\right) \quad (2.2)$$

Where,

$\phi(\vec{r},E,\Omega,\mathrm{t})$ is theneutron flux (neutrons per cm^2 per second), which is dependent on energy *E*, distance *r*, solid angle Ω and time *t*.

Σ_t is the total macroscopic cross-section.

Σ_s is the Macroscopic scattering cross-section.

The source term, $S(\vec{r},E,\hat{\Omega},t)$, represents the total contribution of neutrons generated from the fission process and those originating from external sources. This is mathematically expressed in Equation 2.3 [12, 5].

$$S(\vec{r},E,\hat{\Omega},t) = S_{ext} + \chi(E)\int dE' \int d\hat{\Omega}'\nu(E')\Sigma_f(E')\phi(r,E,\hat{\Omega}',t) \quad (2.3)$$

Where

S_{ext} is the external source of neutrons.

$\chi(E)dE$ is the number of fission neutrons with energy between E and $E + dE$.

$\Sigma_f(E')$ is the macroscopic fission cross-section at energy E.

$\nu(E')$ is the number of neutrons born per fission.

In a steady state, the rate of neutron production through the fission process equals the rate of neutron losses, leading to a criticality parameter k_{eff} = 1. The solution of Boltzmann equation, a pivotal aspect in understanding neutron transport, will now be examined in the subsections below.

2.4.2.1. Methods of solving Boltzmann transport equation

Understanding and solving the Boltzmann transport equation is fundamental to nuclear reactor physics. There are two main methods to solve this equation, each with its own advantages and limitations.

2.4.2.1.1. Deterministic method

Deterministic methods are a class of numerical techniques employed to solve the Boltzmann transport equation in neutron transport simulations. Unlike stochastic methods, deterministic approaches utilize a set of equations that describe the average behaviour of neutrons over space, energy, and angle. This involves discretizing the spatial and energy domains and solving the resulting system of coupled partial differential equations. Deterministic solvers, such as finite element methods, offer a systematic and deterministic way to model neutron behaviour within a medium. While they are computationally efficient and suitable for a wide range of scenarios, deterministic methods may face challenges in handling complex geometries and strongly anisotropic neutron fluxes. Despite these limitations, deterministic solvers play a crucial role in reactor physics simulations, radiation shielding analyses, and other nuclear engineering applications, providing a deterministic and averaged solution to the Boltzmann equation for neutron transport [4].

2.4.2.1.2. Monte Carlo method

The Monte Carlo (MC) method is a stochastic numerical technique employed for solving the Boltzmann transport equation in neutron transport simulations. In essence, it utilizes random sampling to model the individual trajectories of neutrons as they travel through a medium. The method involves simulating the interactions of neutrons with materials, incorporating probabilistic processes such as scattering, absorption, and fission. By combining numerous random neutron histories, the Monte Carlo method statistically approximates the neutron flux distribution and other relevant

parameters, providing a powerful tool for precise and detailed analyses in nuclear reactor physics and radiation shielding. Despite its computational intensity, the Monte Carlo method is particularly advantageous for handling complex geometries and complex nuclear systems, offering a versatile and accurate approach to solving the Boltzmann equation in different scenarios [4].

For instance, the fission cross section of a neutron travelling through matter represents a probability that of an interaction, which depends on, among other variables, on incident energy and atom density, will occur. However, it is uncertain whether a neutron will indeed cause fission when it interacts with fissile material. Various events within the medium, such as scattering collisions, capture, and fission, are also probabilistic in nature. These processes lack certainty due to the inherent randomness associated with neutron transport through a multiplying medium.

The MC simulation operates by generating random numbers to determine various parameters in the neutron transport process. Initially, it selects spatial fission distribution values from the Continuous Distribution Function (CDF), defining the location of source neutrons. Subsequently, it generates random numbers to determine the energy and angular variables of the source neutrons, selected from their respective CDFs [4]. The inherent randomness of the MC technique renders it suitable for solving the neutron transport equation, effectively mimicking the stochastic nature of neutron movement within the system.

In the next sections, codes that are used to solve the neutron transport equation are discussed.

2.4.2.2. Tools for solving Boltzmann transport equation

Several computational tools and software packages are available for solving the Boltzmann transport equation, each tailored to different methods and applications in nuclear engineering.

MCNP (Monte Carlo N-Particle) and SERPENT are two widely used Monte Carlo codes that solves the Boltzmann Transport Equation and interactions for criticality safety calculations. MCNP, developed by Los Alamos National Laboratory, employs Monte Carlo methods to model neutron transport and interactions, providing detailed simulations to ensure nuclear systems remain subcritical under various conditions [12]. SERPENT, developed by VTT Technical Research Centre of Finland, offers advanced capabilities for reactor physics and burnup calculations, making it suitable for detailed criticality safety analyses of spent fuel and reactor cores [13]. CASMO, developed by Studsvik, is a deterministic code that solves the Boltzmann Transport Equation for lattice physics and fuel assembly calculations. It is typically used for burnup credit applications in Boiling Water Reactors wet storage systems [14].

Due to the complex nature of SNF casks and the need for comprehensive safety evaluations, a SCALE code package is utilized, and it is discussed in the following section.

2.4.2.2.1. Overview of SCALE code

The Standardized Computer Analyses for Licensing Evaluations (SCALE) code system is a widely used tool for modeling and performing nuclear safety and design assessments [15]. Developed, maintained, tested, and managed by the Nuclear Energy and Fuel Cycle Division (NEFCD) at Oak Ridge National Laboratory (ORNL), the SCALE suite is distributed to licensees through the Radiation Safety Information Computational Center (RSICC). The SCALE code undergoes rigorous verification and validation (V&V) processes and serves as a comprehensive, user-friendly tool for criticality safety analysis and other key nuclear applications. The software includes three deterministic solvers and three Monte Carlo radiation transport solvers, along with tools for both CE and MG neutronic analyses [15].

It is noted that SCALE-6.3.1 was released in 2024, but it is not used in this project. This project uses SCALE (SCALE-6.4.2), which employs the

Fulcrum module to process the input file. For this research, two primary scale suites (KENO-VI and STARBUCS) were utilized, and they are briefly described below.

2.4.2.2.1.1. KENO

KENO is a MC code used for calculating sequences in both MG and CE modes for criticality safety and neutronic analysis. KENO-V.a and KENO-VI (pronounced KENO 6) are two distinct variants of the KENO code, each capable of determining the k_{eff} of fissile materials in either CE or MG mode. KENO-V.a is run through the Criticality Safety Analysis Sequence with KENO-V.a (CSAS5), whereas KENO-VI is accessed via the Criticality Safety Analysis Sequence with KENO-VI (CSAS6) [15].

KENO-V.a is a streamlined geometry package within the KENO code, designed for efficient modelling of various systems in criticality safety analyses. On the other hand, KENO-VI utilizes the SCALE Generalized Geometry Package, providing greater flexibility for modelling, especially when dealing with complex or nested geometries.

2.4.2.2.1.2. STARBUCS

Criticality safety analysis of spent nuclear fuel (SNF) that incorporates burnup credit is carried out using the Standardized Analysis of Reactivity for Burnup Credit using SCALE (STARBUCS). This tool automatically combines depletion and criticality processes, eliminating the need for manual adjustments of SNF nuclide compositions to align with criticality safety codes. STARBUCS calculates the k_{eff} of the system by accounting for the burnup credit of the SNF. It is important to note that the Origen module is integrated into STARBUCS and is called automatically to perform depletion calculations, without requiring input or prompt from the user [15].

To summarise, SCALE emerges as the preferred code for the research on SNF storage casks due to its comprehensive suite of specialized and focused modules. The integrated approach of SCALE, incorporating modules such as KENO-VI for criticality safety and STARBUCS for burnup

credit, flawlessly aligns with the complex requirements of the study. The dedicated nature of these modules ensures a focused and efficient analysis of SNF storage configurations, covering criticality assessments and burnup calculations.

2.5. Fuel burnup

Nuclear fuel burnup refers to the energy produced by the fission process, primarily from the fissile material (e.g., ^{235}U) in the fuel, which also contains other materials such as ^{238}U. Burnup is typically measured in Gigawatt Days per metric tonne of Uranium (GWd/MTU) [5]. As fission occurs in the core, the amount of fissile material decreases, eventually reaching a point where the fuel can no longer generate power efficiently. Consequently, fuel with higher burnup remains in the core longer than fuel with lower burnup. The fuel is classified as SNF when it is no longer economically viable for power generation.

In the context of criticality safety analysis, the composition and behaviour of SNF become crucial due to the presence of various nuclides that impact reactivity. For this research, the most significant combinations of nuclides considered for analysis are given in Table 2.1 [3, 16]:

Table 2.1: Nuclide groups used in burnup credit.

Nuclide Group	**Nuclide Sets**
Actinides Only	^{235}U, ^{235}U, ^{238}U, ^{238}Pu, ^{239}Pu, ^{240}Pu, ^{241}Pu, ^{242}Pu, ^{241}Am
Minor Fission Products	^{236}U, ^{237}Np, ^{243}Am, ^{133}Cs, ^{143}Nd, ^{151}Sm, ^{155}Gd
Principal Fission Products	^{237}Np, ^{99}Tc, ^{143}Nd, ^{145}Nd, ^{147}Sm, ^{150}Sm, ^{151}S, ^{152}Sm, ^{151}Eu, ^{153}Eu.

The impact of fuel burnup on k_{eff} for the aforementioned nuclide groups is illustrated in Figure 2.8 [3]. The figure demonstrates that k_{eff} decreases as fuel burnup increases. This occurs because, as the fuel undergoes depletion in the core due to the fission process, the concentration of fission products rises. These fission products, which include nuclides with high neutron absorption, contribute to increased neutron absorption, thereby reducing k_{eff}.

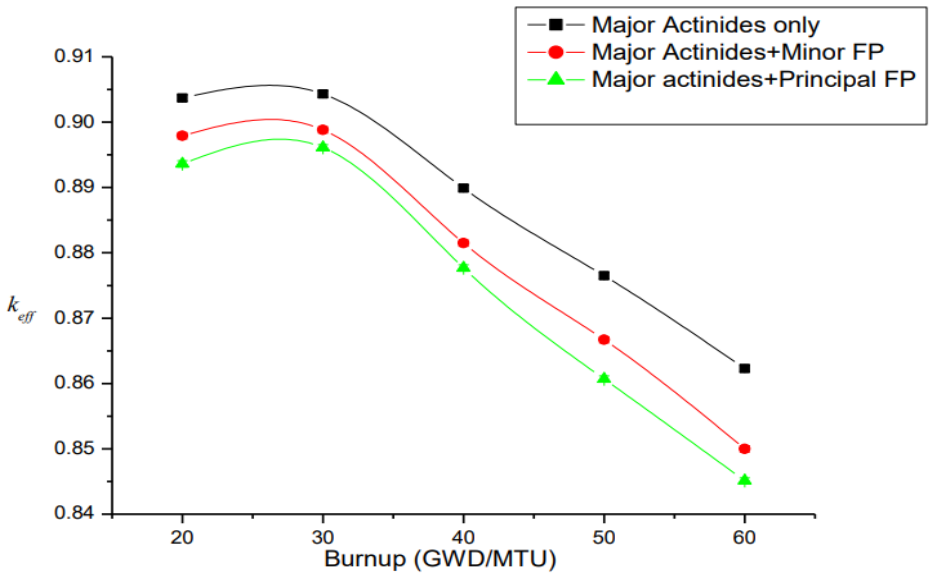

Figure 2.8: Effect of burnup on k_{eff} for different nuclides groups [6].

The decrease in k_{eff} is attributed to the depletion of fissile materials such as ^{235}U, ^{239}Pu, and ^{241}Pu, as well as fertile isotopes like ^{238}U and ^{240}Pu. Additionally, the increase in major actinides, as listed in Table 2.2 and shown in Figure 2.3, contributes to this decrease. While some of these actinides are fissile and can increase k_{eff}, certain fission products with high neutron absorption cross sections, such as ^{155}Gd and ^{150}Sm, significantly contribute to the decrease in k_{eff} .

2.6. Overview of the spent nuclear fuel casks

When nuclear reactors were designed during the 1960s and 1970s, temporary storage solutions, such as fuel pools, were included for SNF, with the expectation of reprocessing the SNF for future reuse [16]. However, the reprocessing did not progress as anticipated, leading to spent fuel pools quickly reaching capacity and leaving nuclear power plant operators with limited space for additional fuel storage [16]. During the standard 18-month refuelling outage at a nuclear power plant, approximately one-third of the SNF is replaced with fresh fuel. Since SNF generates significant amounts of decay heat and radiation, it must be stored underwater and cooled to prevent overheating, which could lead to fuel rod melting or cladding failure due to heat and radiation. One alternative solution to the storage space issue is the use of SNF casks. As part of the strategy to address the storage challenge, it is proposed that SNF be transferred to these casks after cooling for at least 5 years [17].

2.6.1. Transportation casks

Transportation casks are specialized containers designed for the secure and regulated transport of radioactive materials, including fresh and spent nuclear fuel. These casks adhere to stringent safety standards to ensure the containment and shielding of radioactive contents during transportation. They are constructed with impact-resistant materials and may include cooling systems for fresh fuel. Transportation casks play a pivotal role in the movement of nuclear materials between facilities, such as from reactors to storage or reprocessing sites, and are integral to maintaining the safety and security of the nuclear fuel [16].

2.6.2. Dual-purpose casks

Dual-purpose casks, also known as transportation and storage casks, are versatile containers designed to serve both as transportation vessels and long-term storage solutions for SNF. These casks integrate features necessary for safe transportation, such as impact integrity and additional

shielding, while also providing the required attributes for extended storage. The dual-purpose design streamlines logistical operations, reducing the need for separate casks for transportation and storage. This approach enhances the efficiency and cost-effectiveness of managing SNF, particularly in scenarios where fuel must be transported before entering long-term storage [16].

2.6.3. Dry storage casks

Dry storage casks are robust containers designed for the safe and secure storage of SNF outside of a reactor's fuel pool. Typically constructed with materials such as steel and concrete, these casks are structurally sound and offer radiation shielding. The design allows for the passive cooling of the stored SNF, eliminating the need for active cooling systems. Dry storage casks are employed at nuclear power plants as an interim storage solution and will eventual be moved offsite to be stored in long term repository [7, 16].

There are diverse types of dry storage cask designs, each is designed to accommodate specific fuel assembly types and other considerations in fuel design. The selection of a particular cask design is dependent on factors such as reactor type, fuel composition, and regulatory requirements. Some of the commercially available dry storage casks and their fuel assembly capacities are given in Table 2.2 [16].

Table 2.2: SNF dry storage casks [16].

Name	**Model**	**Type of Reactor**	**Fuel Assembly Capacity**
ENSA	DPT [16]	PWR	21
GNS	CASTOR X/28 [16]	PWR	28
MHI	MSF-69B [16]	BWR	69
REA	REA-2023 [16]	PWR / BWR	24 PWR 52 BWR

The properties and design specifics of CASTOR X/28 are further discussed in the following section, as it is the primary focus of this research.

2.6.3.1. CASTOR X/28

The storage cask examined in this study is the CASTOR X/28, developed in Germany by Gesellschaft für Nuklear-Behalter mBH (GNB). This cask is designed to hold twenty-eight spent fuel assemblies (indicated by "28" in CASTOR X/28), which must have been stored in the SNF pool for at least 10 years (represented by "X" in CASTOR X/28). The 10-year storage period exceeds the minimum 5-year requirement for SNF storage. The CASTOR X/28 cask is constructed from various materials, each serving specific functions, as outlined in Figure 2.9 [3]:

- Cast iron: offers mechanical support and enhances nuclear criticality safety due to its high carbon content.
- Iron and nickel: provide mechanical and structural support.
- Borated steel: Boron is a neutron absorber and steel serves as a structural material that provides mechanical strength and corrosion resistance.

- Polyethylene: neutron shielding.

CASTOR X/28 casks are designed to store SNF in a vertical orientation. Thanks to their durable construction, these casks effectively prevent radiation and nuclides from escaping, ensuring the integrity of the system.

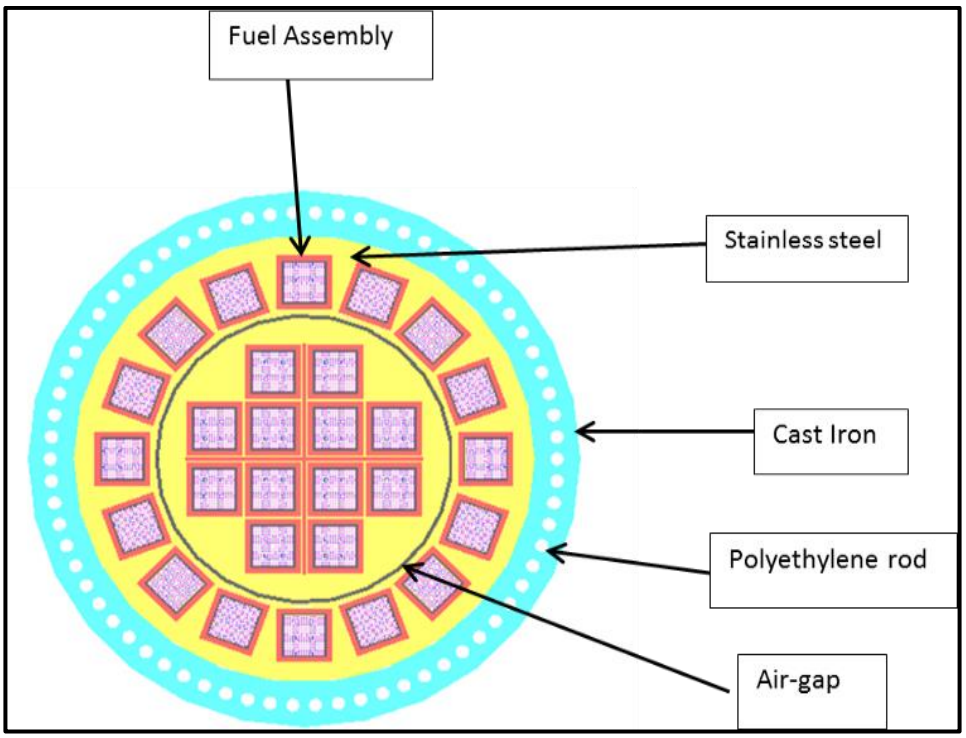

Figure 2.9: A typical spent nuclear fuel cask [6].

The following section provides a brief discussion of the criticality safety analysis of the SNF casks.

2.7. Application of burnup credit on various facilities around the world

This section discusses the application of burnup credit on both dry and wet SNF storage facilities. Additionally, it explores how burnup credit is applied in the transportation, reprocessing, and disposal stages of SNF management. This comprehensive examination aims to provide insights

into the complex utilization of burnup credit across various stages of the nuclear fuel cycle.

2.7.1. Application of burnup credit on transportation, reprocessing and disposal systems

Some countries apply burnup credit when transporting their SNF. Countries such as France, Germany, USA, Switzerland and Netherlands take credit for actinides only when transporting the SNF from their PWR facilities. The rest of the countries, including South Africa do not take credit for burnup when transporting the SNF casks [7].

France's La Haugue reprocessing facility is one of the few facilities that engage in SNF reprocessing. The La Hague facility takes credit for actinides only for 10 years. The 10-year period covers the storage and reprocessing of the SNF [7].

Fuel reprocessing typically eliminates the necessity for burnup credit during the disposal of SNF. Similarly, SNF consolidation removes the need for burnup credit as long as the cask or container remains intact. SNF consolidation is defined as a process in which SNF assemblies are physically reconfigured to increase the efficiency of storage. Consequently, countries such as the USA and Sweden opt to apply burnup credit, particularly for the disposal of SNF within failed or broken casks [7].

2.7.2. Application of burnup credit on dry and wet SNF storages around the world

Facilities around the world have adopted both wet and dry storage methods for storing SNF. In dry storage, SNF is securely housed within casks and similar facilities, without water. Dry storage facilities are commonly situated either on-site or offsite from the reactor facility, providing a flexible approach to SNF management [7].

Conversely, wet storage involves submerging SNF in pools or basins filled with water, serving as a coolant and radiation shield. These wet storage facilities are typically located on-site at nuclear power plants, providing

immediate cooling for recently discharged SNF. The utilization of both wet and dry storage methods reflects the diversity of approaches in managing SNF, considering factors such as space availability, safety considerations, and the immediate cooling needs of freshly discharged fuel [7].

In countries with Pressurized Water Reactors (PWRs), the application of burnup credit in wet storage facilities varies. Notably, Belgium adopts burnup credit for actinides only. On the other hand, South Africa, Brazil, Germany, and the United States of America (USA) extend burnup credit to both actinides and fission products in their wet storage of SNF. Meanwhile, the United Kingdom (UK) is in the process of preparing documentation to enable the adoption of burnup credit for actinides only in its wet storage facility [7].

In contrast, burnup credit practices differ among countries with PWRs for their dry storage. South Africa, France, the United Kingdom, and Sweden do not apply burnup credit in their dry storage facilities for their PWRs. Conversely, USA and Germany take burnup credit for actinides only in their PWR facilities [7].

This research will focus on taking credit for burnup in dry storage facilities. However, for purposes of analysis and calculation, it is assumed that the SNF casks are filled with water to simulate water ingress.

2.8. Regulations of SNF in South Africa

The nuclear industry and the disposal of nuclear waste are highly regulated in South Africa. The following regulations apply to the storage of SNF in South Africa [18]:

- Nuclear Energy Act, 1999 (Act No. 46 of 1999)
- Nuclear Regulatory Act, 1999 (Act No. 47 of 1999)
- National Radioactive Waste Disposal Institute Act, 2008 (Act No. 53 of 2008)

These Acts, along with related legislation such as the National Environmental Management Act, 1998 (Act No. 107 of 1998), aim to regulate the industry and protect the public from hazardous nuclear waste. It is also noted that the country allows the storage of SNF in wet storage pools as well as the dry storage casks [18].

Chapter 3 : Methodology and Modelling

In this chapter, the research approach and techniques employed in this study are outlined. This includes the research design, data collection methods, and analytical tools. A comprehensive understanding of the methodology is crucial for evaluating the reliability and validity of the study's findings.

3.1. Modelling and simulation overview

The present study involves modelling the k_{eff} of spent fuel casks using SCALE 6.2.4, taking credit for three sets of nuclides as detailed in [1, 2, 19, 20, 21, 22, 22 & 23], and also given in Table 2.1, along with NUREG 6747 [24]. Fresh fuel scenario analysis utilized the KENO-VI module of the SCALE code, with the calculation sequence shown in Figure 3.1.

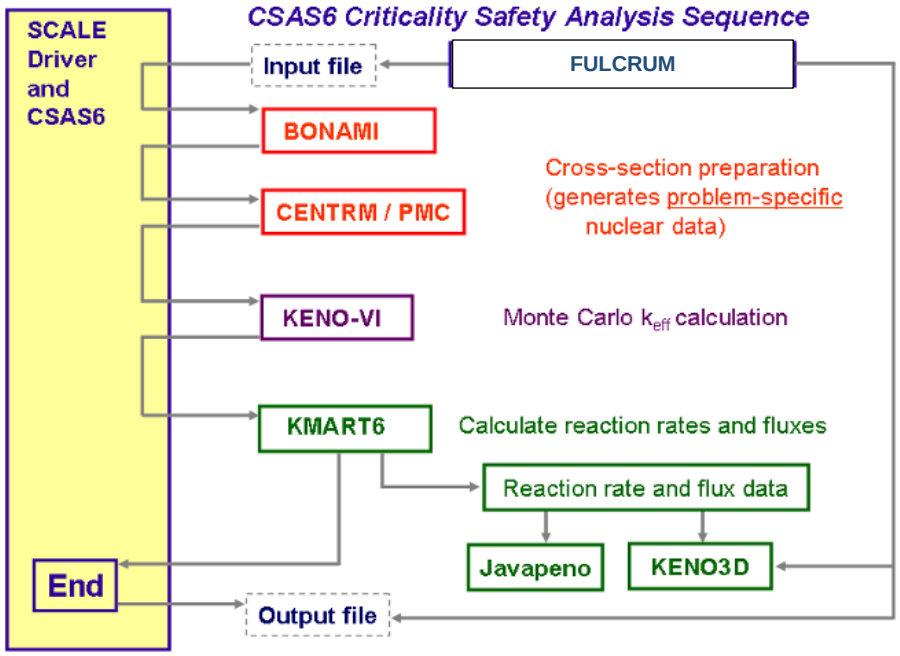

Figure 3.1: Calculation sequence for CSAS6 [15].

The MG energy library (ENDF V7-238) was used in the execution of the KENO-VI module of the SCALE code (the library is given in reference [6]). The use of the MG library invokes CSAS6 to execute XSProc, which processes the MG library to generate cross-sections that include temperature corrections and consider the geometry of the system to be used by KENO-VI module.

Burnup credit was taken using the STARBUCS module of the SCALE code, with its running sequence shown in Figure 3.2. It can be seen in Figure 3.2 that the use of MG invokes XSProc to process cross section library and then run KENO-VI module to calculate k_{eff} of the system.

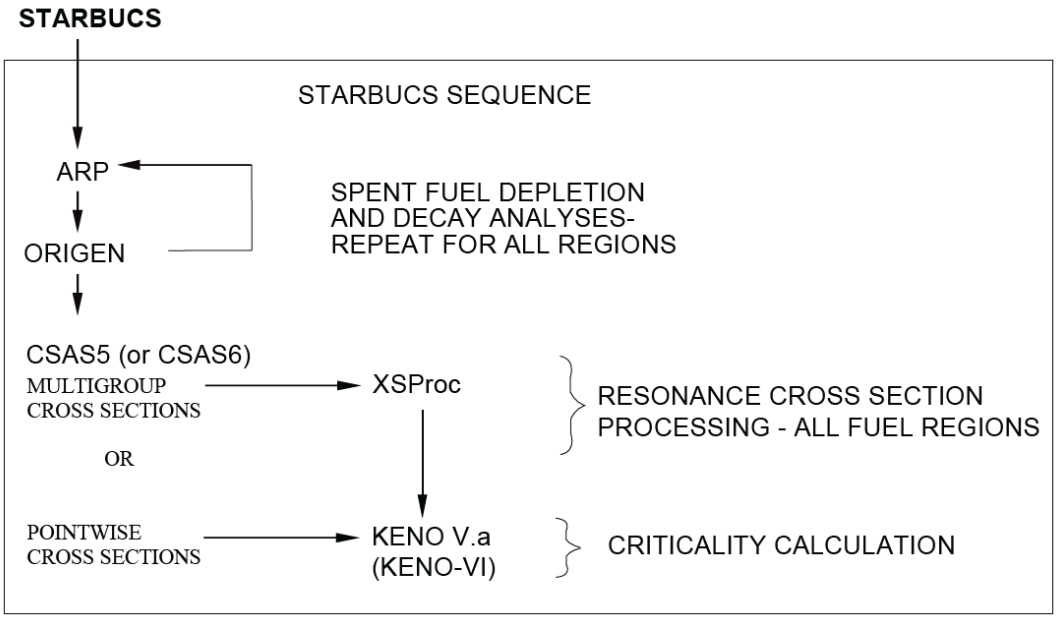

Figure 3.2: STARBUCS running sequence [15].

To accurately model the system, the isotopic correction factor (ICF) recommended by the United States Nuclear Regulatory Commission (U.S. NRC) and utilized in NUREG 6747 [19] was applied for this study. ICFs are defined as adjustments applied to account for variations in the isotopic composition of nuclear materials, which can affect the accuracy of

calculations and measurements [19]. These adjustments were determined based on experimental data and are used to calculate and adjust the value of k_{eff} in the STARBUCS module.

The calculations were conducted on Castor X/28 casks, and the distances between them were varied. The k_{eff} of the SNF storage casks were calculated as a function of varying distances for each nuclide set. Subsequently, the changes in k_{eff} for fresh fuel and different nuclide groups (major actinides, fission products, etc.) per storage space were computed. Finally, Δk was calculated as a function of ΔA, representing the storage saved by taking credit for burnup. It is important to note that this project explored on determining economic benefits based on ΔA relative to the k_{eff} of fresh fuel.

3.2. Calculation techniques and design

This section presents the methodology employed for simulating the k_{eff} of the SNF storage casks, using SCALE code. The simulations involve changing the distance between SNF storage casks and taking credit for fuel burnup by introducing different nuclide groups in the fuel. Furthermore, this section presents a detailed summary of the fuel used, a comprehensive description of Castor X/28 casks, and an in-depth discussion of other input parameters.

3.3.1. Fuel assembly design

At the core of nuclear power, controlled fission reactions occur within fuel assemblies. The fuel assembly used in this research is designed for PWR reactors. These assemblies comprise an arrangement of fuel rods, thimble guides, and an instrument hole, as illustrated in Figure 3.3.

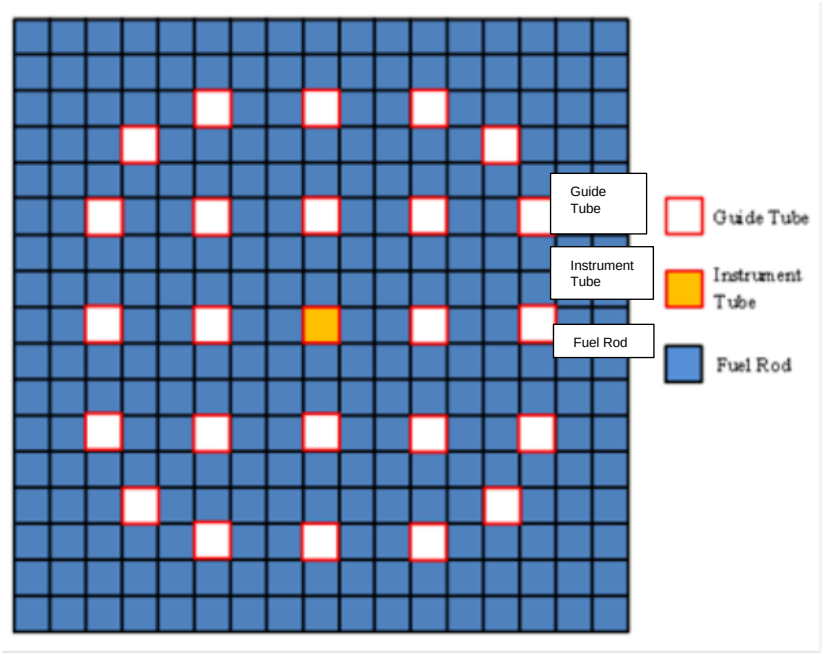

Figure 3.3: A 17x17 Westinghouse Fuel Assembly Showing Fuel Rod, Guide tube and Instrument Tube Arrangement [20].

Additionally, Table 3.1 shows other crucial design properties used as an input for the SCALE code.

Table 3.1: Fuel Assembly Design Description

Parameter	**Value**
Number of fuel rods/assembly	264
Assembly pitch (mm)	215
Array type	17 x 17
Number of instrumentation tubes	1
Number of guide thimbles	24
Fuel rod pitch (mm)	12.60

Parameter	Value
Cladding outer diameter (mm)	9.50
Cladding inner diameter (mm)	8.36
Active height (mm)	3657.6
Overall assembly height (mm)	3867.1
Pellet diameter (mm)	8.192
Pellet height (mm)	13.46
Pellet density (g/cm3)	10.96

In addition to Table 3.1, the following assumptions were made about the fuel assembly used in the calculations:

- Power: 30 MW;
- Burnup: 28 GWd/MTU;
- Fuel Temperature: 296 K (~23 ^{o}C);
- Fuel Density: 10.96 g/cm^{3};
- Moderator Temperature: 296 K (~23 ^{o}C);
- Moderator Density: 1 g/cm^{3};
- Cooling Period: 20 years; and
- Axial Profile: Fuel Assembly is divided into 18 nodes.

It is also assumed that the SNF casks are filled with the moderator, this allows the simulation of accidental water ingress into the casks.

The information provided in Table 3.1, along with the assumptions mentioned above, are necessary input for the SCALE code to calculate the k_{eff} of the SNF casks.

3.3.1.1. Characteristics of fresh fuel and SNF

Fresh fuel is assumed to be un-irradiated and contains the following nuclides characteristics:

- 238U: 96.69 %
- 235U: 3.25 %
- 234U: 0.04 %
- 236U: 0.02%

The characteristics of SNF, depends on the nuclide group that is used to take credit for the burnup and are summarised in Table 2.1.

3.3.1.2. Neutron axial profile of the fuel assembly

To assess the results of the k_{eff} analysis on SNF, nodalization calculations were conducted for the fuel assembly to determine the axial profile of neutron flux distribution. The fuel assembly was discretized into 18 nodes, and the resulting axial profile is illustrated in Figure 3.4.

Since the burnup of the fuel assemblies in the cask and the reactor is uneven, there will be an axial neutron flux profile, indicating unevenness along the length of the cask, as shown in Figure 3.4. This uneven neutron flux profile affects the calculation of k_{eff} at different axial nodes.

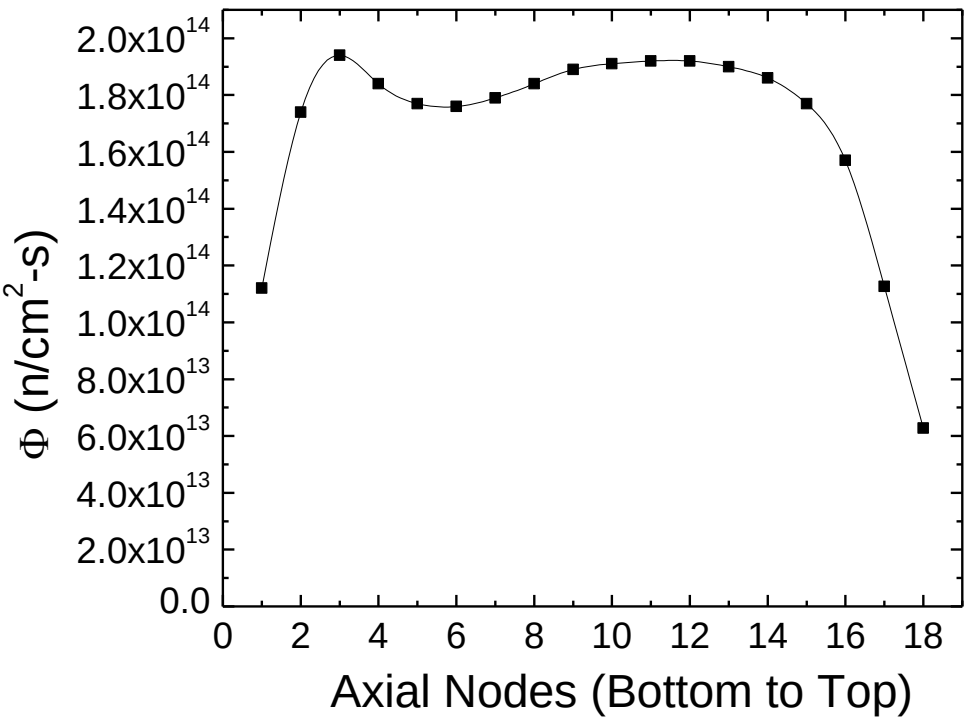

Figure 3.4: Axial profile of the Fuel Assembly taken at fuel burnup of 28 GWD/MTU.

3.3.2. Castor x/28 cask design

As discussed in Section 2.6.3.1, the SNF storage casks used in this study can accommodate 28 fuel assemblies. Figure 3.6 shows CASTOR X/28 cask and how they are currently installed at the Koeberg power station. The SCALE code requires the precise coordinates of the fuel assemblies to accurately determine the k_{eff} of the system. As seen in Figure 2.9 and repeated in Figure *3.5*, the SNF cask has 16 fuel assemblies on the outer layer, and the remaining 12 are placed on the inner core. It must also be noted that the fuel assemblies are surrounded by stainless steel.

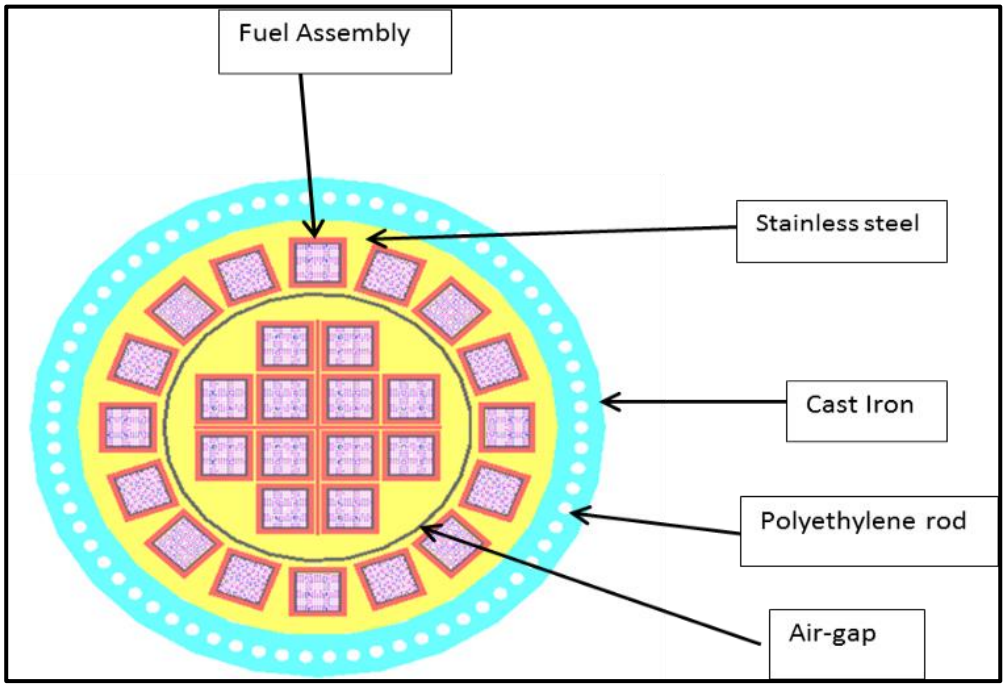

Figure 3.5: A typical spent nuclear fuel cask [6].

For illustration purposes, Figure 3.6 demonstrate how Koeberg SNF casks are stored in horizontal configuration. However, it should be noted that this study focuses solely on vertical SNF storage configurations to analyse the effects of burnup credit.

Figure 3.6: Castor X/28 casks installed horizontally at Koeberg Power Station [31].

The positions of the outer fuel assemblies were determined by dividing 2π by the number of fuel assemblies that are placed on the outer ring, resulting in separation angle of:

$$\theta = \frac{2\pi}{16} = 0.393 \text{ radians} \quad (3.1)$$

This gives the separation angle between adjacent fuel assemblies.

The actual coordinates are calculated by using Equation 3.1 together with distance between the centre of the castor x/28 cask and the middle of the fuel assembly (represents radius, R, for outer fuel assemblies). These coordinates are presented in Table 3.2. Angle θ, also represent the rotation of the fuel assembly about x-y plane.

Table 3.2: Fuel assembly coordinates inside CASTOR X/18 cask

$\boldsymbol{\theta}$ $(\boldsymbol{degrees})$	$\boldsymbol{\theta}$ $(\boldsymbol{radians})$	**x-coordinates (cm)**	**y-coordinates (cm)**
0	0.000	94.90	0.00
22.5	0.393	87.68	36.32
45	0.785	67.10	67.10
67.5	1.178	36.32	87.68
90	1.571	0.00	94.90
112.5	1.963	-36.32	87.68
135	2.356	-67.10	67.10
157.5	2.749	-87.68	36.32

$\theta\ (degrees)$	$\theta\ (radians)$	**x-coordinates (cm)**	**y-coordinates (cm)**
180	3.142	-94.90	0.00
202.5	3.534	-87.68	-36.32
225	3.927	-67.10	-67.10
247.5	4.320	-36.32	-87.68
270	4.712	0.00	-94.90
292.5	5.105	36.32	-87.68
315	5.498	67.10	-67.10
337.5	5.890	87.68	-36.32
360	6.283	94.90	0.00

In an equivalent manner, the remaining 12 fuel assemblies were placed inside the CASTOR X/28, and their x-y coordinates are given in Table 3.3.

Table 3.3: Inner fuel assembly placement inside CASTOR X/28.

Inner Fuel Assemblies	
x (cm)	**y (cm)**
16.25	16.25
46.95	16.25

Inner Fuel Assemblies	
x (cm)	**y (cm)**
16.25	46.95
-16.25	16.25
-16.25	-46.95
-46.95	16.25
-16.25	46.95
-16.25	-16.25
-46.95	-16.25
16.25	-46.95
16.25	-16.25
46.95	-16.25

The coordinates for the 70 polyethylene rods were determined following a methodology like that of the SNF casks, using Equation 3.1. To accommodate the 70 polyethylene rods, the equation was modified, resulting in an angle θ = 0.087266 radians (θ = 5.1429 degrees). The radius from the origin to the centre of the polyethylene rods is 141.7 cm [3]. The computed coordinates are outlined in Appendix B. Figure 3.7 visually portrays the CASTOR X/28 cask arrangement, generated through the SCALE code by using the coordinates given in Table 3.2, Table 3.3 and Appendix B.

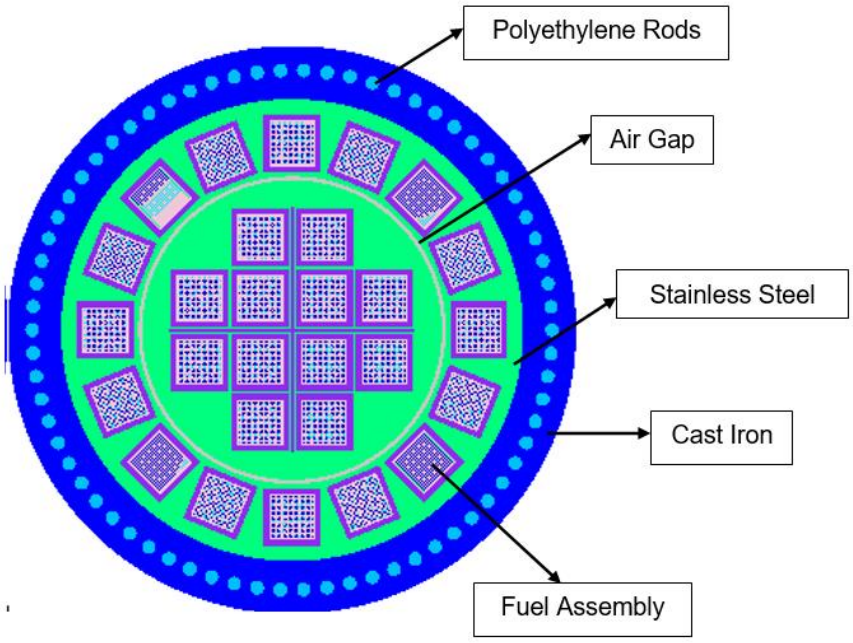

Figure 3.7: Castor x/28 cask generated by SCALE code in this current research project.

The housing, with dimensions of 60 x 23.5 x 8.97 m, was used as a building that could store the SNF casks [3]. In this research, four SNF casks were used and arranged in a 2 x 2 matrix, as depicted in Figure 3.8.

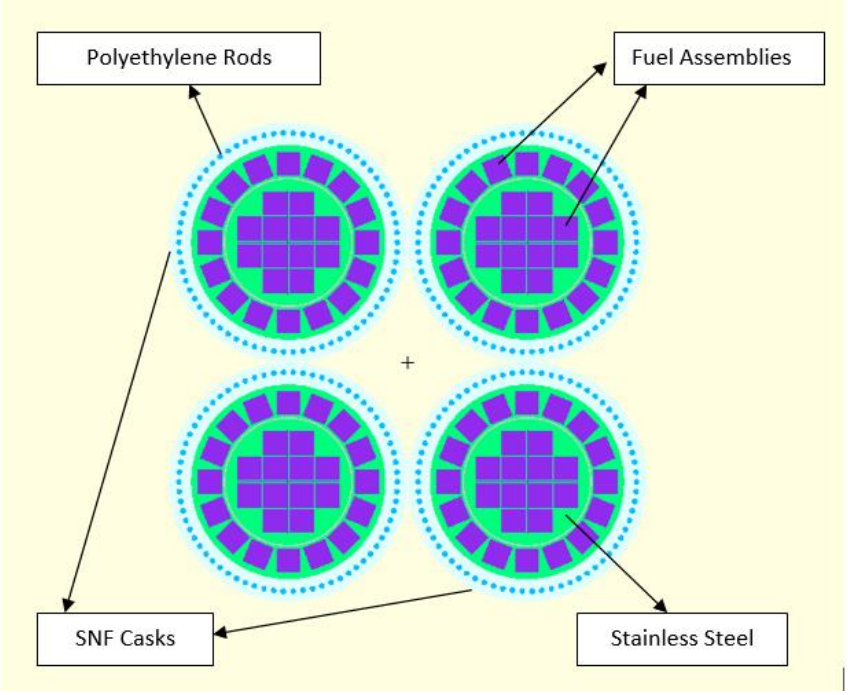

Figure 3.8: A cut through of the SNF casks arranged in 2 x 2 matrix generated by SCALE code in this research project.

The separation between the SNF casks was increased from contact (0 cm) to 200 cm, with intervals of 10 cm each time. At each separation, the k_{eff} of the system was calculated. The area taken up by the SNF casks at each separation was then determined as follows:

$$A = (2d + c) \times (2d + c) = (2d + c)^2 \quad (3.2)$$

Where,

d = 288.6 cm is the diameter of the SNF cask [6].

c is the separation distance (distance between 2 adjacent casks).

The coordinates of the SNF casks were also calculated and used as an input in the SCALE code. These coordinates were determined from the origin of the $x - y$ plane (centre of the housing) to the centre of each SNF cask, considering all distances from 0 cm to 200 cm at intervals of 10 cm.

As an example, the coordinates of the first cask (first quadrant in Figure 3.8) when in contact are given by:

$$x_i = r \tag{3.3}$$

$$y_i = r \tag{3.4}$$

The subsequent coordinates for the first cask are determined by adding half the separation interval (5 cm) to previous x and y values, and that gives the coordinates of:

$$x_{i+1} = x_i + \frac{l}{2} \tag{3.5}$$

$$y_{i+1} = x_i + \frac{l}{2} \tag{3.6}$$

Where,

l is the separation interval = 10 cm (constant value).

r = 144.3 cm is the radius of the SNF cask.

Equations 3.3 to 3.6 are used to calculate the coordinates of the remaining SNF casks at separation distances, ranging from 0 cm to 200 cm, at interval of 10 cm. The outcomes of these calculations are provided in Appendix C for reference.

Chapter 4 : Results and Discussions

This chapter presents and analyses the results obtained from the SCALE code, employed to determine the k_{eff} of SNF storage casks. The SNF casks were arranged in a 2 x 2 matrix pattern, and their separation distances were varied to calculate k_{eff} at different distances for fresh fuel, major actinides, actinides plus minor fission products, and actinides plus principal fission products. The primary purpose of the simulation was to assess the area saved by taking credit for fuel burnup, compared to a scenario with fresh fuel. Calculations for the fresh fuel scenario were conducted using KENO-VI, while simulations for the 'credit for burnup' scenario were performed using the STARBUCS model within the SCALE code.

4.1. Uncertainty of the results

In nuclear engineering, precise calculations are crucial for ensuring the safety, efficiency, and reliability of nuclear systems. However, all calculations inherently carry some level of uncertainty, stemming from various sources such as modelling approximations, measurement errors, and uncertainties in nuclear data as well as statistical uncertainty inherent to Monte Carlo simulations. Understanding and quantifying these uncertainties is essential, particularly in criticality safety analysis, where the accurate prediction of the k_{eff} is vital for preventing unintended criticality events.

In Monte Carlo simulations, the statistical nature of the process introduces uncertainty. This is typically represented by the standard deviation δ of the calculated k_{eff}, reflecting the variability in the simulation results due to the finite number of neutron generations sampled. The average value of calculated k_{eff} is given by Equation 4.1 [1]:

$$\overline{k_{eff}} = \frac{1}{N} \sum_{i=1}^{N} k_{eff,i} \quad (4.1)$$

Where,

N is the total number of neutron generations; and

$k_{eff,i}$ is the effective multiplication factor for the i^{th} neutron generation.

The standard deviation is calculated as a square root of the variance, and it is given by Equation 4.2:

$$\delta = \sqrt{\frac{1}{N}\sum_{i=1}^{N}\left(k_{eff,i} - \overline{k_{eff}}\right)^2} \tag{4.2}$$

The results in both KENO-VI and STARBUCS are presented with this uncertainty as shown in Equation 4.3,

$$k_{eff} \pm \delta \tag{4.3}$$

To test whether changes in k_{eff} are due to statistical uncertainty or are attributable to a physical phenomenon, the two-sample $t-test$ can be applied. This statistical method compares the difference between two k_{eff} values while accounting for their associated uncertainties ($\pm\delta$). The t-value is calculated using Equation 4.4 [32]:

$$t = \frac{|k_{eff,i} - k_{eff,j}|}{\sqrt{\delta_i^2 + \delta_k^2}} \tag{4.4}$$

Here, $k_{eff,i}$ and $k_{eff,j}$ are the two values being compared, and δ_i and δ_j are their respective standard deviations. This formula quantifies the magnitude of the difference relative to the combined uncertainties. If the computed t-value exceeds a critical threshold of $t \geq 2$ (e.g., 95% confidence level), the difference is statistically significant, suggesting a physical cause. Otherwise ($t < 2$), the variation is likely due to statistical noise associated with Monte Carlo method [32]. This test provides a systematic approach to interpreting fluctuations in simulation results and is used to evaluate the significance of observed fluctuations in k_{eff}.

In criticality safety analysis, understanding the uncertainty in the k_{eff} is essential to prevent unintended criticality events. By rigorously analysing and managing uncertainty, the nuclear industry can ensure that its designs and operations remain safe, even in the face of data variability and modelling approximations.

- The final edit of the results was extracted from KENO-VI and STARBUCS for all scenarios discussed in the sections below:
- “k-effective satisfies the chi**2 test for normality at the 95 % level”
- “source convergence tests passed”

4.2. Fresh fuel scenario

In the fresh fuel scenario, the assumption is that the fuel has not undergone any irradiation. The initial composition includes an enrichment of 3.25% for ^{235}U, while the other uranium isotopes are present as follows: ^{238}U at 96.69%, ^{234}U at 0.040%, and ^{236}U at 0.02%. These specifications set the starting conditions for the analysis, forming the basis for comparison with scenarios involving irradiated fuel, which will be discussed in the following sections.

The following methodology was employed to run the KENO-VI module of the SCALE code:

- Set up material compositions: Define the specific material compositions used in the simulation, including the isotopic makeup of the fuel and any other relevant materials in the system.
- Set up fuel dimensions: Input the dimensions of the fuel rods, including length, diameter, and cladding thickness.
- Set up geometry of fuel assembly and casks: Configure the geometric arrangement of the fuel assembly and the storage casks, ensuring accurate spatial representation.

- Separate cask distances and calculate area: Systematically adjust the distances between casks and compute the area occupied at each separation distance.
- Calculate k_{eff}: Determine the k_{eff} for the configuration at each calculated area, for the 4 casks arranged in a 2 x 2 matrix.

The effect of changing the area occupied by the SNF casks on k_{eff} is shown in Figure 4.1 (see Appendix D).

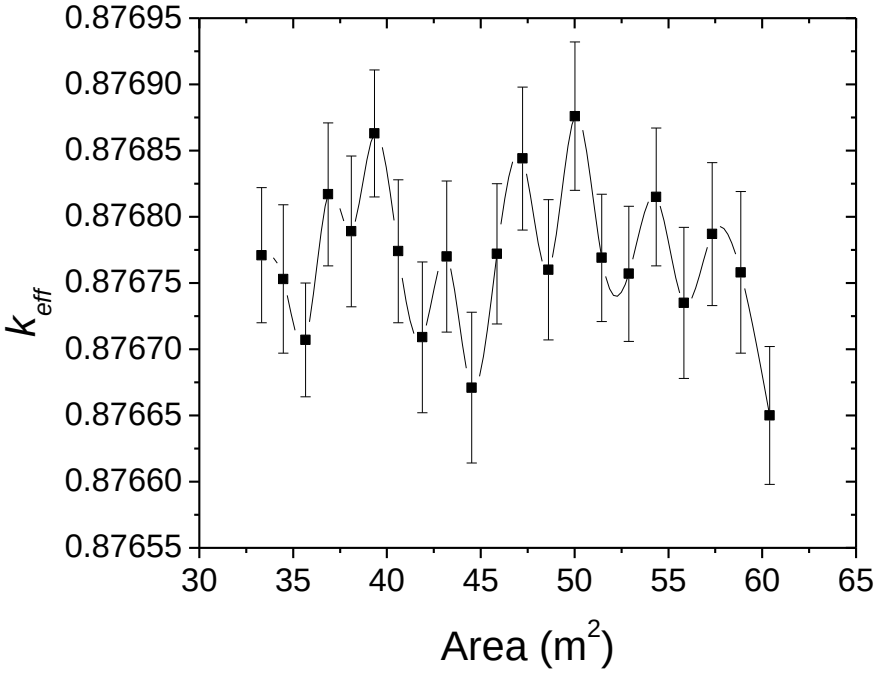

Figure 4.1: k_{eff} as a function of area occupied by the SNF casks for fresh fuel.

The results also show that the k_{eff} of the SNF casks for fresh fuel remains below 0.95, which is the regulatory limit for SNF storage [3]. This suggests that the storage configuration is effective in maintaining subcritical conditions, ensuring the safety of the storage system.

The findings indicate fluctuations in k_{eff} as the area occupied by the SNF casks is increased. To determine whether these fluctuations are caused by

physical factors or statistical noise inherent to the Monte Carlo method, Equation 4.4 is used to calculate t-values, focusing particularly on outliers and using the k_{eff} of the contact area at $33.32\ m^2$ as a reference point. The following pairs are selected based on observations from Figure *4.1*:

Pair number 1 (see Appendix D1):

$$A_1 = 33.32;\ k_{eff,1} = 0.87677;\ \delta_1 = 5.1 \times 10^{-5}$$

$$A_2 = 60.40\ ;\ k_{eff,2} = 0.87665;\ \delta_2 = 5.2 \times 10^{-5}$$

Based on Equation 4.4:

$$t = \frac{|k_{eff,1} - k_{eff,2}|}{\sqrt{\delta_1^2 + \delta_2^2}} = 1.44$$

Pair number 2 (see Appendix D1):

$$A_1 = 33.32;\ k_{eff,1} = 0.87677;\ \delta_1 = 5.1 \times 10^{-5}$$

$$A_2 = 50.01;\ k_{eff,2} = 0.87676;\ \delta_2 = 5.6 \times 10^{-5}$$

Based on Equation 4.4:

$$t = \frac{|k_{eff,1} - k_{eff,2}|}{\sqrt{\delta_1^2 + \delta_2^2}} = 0.15$$

Pair number 3 (see Appendix D1):

$$A_1 = 33.32;\ k_{eff,1} = 0.87677;\ \delta_1 = 5.1 \times 10^{-5}$$

$$A_2 = 39.34;\ k_{eff,2} = 0.87686;\ \delta_2 = 4.8 \times 10^{-5}$$

Based on Equation 4.4:

$$t = \frac{|k_{eff,1} - k_{eff,2}|}{\sqrt{\delta_1^2 + \delta_2^2}} = 1.27$$

Since the t-values of the outliers are less than 2, it can be deduced that all other values are also below this threshold. Therefore, the observed fluctuations in k_{eff} of the system can be attributed to the random nature of

the Monte Carlo method used in the calculations, rather than to physical factors.

4.3. Burnup credit for different nuclide groups

When taking credit for major actinides, actinides plus minor fission products and actinides plus principal fission products, the STARBUCS model of SCALE code was used to determine the k_{eff} of the system.

To calculate the reactivity savings (Δk_{eff}) when accounting for different nuclide groups mentioned above, the k_{eff} of the SNF casks, were computed at various distances (in other words, at different areas occupied by the SNF casks). These values were then subtracted from the k_{eff} of the SNF storage casks calculated for fresh fuel. Δk_{eff} is represented by Equation 4.5:

$$\Delta k_{eff} = k_{eff}(Fresh\ Fuel) - k_{eff}(Burnup\ Credit) \quad (4.5)$$

where,

$k_{eff}(Fresh\ Fuel)$ is the multiplication factor of the fresh fuel calculated at different areas of SNF casks.

$k_{eff}(Burnup\ Credit)$ is the multiplication factor of the SNF casks when taking credit for fuel burnup at different areas.

The method used to calculate $k_{eff}(Burnup\ Credit)$ is similar to the one outlined in Section 4.2, except that the STARBUCS module of the SCALE code is used instead of direct use of KENO-VI. In addition, the relevant nuclides considered in the burnup calculations were defined, and their ICFs were also entered. Other crucial factors included in the calculation are the power produced by the SNF, the burnup of the SNF (28 GWD/MTU), and the cooling period (20 years).

Equation 4.5 was employed to calculate reactivity savings for each of the various nuclide groups investigated in this study. The following sections will delve into detailed discussions on the reactivity savings for each specific nuclide group.

4.3.1. Taking credit for major actinides

This section presents the results for taking credit for major actinides within the SNF casks. Figure 4.2 depicts the relationship between k_{eff} and the area occupied by four SNF casks arranged in a 2 x 2 matrix.

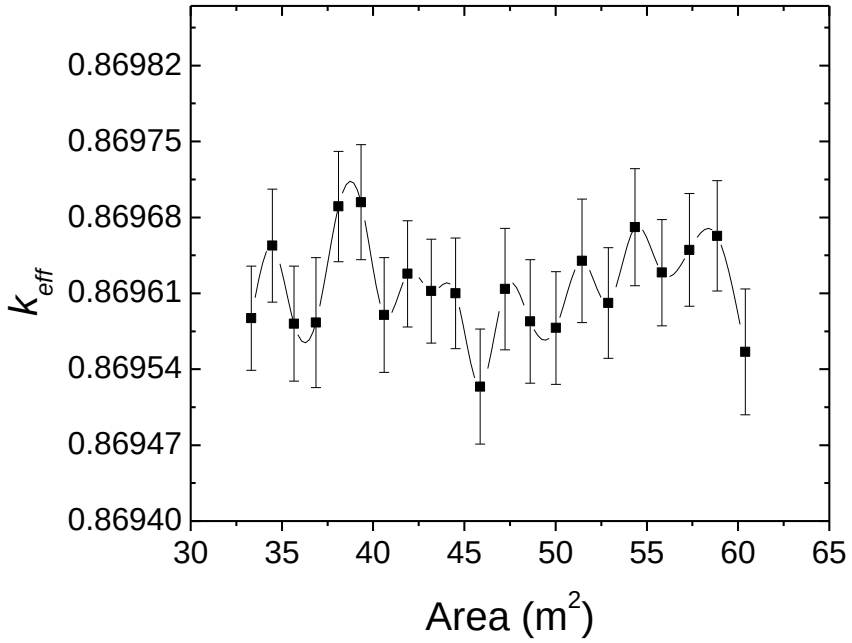

Figure 4.2: Effect of changing area on k_{eff} when taking credit for burnup of major actinides only.

The results indicate that as the area occupied by the SNF casks increases, the system's k_{eff} fluctuates. To assess whether these fluctuations are caused by physical factors or statistical noise inherent to the Monte Carlo method, Equation 4.4 is applied to compute the t-values, with particular focus on outliers, using k_{eff} of contact area as a reference point. The

following pairs of outliers are selected based on observations from Figure *4.4*:

Pair number 1 (see Appendix D1):

$$A_1 = 33.32;\ k_{eff,1} = 0.869587;\ \delta_1 = 4.8 \times 10^{-5}$$

$$A_2 = 39.34;\ \ k_{eff,2} = 0.869643;\ \delta_2 = 5.3 \times 10^{-5}$$

Based on Equation 4.4:

$$t = \frac{|k_{eff,1} - k_{eff,2}|}{\sqrt{\delta_1^2 + \delta_2^2}} = 0.783159$$

Pair number 2 (see Appendix D1):

$$A_1 = 33.32;\ k_{eff,1} = 0.869587;\ \delta_1 = 4.8 \times 10^{-5}$$

$$A_2 = 39.34;\ \ k_{eff,2} = 0.869524;\ \delta_2 = 5.3 \times 10^{-5}$$

Based on Equation 4.4:

$$t = \frac{|k_{eff,1} - k_{eff,2}|}{\sqrt{\delta_1^2 + \delta_2^2}} = 0.881054$$

Pair number 3 (see Appendix D1):

$$A_1 = 33.32;\ k_{eff,1} = 0.869587;\ \delta_1 = 4.8 \times 10^{-5}$$

$$A_2 = 39.34;\ \ k_{eff,2} = 0.869556;\ \delta_2 = 5.8 \times 10^{-5}$$

Based on Equation 4.4:

$$t = \frac{|k_{eff,1} - k_{eff,2}|}{\sqrt{\delta_1^2 + \delta_2^2}} = 0.411762$$

Since the t-values of the outliers are less than 2, it can be deduced that all other values are also below this threshold. Therefore, the observed fluctuations in k_{eff} of the system can be attributed to the random nature of the Monte Carlo method used in the calculations, rather than to physical factors.

The reactivity savings realized by taking credit for major actinides is represented by Δk_{eff} and shown in Equation 4.4, the reactivity savings is plotted against the area occupied by the SNF storage casks, as illustrated in Figure 4.3.

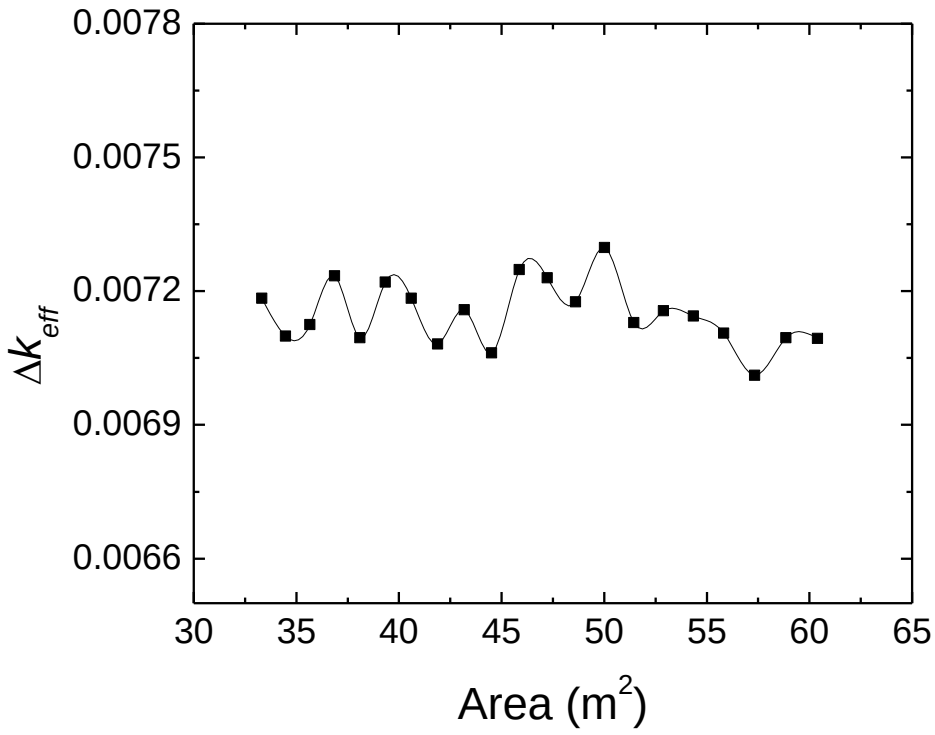

Figure 4.3: Reactivity savings when taking credit for major actinides only.

The results show that as the area occupied by the SNF casks increases, the resulting savings in reactivity fluctuate. These fluctuations are attributed to statistical uncertainties inherent in the Monte Carlo simulations rather than the physical separation of the casks. Overall, the results demonstrate that the k_{eff} of the system decreases when taking credit for major actinides compared to the fresh fuel scenario. This reduction in k_{eff} is primarily due to the presence of neutron-absorbing actinides when taking burnup credit.

4.3.2. Actinides plus principal fission products

Similar to Section 4.3.1, but now taking credit for actinides plus principal fission products, the k_{eff} of the SNF casks was calculated for different areas occupied by the casks. The results are presented in Figure 4.4 (see Appendix D).

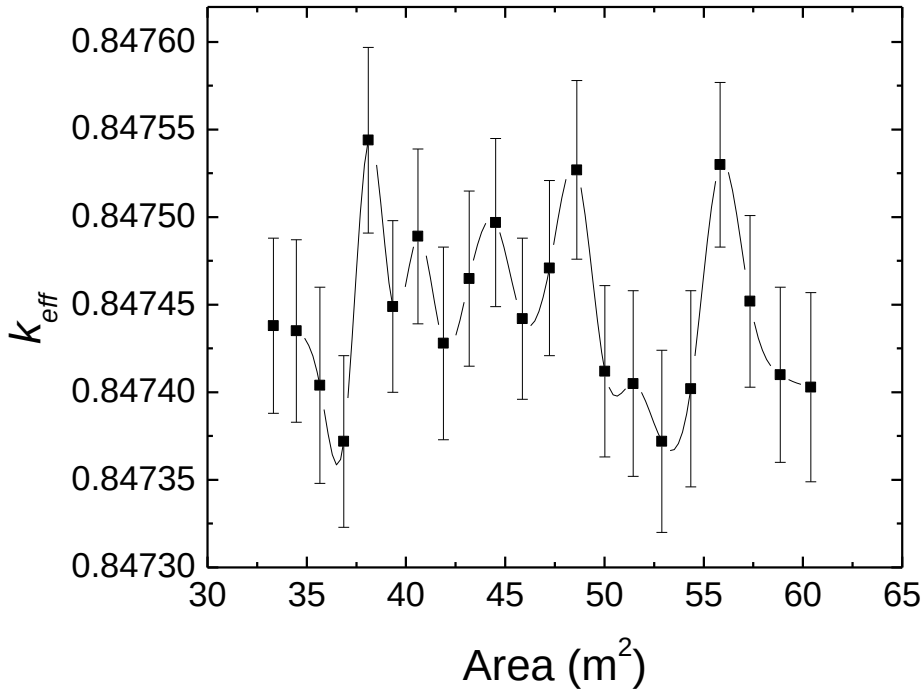

Figure 4.4: Effect of area on k_{eff} when taking credit for burnup on actinides plus principal fission products.

The results of taking credit for actinides plus principal fission products shows fluctuations in k_{eff} when the area occupied by the SNF casks is increased.

Pair number 1 (see Appendix D1):

$$A_1 = 33.32;\ k_{eff,1} = 0.847438;\ \delta_1 = 5.0 \times 10^{-5}$$

$$A_2 = 39.34;\ k_{eff,2} = 0.847530;\ \delta_2 = 4.7 \times 10^{-5}$$

Based on Equation 4.4:

$$t = \frac{|k_{eff,1} - k_{eff,2}|}{\sqrt{\delta_1^2 + \delta_2^2}} = 1.34067$$

Pair number 2 (see Appendix D1):

$$A_1 = 33.32;\ k_{eff,1} = 0.847438;\ \delta_1 = 5.0 \times 10^{-5}$$

$$A_2 = 38.09;\ \ k_{eff,2} = 0.847544;\ \delta_2 = 5.3 \times 10^{-5}$$

Based on Equation 4.4:

$$t = \frac{|k_{eff,1} - k_{eff,2}|}{\sqrt{\delta_1^2 + \delta_2^2}} = 1.45479$$

Pair number 3 (see Appendix D1):

$$A_1 = 33.32;\ k_{eff,1} = 0.847438;\ \delta_1 = 5.0 \times 10^{-5}$$

$$A_2 = 48.61;\ \ k_{eff,2} = 0.847527;\ \delta_2 = 5.1 \times 10^{-5}$$

Based on Equation 4.4:

$$t = \frac{|k_{eff,1} - k_{eff,2}|}{\sqrt{\delta_1^2 + \delta_2^2}} = 1.24613$$

Based on the t-values calculated above, it can be concluded that these fluctuations are not caused by the physical separation of the SNF casks but are instead due to the statistical uncertainties inherent in the Monte Carlo method.

The results of taking credit for major actinides versus actinides plus principal fission products show similar patterns of k_{eff} fluctuations with varying areas occupied by the SNF casks. Deducing from the t-values calculated above, it can be concluded that the fluctuations are not due to physical separation of the SNF casks, rather they are due statistical uncertainty inherent to Monto Carlo method. However, the overall k_{eff} is lower when credit is taken for actinides plus principal fission products.

This can be explained by the additional neutron absorption provided by the principal fission products, which function as neutron poisons and further

reduce the neutron population capable of sustaining the chain reaction. While both scenarios exhibit fluctuations due to factors such as neutron streaming, spatial heterogeneity, neutron reflection, and geometric changes, the presence of principal fission products adds an extra layer of neutron absorption, thereby enhancing the reactivity savings and resulting in a lower overall k_{eff}.

The reactivity savings was calculated using Equation 4.4 and the results are shown in Figure 4.5, respectively.

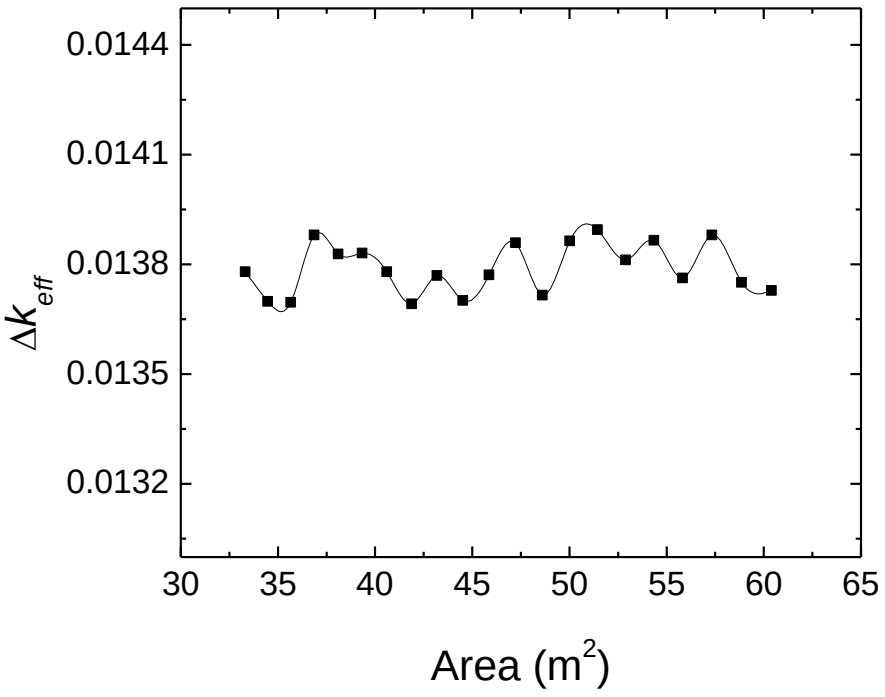

Figure 4.5: Reactivity savings when taking credit for actinides plus principal fission products.

The overall reactivity savings when taking credit for actinides plus principal fission products is higher than that when taking credit for major actinides only, as shown in Figure 4.3 and Figure 4.5.

4.3.3. Actinides Plus Minor Fission Product

The identical calculations were replicated to account for actinides plus minor fission products. The results are shown in Figure 4.6 (see Appendix D).

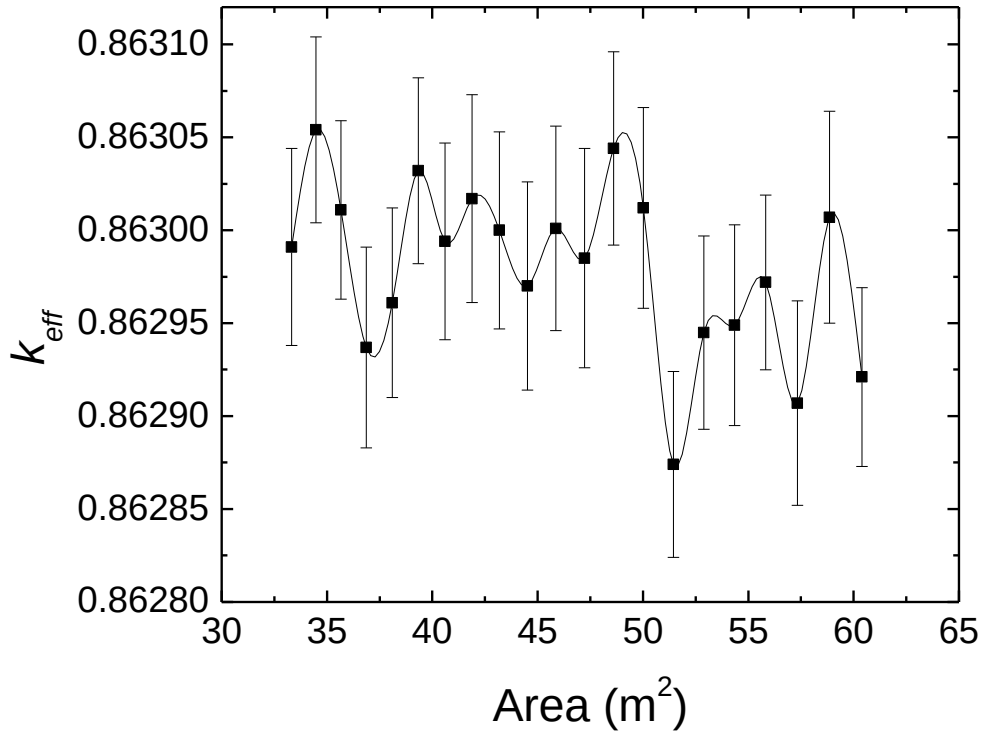

Figure 4.6: Effect of area on k_{eff} when taking credit for burnup on actinides + minor fission products.

Pair number 1 (see Appendix D1):

$$A_1 = 33.32;\ k_{eff,1} = 0.862991;\ \delta_1 = 5.3 \times 10^{-5}$$

$$A_2 = 34.48;\ \ k_{eff,2} = 0.863054;\ \delta_2 = 5.0 \times 10^{-5}$$

Based on Equation 4.4:

$$t = \frac{|k_{eff,1} - k_{eff,2}|}{\sqrt{\delta_1^2 + \delta_2^2}} = 0.86464$$

Pair number 2 (see Appendix D1):

$$A_1 = 33.32;\ k_{eff,1} = 0.862991;\ \delta_1 = 5.3 \times 10^{-5}$$

$$A_2 = 34.48;\ \ k_{eff,2} = 0.862874;\ \delta_2 = 5.0 \times 10^{-5}$$

Based on Equation 4.4:

$$t = \frac{|k_{eff,1} - k_{eff,2}|}{\sqrt{\delta_1^2 + \delta_2^2}} = 1.65756$$

Pair number 2 (see Appendix D1):

$$A_1 = 33.32;\ k_{eff,1} = 0.862991;\ \delta_1 = 5.3 \times 10^{-5}$$

$$A_2 = 48.61;\ \ k_{eff,2} = 0.863044;\ \delta_2 = 5.2 \times 10^{-5}$$

Based on Equation 4.4:

$$t = \frac{|k_{eff,1} - k_{eff,2}|}{\sqrt{\delta_1^2 + \delta_2^2}} = 0.71381$$

The results show that the overall k_{eff} when taking credit for actinides plus minor fission products falls between the k_{eff} values obtained when taking credit for major actinides only and actinides plus principal fission products. This indicates that minor fission products contribute to neutron absorption, though less significantly than principal fission products. The presence of minor fission products adds to the overall neutron absorption capacity, leading to additional reactivity savings compared to when taking credit for major actinides only, but not as much as when taking credit for actinides plus principal fission products.

The overall trend shows that taking credit for actinides plus minor fission products provides intermediate reactivity savings, but not to the extent achieved when taking credit for actinides plus principal fission products. Once again, Equation 4.4 was applied to compute Δk_{eff} when taking credit for actinides plus minor fission products, with the results depicted in Figure 4.7.

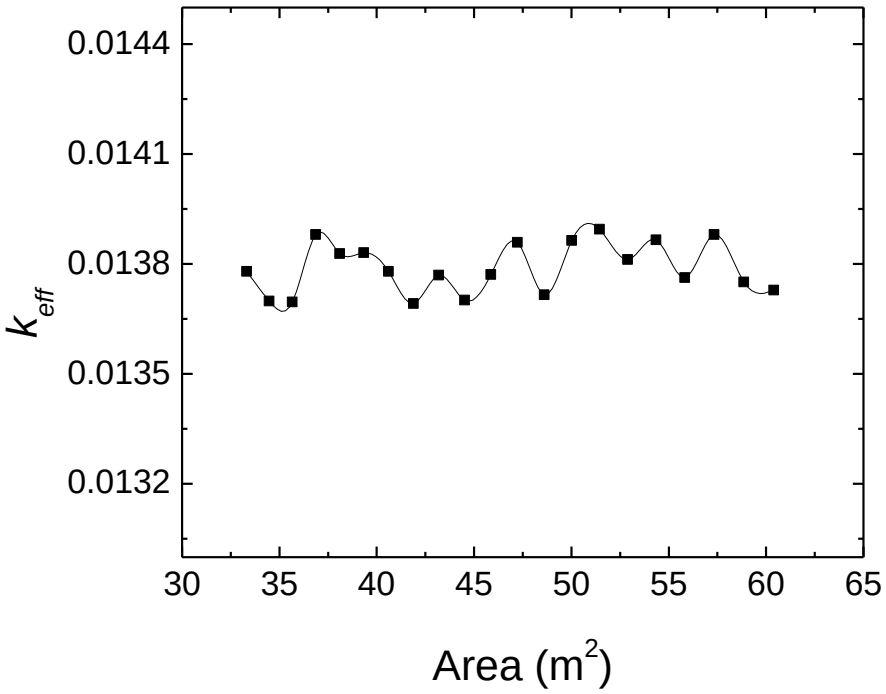

Figure 4.7: Reactivity savings when taking credit for actinides plus minor fission products.

4.4. Determining storage space saving

Building upon the preceding discussions on reactivity savings when taking credit for burnup in various nuclide groups compared to fresh fuel, this section delves into the assessment of ΔA. This analysis aims to quantify the reduction in storage area achieved through taking credit for burnup, using fresh fuel as a reference point.

As mentioned before, the reactivity savings for different nuclides groups is given in Equation 4.4. To determine the space saved, denoted by ΔA, the reference area was taken when the SNF casks were in contact (0 cm separation) and is given in Equation 4.5:

$$\Delta A = A_0 - A_i \tag{4.5}$$

Where,

A_0 is the area of the SNF casks when they are in contact with each other.

A_i is the area at different separations (at 10 cm intervals, ranging from 0 cm to 200 cm).

The calculations of k_{eff} to determine the space savings were performed for major actinides, actinides plus principal fission products, and actinides plus minor fission products with fresh fuel serving as a reference point. The results illustrated in Figure 4.8 (see Appendix E)

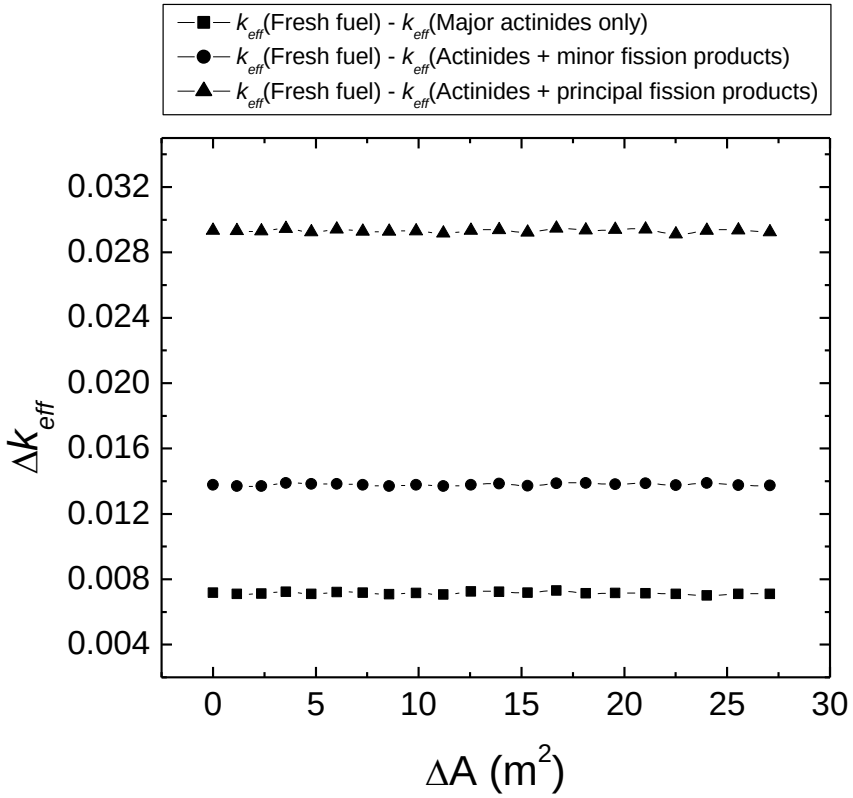

Figure 4.8: Space saved due to taking credit for major actinides, actinides plus principal fission products and actinides plus minor fission products.

Major actinides plus principal fission products have a higher number of nuclide than that of major actinides only and actinides plus minor fission products. When the number of nuclides is increased, they come with their own absorption cross section, some of which are high e.g., ^{155}Gd. The total

absorption cross section for actinides plus principal fission products will therefore be higher than for the other two nuclide sets, consequently the actinides plus principal fission products will have a greater decrease in k_{eff}. Since actinides plus principal fission products have lower k_{eff},, subtracting their k_{eff} from that of the fresh fuel will result in larger differences, as shown in Figure 4.8. It was found that the changes in the storage area did not produce any change in k_{eff}; the differences observed were due to statistical noise. Since the change in area effectively corresponds to a change in the distance between fuel assemblies, one can conclude that the distance between fuel assemblies can be reduced to as much as 0 cm, as shown in this study, without affecting the value of k_{eff}. This can allow the storage area to be reduced.

The k_{eff} of the system depends on other factors such as fuel temperature, fuel density, moderator temperature and moderator density in the SNF casks. The effects of these factors are discussed in the following section.

4.5. Effect of fuel temperature and fuel density on k_{eff}.

In this section, the effects of fuel temperature and fuel density on k_{eff} of the SNF is presented for fresh fuel. The results are shown in Table 4.1.

Table 4.1: Effects of Fuel and Moderator Properties on k_{eff}.

Fuel Density		
Density, ρ (g/cm³)	k_{eff}	$\pm\delta$
8.96	0.848747	0.000058
9.96	0.863789	0.000048
10.96	0.876771	0.000051
11.96	0.887796	0.000050
12.96	0.897471	0.000056
Fuel Temperature		
Temperature, T (K)	k_{eff}	$\pm\delta$
298	0.876578	0.00005
308	0.876291	0.000054
318	0.875874	0.000056
328	0.875629	0.00005
338	0.87529	0.000055
Moderator Density		
Density (g/cm³)	k_{eff}	$\pm\delta$
0.6	0.701048	0.000046
0.7	0.755035	0.000055
0.8	0.801638	0.000051
0.9	0.842255	0.000054
1	0.907914	0.000051
1.1	0.934417	0.000053
Moderator Temperature		
Temperature, T (K)	k_{eff}	$\pm\delta$
298	0.876561	0.000051
308	0.87584	0.000056
318	0.875136	0.000056
328	0.874595	0.000049
338	0.873781	0.000049

4.5.1. Effect of fuel temperature on k_{eff}.

The k_{eff} for the fresh fuel was calculated to determine the effect of fuel temperature on the system. The fuel temperature was varied from 298 K (~26 degrees Celsius) to 338 K (~65 degrees Celsius) at intervals of 10 K.

At each interval, the k_{eff} of the system (SNF casks) was calculated using KENO-VI. The results are shown in Table 4.1 and Figure 4.9.

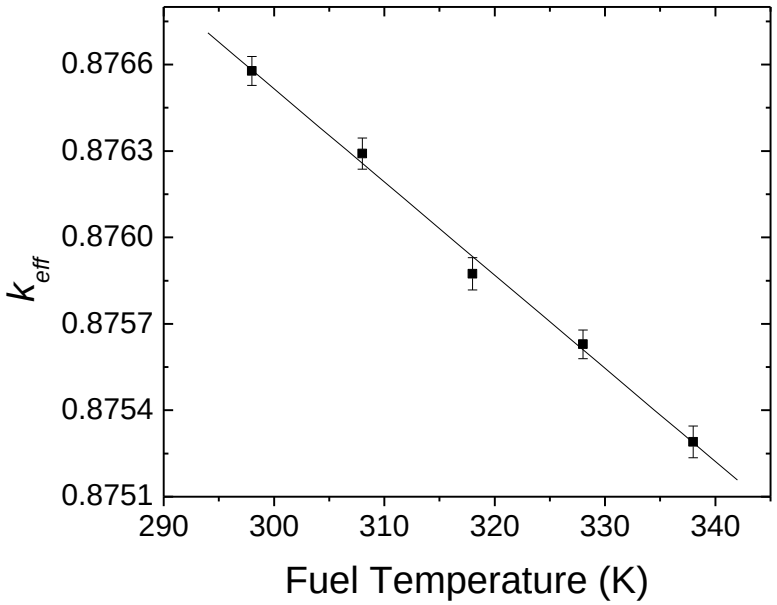

Figure 4.9: Effect of increasing fuel temperature on k_{eff}.

The decrease in k_{eff} with increasing fuel temperature in SNF casks can be attributed to Doppler broadening [4]. As the temperature rises, Doppler broadening enhances neutron absorption in the fuel, particularly in resonance regions of fissile and fertile isotopes, leading to a decrease in k_{eff}, as shown in Figure 4.9. This negative temperature feedback effect enhances the inherent safety of SNF storage by reducing reactivity as temperatures increase.

4.5.2. Fuel density

In this section, the effect of fuel density on k_{eff} for fresh fuel in SNF casks is determined. The fuel density was varied from 9.96 g/cm³ to 12.9 g/cm³ at intervals of 1 g/cm³. This range includes variations of both above and below the standard fuel density of 10.96 g/cm³ to observe the effects of increasing and decreasing fuel density. At each interval, k_{eff} of the casks was calculated using KENO-VI. The results, presented in Table 4.1 and Figure

4.10, provide insights into how fuel density influences the criticality of SNF casks, which is crucial for optimizing storage configurations and ensuring safety.

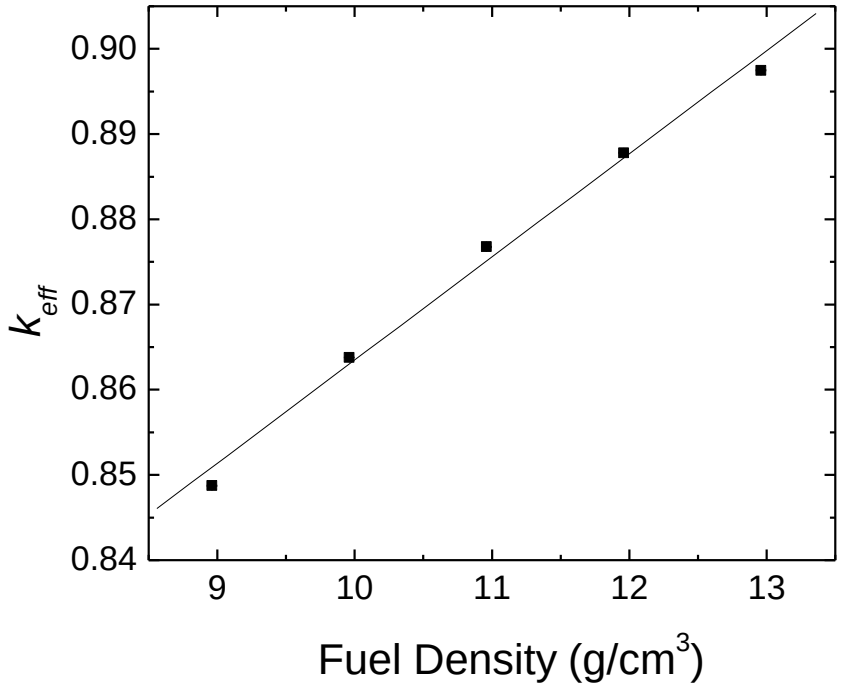

Figure 4.10: Effect of Fuel Density on k_{eff}.

The results show that as the fuel density increases, the k_{eff} of the SNF casks also increases. This phenomenon is due to the following factors:

- When fuel density increases, the concentration of fissile materials such as ^{235}U rises, enhancing k_{eff}, while the increase in fertile material such as ^{238}U tends to reduce k_{eff} through neutron capture. The net effect of these competing processes results in an increase in k_{eff} due to the dominance of fissile material contributions and the eventual production of additional fissile isotopes such as ^{239}Pu from ^{238}U [4].
- The likelihood of neutron interactions with fissile nuclei rises significantly due to closer proximity of fuel nuclei [4].

4.6. Effect of moderator temperature and moderator density on k_{eff}.

In this section, the effects of moderator temperature and moderator density on k_{eff} are presented. These factors are crucial for understanding how changes in moderator properties influence the criticality of the system. The results offer insights into optimizing SNF cask storage.

4.6.1. Moderator temperature

The k_{eff} for the fresh fuel was calculated to investigate the effect of moderator temperature on the SNF cask system. The moderator temperature was varied from 298 K (~26 degrees Celsius) to 338 K (~65 degrees Celsius) at 10 K intervals. This temperature range was selected to cover the effects of temperature on storage conditions. At each interval, the k_{eff} of the SNF cask system was computed using KENO-VI. The results are depicted in Table 4.1 and Figure 4.11.

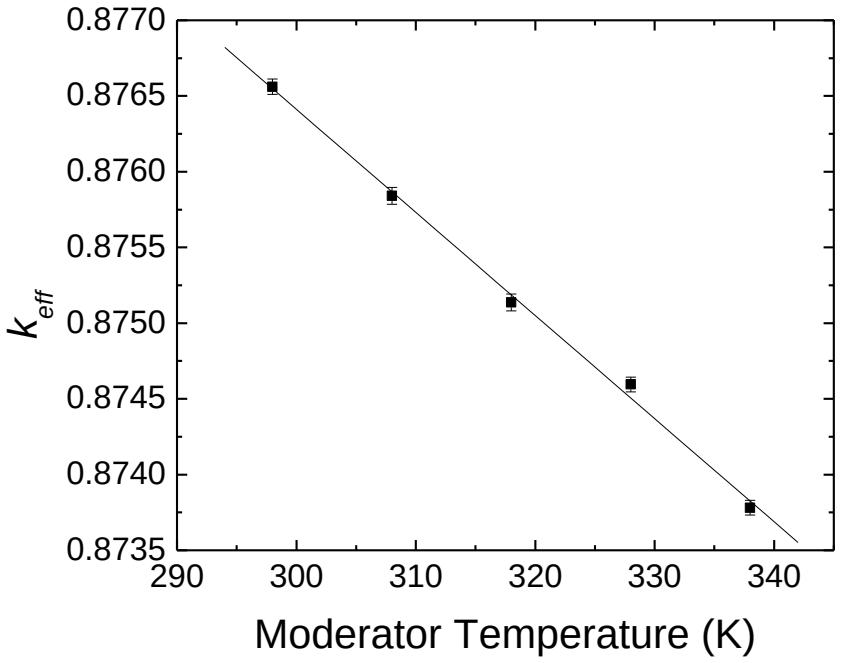

Figure 4.11: Effect of moderator temperature on k_{eff}.

The decrease in k_{eff} with increasing moderator temperature can be attributed to several factors (see Figure 4.11). As the moderator temperature rises, the increased thermal motion of water molecules reduces the effectiveness of neutron thermalization, leading to fewer neutrons being slowed to the thermal energy range required for fission. This effect is influenced primarily by the S(α,β) scattering of neutrons in water. Additionally, while neutron scattering increases with temperature, these neutrons are less likely to thermalize effectively due to competition between neutron scattering and absorption in water. Furthermore, at higher moderator temperatures, the reduction in moderator density further decreases the system's k_{eff} (see Section 4.6.2 below) [4, 5].

4.6.2. Moderator density

The k_{eff} for the fresh fuel was calculated to assess the impact of moderator density on the system. Moderator density was varied from 0.6 g/cm³ to 1 g/cm³ at intervals of 0.1 g/cm³. These variations were intended to determine the effects of decreasing moderator density on the k_{eff} of the system. At each interval, the k_{eff} of the casks was calculated using KENO-VI, and the results are presented in Table 4.1 and Figure 4.12.

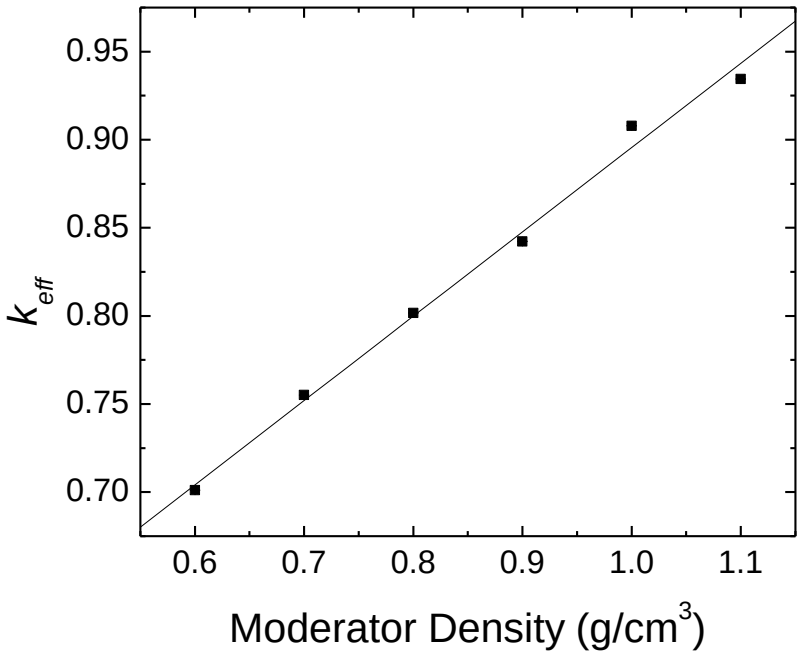

Figure 4.12: Effect of Moderator **Density on k_{eff}.**

The results show that the k_{eff} increases as the density of the moderator increases. The observed increase in k_{eff} is attributed to the greater probability of neutron moderation and reduced neutron leakage as moderator density increases, thereby enhancing neutron thermalization and improving the overall k_{eff} of the system [4, 5].

4.7. Summary of the results

It was concluded that changing the area of the SNF casks for fresh fuel results in fluctuations in the k_{eff} of the system. These fluctuations were determined to be due to the statistical uncertainties inherent in Monte Carlo calculations. Similar fluctuations were observed when accounting for fuel burnup across all considered nuclide groups: major actinides, actinides plus minor fission products, and actinides plus principal fission products. Therefore, it can be concluded that changing the area of the SNF casks does not affect the k_{eff} of the system.

The study also demonstrates that a decrease in the k_{eff} when taking credit for various nuclide groups compared to the baseline k_{eff} of the fresh fuel. Whether taking credit for major actinides, actinides plus principal fission products, or actinides plus minor fission products, the application of Equation 4.4 consistently reveals reactivity savings. This indicates that taking credit for fuel burnup of different nuclide groups results in reduced k_{eff}, emphasizing the impact of fuel depletion and the associated changes in nuclear composition on the SNF. The graphical representations in Figure 4.3, Figure 4.5 and Figure 4.7 provide a visual summary of these observed trends. It is noteworthy that a greater reactivity saving is observed when taking credit for actinides plus principal fission products, in comparison to scenarios where credit is taken for actinides plus minor fission products (which has higher savings than major actinides only) and major actinides only.

It is concluded that increasing the area of SNF casks does not affect k_{eff}. However, it is noted that for a given area, accounting for burnup results in a lower k_{eff} compared to fresh fuel. Among the considered nuclide groups, actinides and principal fission products contribute the most to reactivity savings (Figure 4.8). This suggests that, from the standpoint of optimizing space utilization, taking credit for actinides plus principal fission products offers the most substantial benefits.

Chapter 5 : Sensitivity Analysis

Sensitivity analysis is a valuable method for investigating the impact of variations in the distance between the SNF casks, treated as the independent variable (*A*), on the k_{eff}, considered as the dependent variable. This analysis seeks to identify the minimum change in the separation distance necessary to induce the minimum change in k_{eff}. By systematically exploring these relationships, sensitivity analysis provides crucial insights into how alterations in SNF cask spacing influence the criticality of the system, guiding the optimization of safety and efficiency in nuclear configurations.

In this chapter, the sensitivity exhibited by different nuclide groups (e.g., major nuclides) to changes in separation distance is explored. The objective is to discern which nuclide group is more susceptible to variations in spacing. In this investigation, the goal is to uncover valuable insights into the impact of different nuclide groups on the SNF cask system's response to changes in separation distance (Section 5.1).

Section 5.2 delves into a sensitivity analysis, exploring the impact of both fuel temperature and moderator density on the k_{eff} for major actinides.

5.1. Sensitivity analysis of different nuclide groups

This section explores the sensitivity analysis of various nuclide groups. The analysis involved selecting a nominal area for SNF casks at a separation of 100 cm, corresponding to an area of 45.8600 m² (see Table 5.1). Sensitivity was assessed by varying the area by ±1% and ±5% [21]. For each area, k_{eff} was calculated, and normalized values were computed. This comprehensive approach was repeated for all nuclide groups considered in this study.

Table 5.1: Sensitivity of k_{eff} as a function of SNF casks area.

Fresh Fuel					
Percentage Change	**Area, $A\ (m^2)$**	A/A_{nom}	k_{eff}	k/k_{nom}	$\pm\delta$
Nominal Area -5%	43.57	0.950	0.876786	1.010448	0.000055
Nominal Area -1%	45.40	0.99	0.876855	1.010528	0.000054
Nominal Area	45.86	1.00	0.867720	1	0.000053
Nominal Area +1%	46.32	1.00994	0.876711	1.010362	0.000056
Nominal Area +5%	48.15	1.05	0.876710	1.01036	0.000053
Major Actinides					
Percentage Change	**Area, $A\ (m^2)$**	A/A_{nom}	k_{eff}	k/k_{nom}	$\pm\delta$
Nominal Area -5%	43.567	0.95	0.869624	1.000115	0.000055
Nominal Area -1%	45.4014	0.99	0.869613	1.000102	0.000050
Nominal Area	45.86	1.00	0.869524	1.00	0.000053
Nominal Area +1%	46.3158	1.00994	0.869545	1.000024	0.000055
Nominal Area +5%	48.153	1.05	0.869588	1.000074	0.000058
Actinides + Principal Fission Products					
Percentage Change	**Area, $A\ (m^2)$**	A/A_{nom}	k_{eff}	k/k_{nom}	$\pm\delta$
Nominal Area -5%	43.567	0.95	0.847398	0.999948	0.000049
Nominal Area -1%	45.4014	0.99	0.847419	0.999973	0.000051
Nominal Area	45.86	1.00	0.847442	1.00	0.000046
Nominal Area +1%	46.3158	1.00994	0.847428	0.999983	0.000050
Nominal Area +5%	48.153	1.05	0.847454	1.000014	0.000054
Actinides + Minor Fission Products					
Percentage Change	**Area, $A\ (m^2)$**	A/A_{nom}	k_{eff}	k/k_{nom}	$\pm\delta$
Nominal Area -5%	43.567	0.95	0.862923	0.99991	0.000054
Nominal Area -1%	45.4014	0.99	0.862943	0.999933	0.000053
Nominal Area	45.86	1.00	0.863001	1.00	0.000055
Nominal Area +1%	46.3158	1.00994	0.862922	0.999908	0.000050
Nominal Area +5%	48.153	1.05	0.862889	0.99987	0.000054

The normalised area was calculated by dividing each point calculated at areas of $\pm 1\%$ and $\pm 5\%$ of nominal value by nominal area of 45.86 m^2 (see Table 5.1 for normalised values). Similarly, the corresponding multiplication factors were divided by the nominal values of k_{eff} (Figure 5.1) for each nuclide group [21].

5.1.1. Sensitivity of fresh fuel

The normalised values for both the area and k_{eff} of fresh fuel are presented in Figure 5.1 and summarized in Table 5.1.

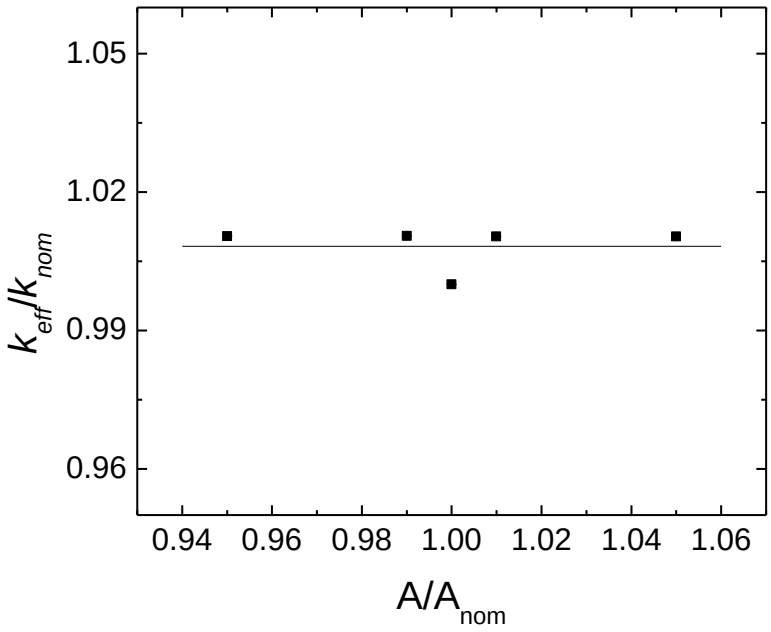

Figure 5.1: Sensitivity analysis of the fresh fuel.

The relationship between the normalised area A and the normalised k_{eff} is described by Equation 5.1, as illustrated in Figure 5.1.

$$k_{eff} = 1.00818 + 6.73 \times 10^{-5} A \tag{5.1}$$

The sensitivity coefficient ($s_{fresh\ fuel}$) is derived by calculating the slope of Equation 5.1 (i.e., first derivative), resulting in Equation 5.2 [22].

$$s_{fresh\ fuel} = \frac{dk_{eff}}{dA} = \frac{d}{dA}(1.00818 + 6.73 \times 10^{-5} A) \tag{5.2}$$

$$s_{fresh\ fuel} = \left.\frac{dk_{eff}}{dA}\right|_{A/A_{nom}=1} = 6.73 \times 10^{-5}$$

This yields a sensitivity coefficient for fresh fuel of $s_{fresh\ fuel} = 6.73 \times 10^{-5}$ when evaluated at the normalised nominal area. The magnitude of $s_{fresh\ fuel}$ is relatively small, suggesting that the system's response is not highly sensitive to changes in the area of SNF casks, as seen in Figure 5.1. The small sensitivity coefficient indicates that, at the nominal area, the k_{eff} of the SNF casks for fresh fuel is slightly increasing. It can be concluded that slight changes in area of the SNF casks does not change the k_{eff} of the system.

5.1.2. Sensitivity analysis of major actinides

In a similar fashion, for major actinides, the normalised values of both the area and k_{eff} were computed and shown in Figure 5.2 (also see Table 5.1 for normalised values).

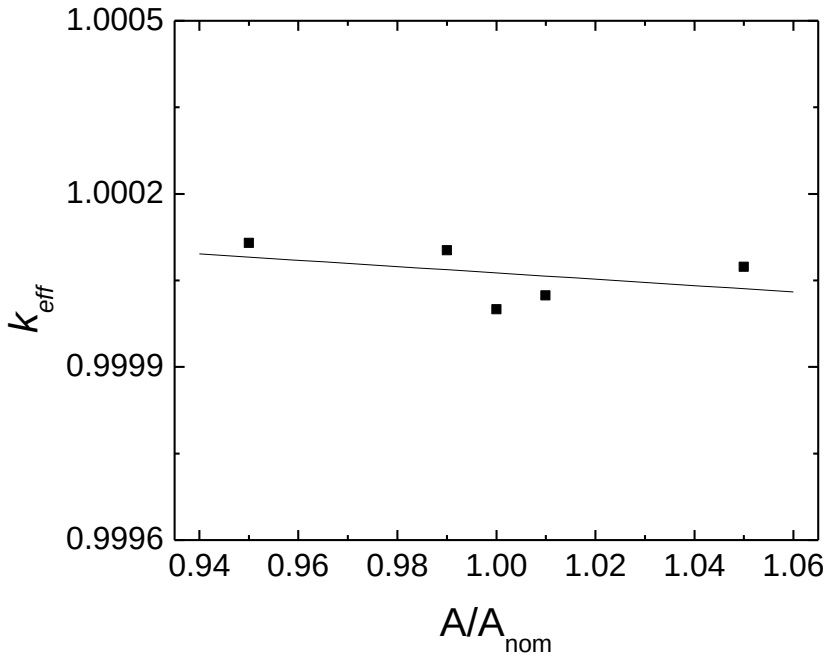

Figure 5.2: Sensitivity analysis of major actinides

The relationship between normalised area and normalised k_{eff} is expressed by a linear fit presented in Equation 5.3.

$$k_{eff} = 1.00061 - 5.48 \times 10^{-4} A \quad (5.3)$$

The sensitivity coefficient for major actinides (s_{major}) is calculated by taking the determining the slope of Equation 5.3, at $A = 1$, and the derivative is shown in Equation 5.4.

$$s_{major} = \frac{dk_{eff}}{dA} = \frac{d}{dA}(1.00061 - 5.48 \times 10^{-4} A) \quad (5.4)$$

$$s_{major} = \left.\frac{dk_{eff}}{dA}\right|_{A/A_{nom}=1} = -5.48 \times 10^{-4}$$

This yields a sensitivity coefficient for major actinides of $s_{major} = -5.48 \times 10^{-4}$ when evaluated at normalised nominal value of the area (see Figure *5.2*). The negative value of the sensitivity coefficient means that the k_{eff} of the SNF casks, when taking credit for major actinides only, is decreasing, as shown in Figure 5.2. The magnitude of $s_{fresh\ fuel}$ is exceedingly small, suggesting that the system's response is not overly sensitive to changes in the area of SNF casks. Comparing the sensitivity coefficient values for fresh fuel and a case where credit is taken for major actinides, it can be concluded that k_{eff} is not overly sensitive to changes in the area in either case. However, the magnitude of the sensitivity coefficient is higher when credit is taken for major actinides when compared to that of fresh fuel.

5.1.3. Sensitivity analysis of actinides plus minor fission products.

For actinides plus minor fission products, the normalised values of the area and that of the k_{eff} were also calculated and plotted as shown in Figure 5.3.

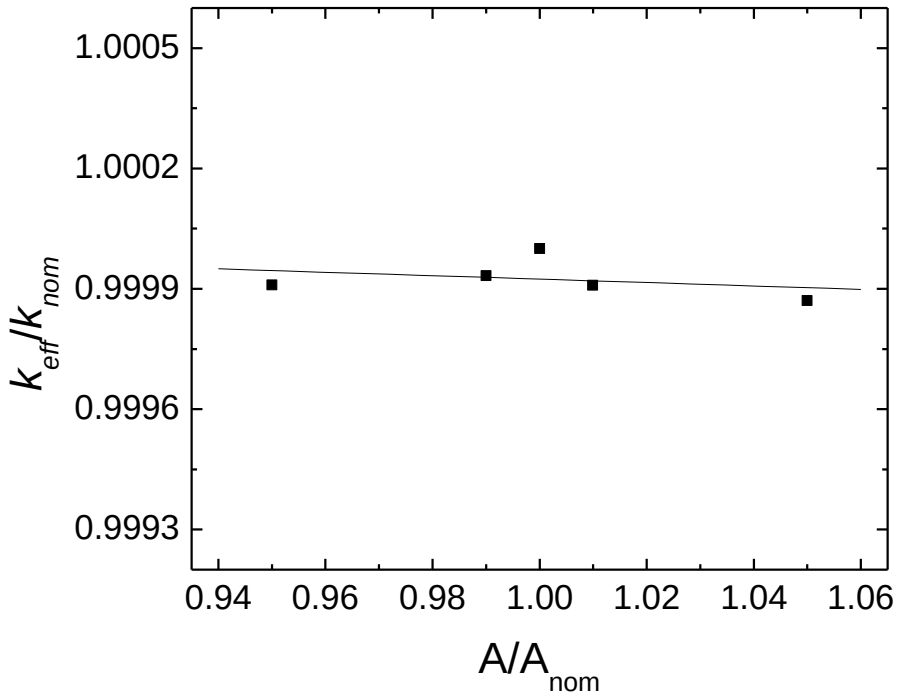

Figure 5.3: Sensitivity analysis of actinides plus minor fission products.

The relationship between normalised area and normalised k_{eff} is given in Equation 5.5:

$$k_{eff} = 1.00035 - 5.24 \times 10^{-5} \, (A/A_{nom}) \tag{5.5}$$

The sensitivity coefficient (s_{minor}) is calculated by taking the first order derivative of Equation 5.5, at $A = 1$, and the derivative is shown in Equation 5.6.

$$s_{minor} = \frac{dk_{eff}}{dA} = \frac{d}{dA}(1.00035 - 5.24 \times 10^{-4} A) \tag{5.6}$$

$$s_{minor} = \left.\frac{dk_{eff}}{dA}\right|_{A/A_{nom}=1} = -5.24 \times 10^{-4}$$

This yields a sensitivity coefficient for actinides plus minor fission products of $s_{minor} = -5.24 \times 10^{-4}$ when evaluated at the nominal value of the area. The negative value of the sensitivity coefficient indicates that the k_{eff} of the SNF casks is decreasing (as seen in Figure 5.3). However, the decrease is

exceedingly small, indicating that k_{eff} is not overly sensitive to changes in area.

5.1.4. Sensitivity analysis of actinides plus principal fission products.

In the case of actinides plus principal fission products, the normalized values for both the area and k_{eff} were calculated and presented in Figure *5.4*.

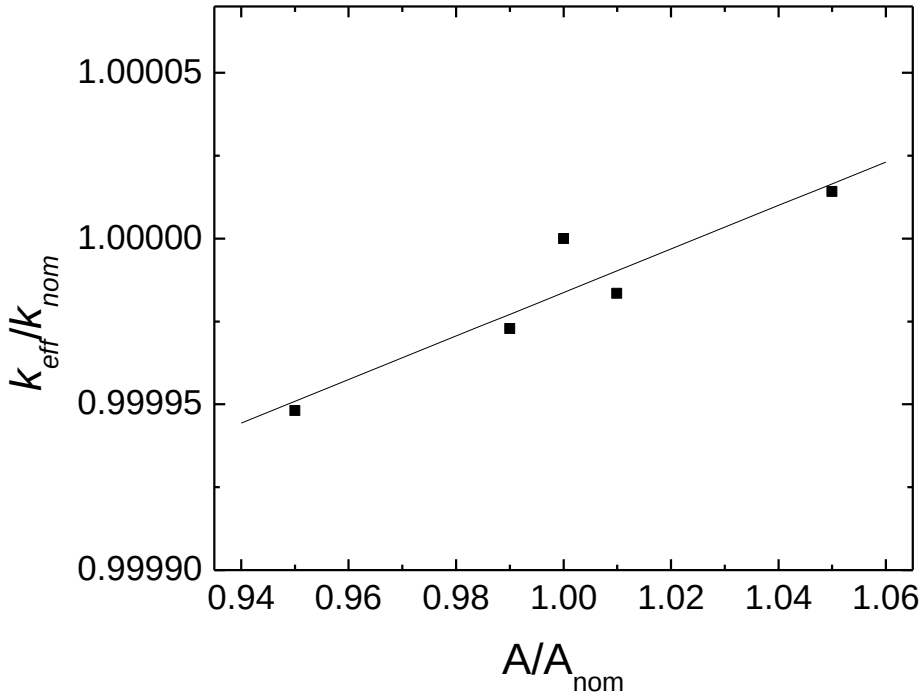

Figure 5.4: Sensitivity analysis of actinides plus principal fission products.

The equation that describes the relationship between normalised area and normalised k_{eff} for actinides plus principal fission products is given by Equation 5.7.

$$k_{eff} = 0.99932 + 6.61 \times 10^{-4} A \qquad (5.7)$$

The sensitivity coefficient ($s_{principal}$) is calculated by determining the slope of Equation 5.5, at $A/A_{nom} = 1$, and this derivative is shown in Equation 5.8.

$$s_{principal} = \frac{dk_{eff}}{dA} = \frac{d}{dA}(0.99932 + 6.61 \times 10^{-4} A) \quad (5.8)$$

$$s_{principal} = \left.\frac{dk_{eff}}{dA}\right|_{A/A_{nom}=1} = 6.61 \times 10^{-4}$$

This yields a sensitivity coefficient for actinides plus principal fission products of $s_{principal} = 6.61 \times 10^{-4}$ when evaluated at the nominal value of the area. The positive value of the sensitivity coefficient indicates that the k_{eff} of the SNF casks is increasing (as seen in Figure 5.4). However, the magnitude of sensitivity coefficient indicates that the k_{eff} is not overly sensitive to the changes in area when taking credit for actinides plus principal fission products.

In conclusion, the sensitivity analysis of fresh fuel, major actinides, actinides plus minor fission products, and actinides plus principal fission products indicates that k_{eff} of the SNF casks does not change with variations in area. This observation is supported by the results shown in Figure 4.1, Figure 4.2, Figure 4.4 and Figure 4.6.

The k_{eff} of the system is dependent on the fuel temperature and moderator density in the SNF casks. The sensitivity of these factors is discussed in the following section.

5.2. Sensitivity Analysis of Important Parameters

The sensitivity analysis of both fuel and moderator temperatures, as well as fuel and moderator densities, is presented in this section. Table 5.2 displays the calculated k_{eff} values based on selected nominal values of fuel and moderator temperatures and densities, which were varied by ±1% and ±5%.

Table 5.2: Sensitivity of k_{eff} as a function of fuel and moderator temperatures and fuel and moderator densities.

Fuel Density					
Percentage Change	**Density, ρ (g/cm^3)**	ρ/ρ_{nom}	k_{eff}	$\pm\delta$	k/k_{eff}
Nominal -5%	10.41	0.95	0.870044	0.000051	0.992328
Nominal -1%	10.85	0.99	0.875522	0.000051	0.998575
Nominal Value	10.96	1.00	0.876771	0.000051	1.000000
Nominal +1%	11.07	1.01	0.877880	0.000053	1.001265
Nominal +5%	11.51	1.05	0.883040	0.000057	1.007150
Fuel Temperature					
Percentage Change	**Temperature, T (K)**	T/T_{nom}	k_{eff}	$\pm\delta$	k/k_{eff}
Nominal Area -5%	302.10	0.95	0.876571	0.000051	1.000796
Nominal Area -1%	314.82	0.99	0.875964	0.000053	1.000103
Nominal	318.00	1.00	0.875874	0.000056	1.000000
Nominal Area +1%	321.18	1.01	0.875828	0.000052	0.999947
Nominal Area +5%	333.90	1.05	0.875329	0.000053	0.999378
Moderator Density					
Percentage Change	**Density ρ (g/cm^3)**	ρ/ρ_{nom}	k_{eff}	$\pm\delta$	k/k_{eff}
Nominal Area -5%	0.76	0.95	0.783743	0.000050	0.977677
Nominal Area -1%	0.79	0.99	0.798118	0.000052	0.995609
Nominal Area	0.80	1.00	0.801638	0.000051	1.000000
Nominal Area +1%	0.81	1.01	0.805202	0.000056	1.004446
Nominal Area +5%	0.84	1.05	0.818543	0.000053	1.021088
Moderator Temperature					
Percentage Change	**Temperature, T (K)**	T/T_{nom}	k_{eff}	$\pm\delta$	k/k_{eff}
Nominal Area -5%	302.10	0.95	0.876328	0.000500	1.001362
Nominal Area -1%	314.82	0.99	0.875389	0.000053	1.000289
Nominal Area	318.00	1.00	0.875136	0.000055	1.000000
Nominal Area +1%	321.18	1.01	0.875090	0.000055	0.999947
Nominal Area +5%	333.90	1.05	0.874099	0.000049	0.998815

5.2.1. Sensitivity Analysis of Fuel Temperature

The calculations performed in Section 5.1 were repeated for fuel temperatures varied by ±1% and ±5%, where the values were divided by

the nominal value of 318K. Correspondingly, the values of k_{eff} were divided by the nominal value as well. The results are depicted in Figure 5.5.

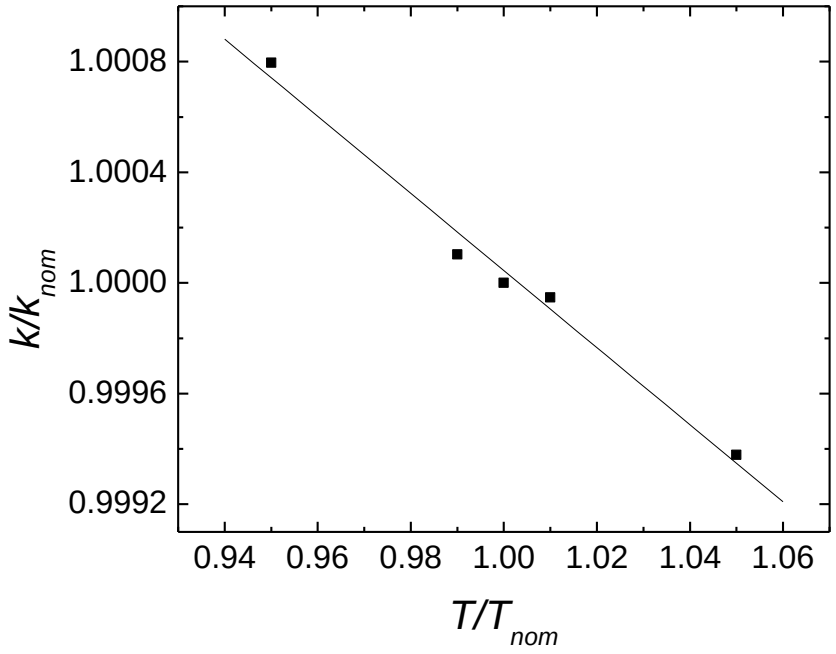

Figure 5.5: Sensitivity of k_{eff} as a function of fuel temperature.

The linear fit for the normalised values is given in Equation 5.9.

$$k_{eff} = 1.01398 - 0.01393\,(T/T_{nom}) \tag{5.9}$$

The sensitivity coefficient is obtained by determining the slope of Equation 5.9, and it is given by:

$$S_{Fuel\ Temperature} = \frac{dk_{eff}}{dT}\Big|_{T/T_{nom}=1} = -0.01393$$

The negative sensitivity coefficient of -0.01393 for fuel temperature indicates that the k_{eff} of the SNF casks, evaluated at $T/T_{nom} = 1$, decreases as fuel temperature increases. The magnitude of this coefficient quantifies how sensitive k_{eff} is to changes in fuel temperature. In summary, the sensitivity coefficient for fuel temperature suggests that small increases in fuel temperature result in a decrease in the k_{eff} of the system.

5.2.2. Sensitivity analysis of fuel density

Similarly, the normalized values of fuel density and k_{eff} are depicted in Figure 5.6. The nominal value of $10.96\ g/cm^3$ was used as a reference to normalize values of fuel density at ±1% and ±5% of nominal value.

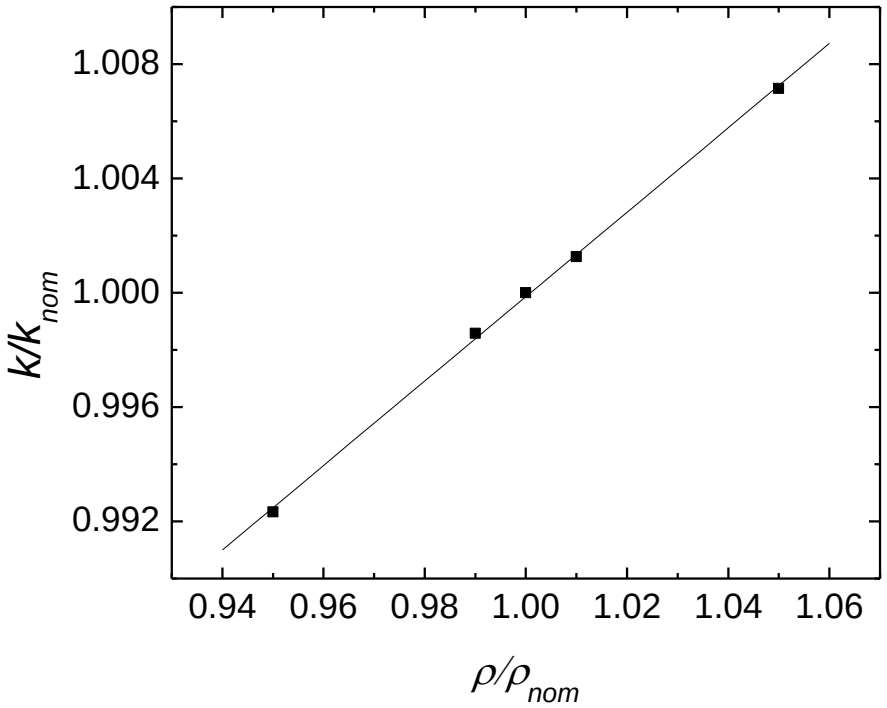

Figure 5.6: Sensitivity of k_{eff} as a function of fuel density.

The corresponding linear fit is represented by Equation 5.10:

$$k_{eff} = 0.85217 + 0.14769(\rho/\rho_{nom}) \tag{5.10}$$

Taking the first order derivative of Equation 5.10 yields the sensitivity coefficient of:

$$s_{Fuel\ Density} = \frac{dk_{eff}}{d\rho}\Big|_{\rho/\rho_{nom}=1} = 0.14769$$

The positive sensitivity coefficient for fuel density indicates that the k_{eff} of the SNF casks, is increasing. The magnitude of this sensitivity coefficient is

greater than that of fuel temperature, indicating that k_{eff} is more sensitive to changes in fuel density compared to changes in fuel temperature.

5.2.3. Sensitivity analysis of moderator density

For moderator density, similar calculations were performed, resulting in the normalized linear fit shown in Figure 5.7.

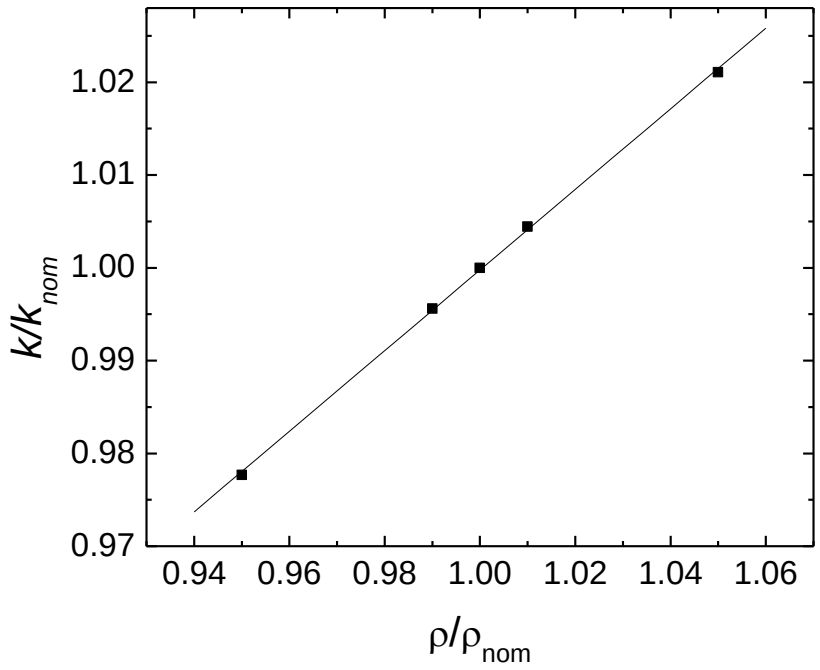

Figure 5.7: Sensitivity of k_{eff} as a function of moderator density.

The corresponding linear fit equation is provided in Equation 5.11:

$$k_{eff} = 0.56536 + 0.43441\ (\rho/\rho_{nom}) \tag{5.11}$$

Again, the sensitivity coefficient is determined calculating the slope of Equation 5.11, resulting in a sensitivity coefficient of:

$$s_{Mod\ Density} = \frac{dk_{eff}}{dT}\Big|_{\rho/\rho_{nom}=1} = 0.43441$$

The sensitivity coefficient of moderator density is 0.43441 and it is positive, indicating that changes in moderator density result in an increase in k_{eff} of the system (see Figure *5.7*). This is because a denser moderator leads to

more neutrons being slowed down, which increases the number of neutrons participating in the fission process. In summary, the sensitivity coefficient of moderator density demonstrates that even minor changes in moderator density can result in significant changes in k_{eff}.

5.2.4. Sensitivity of moderator temperature

Finally, the sensitivity analysis for moderator temperature is conducted in a comparable manner. The normalized values produce the polynomial fit depicted in Figure 5.8.

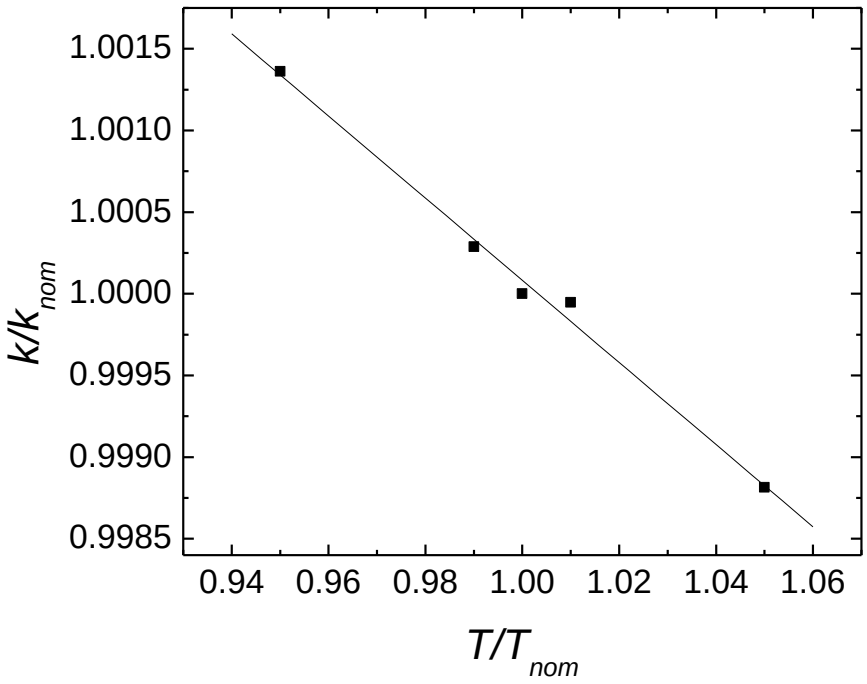

Figure 5.8: Sensitivity of k_{eff} as a function of moderator temperature.

The corresponding polynomial fit equation is provided in Equation 5.12.

$$k_{eff} = 1.02523 - 0.02515\,(T/T_{nom}) \tag{5.12}$$

Taking the first order derivative of Equation 5.12 yields the sensitivity coefficient of:

$$s_{Mod\ Temperature} = \left.\frac{dk_{eff}}{dT}\right|_{T/T_{nom}=1} = -0.02515$$

The sensitivity coefficient of moderator temperature is -0.02515 and it is negative, indicating that k_{eff} decreases when evaluated at normalized nominal temperature. The magnitude of this moderator temperature sensitivity coefficient is less than that of moderator density. This indicates that k_{eff} of the system is more sensitive to changes in moderator density than that of moderator temperature. In summary, the sensitivity coefficient of moderator temperature demonstrates that even minor changes in moderator temperature can influence k_{eff}.

5.3. Summary of Sensitivity Analysis

The sensitivity coefficient for fresh fuel, calculated as $s_{fresh\ fuel} = 6.73154 \times 10^{-5}$, suggests that k_{eff} increases slightly and is not significantly affected by changes in the separation distance. The positive value indicates that small alterations in the spatial arrangement have a minimal impact on the k_{eff} of the system.

The sensitivity coefficient for major actinides, calculated as $s_{major} = -5.48166 \times 10^{-4}$, indicates that k_{eff} decreases slightly and is not significantly affected by changes in the area of the SNF casks. It can be concluded that, in both cases, the k_{eff} of the system does not change appreciably with variations in the area, given the relatively small magnitude of the sensitivity coefficients.

The sensitivity coefficient for actinides plus minor fission products, calculated as $s_{minor} = -5.24478 \times 10^{-4}$, indicates that k_{eff} decreases slightly and is not significantly affected by changes in the area of the SNF casks. The magnitude of sensitivity coefficient for actinides plus minor fission products is similar to that of major actinides, but slightly less responsive. Consequently, given the small magnitude of the sensitivity

coefficient, it can be concluded that changes in the area of the SNF casks have minimal impact on the k_{eff} of the system.

The sensitivity coefficient for actinides plus principal fission products, calculated as $s_{principal} = 6.61438 \times 10^{-4}$, indicates that k_{eff} increases slightly and is not significantly affected by changes in the area of the SNF casks. Given the small magnitude of the sensitivity coefficient, it can also be concluded that changes in the area of the SNF casks have minimal impact on the k_{eff} of the system.

To summarize, it is concluded that slight changes in the area of the SNF casks for fresh fuel, major actinides, actinides plus minor fission products, and actinides plus principal fission products do not significantly affect $\mathrm{k_{eff}}$. The fluctuations in $\mathrm{k_{eff}}$ observed in Figure 4.1, Figure 4.2, Figure 4.4 and Figure 4.6 as the area is increased can be attributed to statistical variations inherent to the Monte Carlo method.

The sensitivity analysis reveals that the magnitude of the sensitivity coefficient for fuel temperature (−0.01393) indicates that k_{eff} decreases as fuel temperature increases. In contrast, the sensitivity coefficient for fuel density (0.14769) indicates that k_{eff} increases with increasing fuel density. The magnitudes of the sensitivity coefficients clearly demonstrate that k_{eff} is more sensitive to changes in fuel density than to changes in fuel temperature.

The sensitivity analysis also reveals that the magnitude of the sensitivity coefficient for moderator density (0.43441) indicates that k_{eff} increases significantly with increasing moderator density. Conversely, the sensitivity coefficient for moderator temperature (−0.02515) indicates that k_{eff} decreases slightly as moderator temperature increases. The magnitudes of the sensitivity coefficients clearly demonstrate that k_{eff} is more sensitive to changes in moderator density than to changes in moderator temperature.

Chapter 6 : Conclusion

This comprehensive study investigated the complex dynamics of burnup credit, specifically focusing on its impact on the effective multiplication factor (k_{eff}) within spent nuclear fuel (SNF) storage casks. The investigation considered major actinides, actinides plus minor fission products, and actinides plus principal fission products, examining both reactivity changes and the associated space savings in comparison to fresh fuel.

6.1. Reactivity of Different Nuclide Groups

The analysis unveiled fluctuations in k_{eff} as the area occupied by SNF casks increased for fresh fuel and all considered nuclide groups, i.e., major actinides, actinides plus minor fission products and actinides plus principal fission products. However, it is concluded that the observed fluctuations are due to statistical uncertainty inherent to Monte Carlo method. Essentially, it is concluded that increasing the area of the SNF casks does not change the keff of the system for the respective nuclide groups. Additionally, it was observed that the k_{eff} of the fresh fuel is comparatively higher than that of configurations considering fuel burnup credit. Specifically, the results for actinides plus principal fission products indicate the lowest k_{eff} value compared to the other configurations (Figure 4.1, Figure 4.2, Figure 4.4 and Figure 4.6).

6.2. Reactivity Saving Due to Taking Credit for Fuel Burnup

The investigation into reactivity savings, which compares fresh fuel to burnup credit scenarios and provides distinctive insights into the impact of different nuclide groups. The findings, as depicted in the respective figures, reveal following trends in reactivity savings:

- **Actinides plus principal fission products:**
  Demonstrates the highest reactivity savings, suggesting a robust potential for effective burnup credit utilization. The inclusion of a comprehensive set of nuclides, including principal fission products, results in significant reactivity reduction, contributing to efficient storage practices.
- **Actinides plus minor fission products:**
  Exhibits substantial reactivity savings, albeit lower than actinides plus principal fission products. The lower reactivity savings are attributed to the consideration of fewer nuclides in this group, emphasizing the importance of nuclide composition in influencing reactivity reduction.
- **Major actinides:** Presents the least reactivity savings among the considered nuclide groups. The limited number of nuclides included in this group contributes to a modest impact on reactivity reduction when compared to fresh fuel.

The conclusion can be drawn that incorporating burnup credit leads to reactivity savings for the SNF casks when compared to fresh fuel. Among the considered configurations, actinides plus principal fission products demonstrate the highest k_{eff} savings, while major actinides exhibit the least savings.

It is also demonstrated that the k_{eff} of the system is influenced by both fuel and moderator temperatures, with k_{eff} decreasing as both fuel and moderator temperatures increase. Additionally, it is concluded that k_{eff} is impacted by both fuel and moderator densities. Specifically, k_{eff} increases with increasing fuel density, as well as with increasing moderator density.

6.3. Sensitivity Analysis

The sensitivity analysis for fresh fuel and various nuclide groups revealed the following findings:

- Fresh fuel sensitivity coefficient: 6.73×10^{-5}, indicating insignificant sensitivity of k_{eff} to spatial changes.
- Major actinides sensitivity coefficient: -5.48×10^{-4}, suggesting insignificant response of k_{eff} to alterations in separation distance within the major actinides group.
- Actinides plus minor fission products sensitivity coefficient: -5.24×10^{-4}, signifying insignificant sensitivity of k_{eff} to changes in separation distance, resulting in no influence on k_{eff}.
- Actinides plus principal fission products sensitivity coefficient: 6.61×10^{-4}, also indicating insignificant changes in k_{eff} of the system.

The magnitude of the sensitivity coefficients indicates that changes in the area of the SNF casks do not affect the k_{eff} of the system. Therefore, it can be concluded that variations in k_{eff} are primarily influenced by taking credit for fuel burnup across various nuclide groups: major actinides, actinides plus minor fission products, and actinides plus principal fission products.

6.4. Space Savings due to taking credit for fuel burnup.

In conclusion, the analysis of area savings (ΔA) for distinct nuclide groups in burnup credit offers crucial insights into reactivity impact, as illustrated in Figure 4.8. The key findings are as follows:

Major actinides burnup credit:

- **Reactivity savings:** Lowest.
- **Space savings (ΔA):** Relatively modest.

Actinides plus principal fission products burnup credit:

- **Reactivity savings:** Highest .
- **Space savings (ΔA):** Substantial, yielding the most significant increase in area savings.

Actinides plus minor fission products burnup credit:

- **Reactivity savings:** Intermediate between major actinides and actinides plus principal fission products.
- **Space savings (ΔA):** Falls between the extremes, showing intermediate reactivity savings.

In conclusion, this study highlights the critical role of burnup credit in optimizing storage space for SNF casks. Actinides plus principal fission products emerge as the key contributors to substantial reactivity and space savings, offering a compelling avenue for enhancing efficiency in nuclear fuel management. These findings carry profound implications for safety assessments and operational strategies, providing a nuanced understanding that empowers the industry to strike a delicate balance between maximizing storage capacity and upholding stringent safety standards.

6.5. Recommendations for future research

The following recommendations are suggested for future research to further investigate these critical areas:

- Investigate the influence of fuel and moderator temperatures on space savings when taking credit for fuel burnup credit.
- Explore the impact of fuel and moderator densities on space savings when taking credit for fuel burnup.
- As future work, exploring the application of burnup credit on the newly proposed HOLTEC HI-STAR 100 Cask for South Africa’s spent nuclear fuel.
- Future research should focus on investigating the implementation of burnup credit for South Africa's Spent Nuclear Fuel. This approach is critical to effectively address the challenges associated with extending the operational lifespan of nuclear power plants from 40 to 60 years.

- These investigations will provide valuable insights into optimizing space utilization while incorporating burnup credit in nuclear systems.

References

[1] Leotlela M.J., “Preserving Spent Fuel Storage Capacity by Taking Credit for Burnup in Nuclear Criticality Safety Analysis: An Alternative Solution to Spent Fuel Storage Shortage,” J Mod Appl Phys, vol. 2, no. 1, pp. 10-12, 2018.

[2] Leotlela M.J., Mueller D.E., “The Effects of Storage Patterns on the Neutron Multiplication Factor of Spent Nuclear Fuel Casks.,” International Safety Nuclear Journal, vol. 1, no. 1, pp. 7-15, 2012.

[3] V.F. Castro, R. Mir´o, C. Pereira and G. Verdú, “A burnup credit methodology for PWR spent fuel storage pools: Application,” Nuclear Engineering and Design, vol. 419, pp. 628 - 633, 2014.

[4] Milosevic M.J. Pesic M.P., “An analysis of burnup reactivity credit for reactor RA spent fuel storage.,” Nuclear Engineering and Design, no. 180, pp. 29 - 35, 1998.

[5] Mahmouda R.F, Shaatb M.K., Nagyc M.E., Agamyc S.A. and Abdelrahmana A.A., “Burn-up credit in criticality safety of PWR spent fuel,” Nuclear Engineering and Design, vol. 280, pp. 628 - 633, 2014.

[6] Leotlela M.J., “Criticality Safety Analysis of the Design of Spent Fuel Cask, Its Manipulation and Placement in a Long-Term Storage.,” Faculty of Science, University of Wirwatersrand, Johannesburg, 2016.

[7] Stacey W.M. , Nuclear Reactor Physics, Wiley-VCH Verlag GmbH & Co. KGaA., 2007.

[8] Gautreau R. Savin W. , Theory and Problems of Modern Physics., Schaum’s Outline Series. , 1978.

[9] Duderstadt J.J. and Hamilton L.J., Nuclear Reactor Analysis., Wiley and Sons, inc., 1976.

[10] “ENDF data,” International Atomic Energy Agency, 2024. [Online]. Available: https://www-nds.iaea.org/exfor/endf.htm.

[11] “Advances in Applications of Burnup Credit to Enhance Spent Fuel Transportation, Storage, Reprocessing and Disposition.,” in Proceedings of a Technical Meeting held in London., IAEA-TECDOC-1547, London, 2005.

[12] Lamarsh J.R. and Baratta A.J. , Introduction to Nuclear Engineering. 3rd Edition. ., Prentice-Hall, inc, 2001.

[13] Leotlela M.J., Nokahle D. H., Petr I and Abraham S., “Prediction of dose rates around the interim spent fuel storage facility.,” Radiation Physics and Chemistry., vol. 180, 2020.

[14] Leotlela M.J., “Time-dependent variations in the radiological health impact of an interim spent fuel storage facility.,” Radiation Physics and Chemistry, vol. 189, no. 109620, 2021.

[15] Wieselquist W.A., Lefebvre R.A. and Jessee M.A., “SCALE Code System,” Oak Ridge National Laboratory, 2020.

[16] “Criticality Safety in the Handling of Fissile Material,” International Atomic Energy Agency, 2022.

[17] Shultis J.K. and Faw R.E., An MCNP Primer, Manhattan: KS 66506, Kansas State University , 2011.

[18] Leppänen J., Serpent– a Continuous-energy Monte Carlo Reactor Physics Burnup Calculation Code, VTT Technical Research of Finland, 2015.

[19] “Implementation of burnup credit in spent fuel management systems,” in Proceedings of a Technical Committee meeting , Vienna, 2001.

[20] Bowman S.M., “ KENO-VI Primer: A Primer for Criticality Calculations with SCALE/KENO-VI Using GeeWiz.,” Oak Ridge National Laboratory. (ORNL/TM-2008/069)., 2008.

[21] Leotlela M.J., Malgas I. and Taviv E., “Sensitivity analysis of parameters important to nuclear criticality safety of Castor X/28F spent nuclear fuel cask.,” KERNTECHNIK 80, vol. 5, p. 485 – 493, 2015.

[22] “Operation and Maintenance of Spent Fuel Storage and Transportation Casks/Containers.,” Internation Atomic Energy Agency, IAEA-TECDOC-1532., 2007.

[23] Alvarez R., “Reducing Hazard from Stored Spent Power-Reactor Fuel in the United States.,” Science and Global Security, 2003.

[24] Radioactive Waste Management Policy and Strategy for the Republic of South Africa, Department of Minerals and Engergy (South Africa), 2005.

[25] Guoshun Y., Chunming Z. and Xinyi P., “. (2012). Introduction of Burn-up Credit in Nuclear Criticality Safety Analysis.,” in International Symposium on Safety Science and Engineering, China, 2012.

[26] Leotlela M.J., Olifant T. and Petr I., “Time-dependent variation of the neutron multiplication factor in spent fuel storage.,” KERNTECHNIK, vol. 6, no. 82, p. 653–661, 2017.

[27] Leotlela M.J, Petr I and Mathye A., “Sensitivity of the neutron multiplication factor to water ingress into a spent fuel cask.,” KERNTECHNIK , vol. 1, no. 85, p. 38 –53., 2020.

[28] “Computational Benchmark for Estimation of Reactivity Margin from Fission Products and Minor Actinides in PWR Burnup Credit. (NUREG 6747) . .,” Oak Ridge National Laboratory, 2001.

[29] Kucukboyaci V, Sung Y and Salko R., “COBRA-TF Parallelization and Application to PWR Reactor Core Subchannel DNB Analysis. ANS MC2015,” in Joint International Conference on Mathematics and Computation (M&C), Supercomputing in Nuclear Applications (SNA) and the Monte Carlo (MC) Method., American Nuclear Society, LaGrange Park, IL., 2015.

[30] Mueller D.E. and Rearden B.T., “ Sensitivity Coefficient Generation for A Burnup Credit Cask Model Using Tsunami-3D.,” Oak Ridge National Laboratory, American Nuclear Society,, LaGrange Park, IL. , 2005.

[31] Krishna T., “Risk Assessment of Additional Metal Casks”. PSA-R-T15-08, 2022.

[32] Sheldon M. Ross. Introduction to Probability and Statistics for Engineers and Scientists. Elsevier, 5th Edition, 2014.

Appendix A: Nuclide build-up

Table A.1: Build-up and decay of various nuclides over a period of 12 months.

Nuclide	Time (days)								
	0.00	6.50	11.55	20.54	36.52	64.95	115.50	205.39	365.24
np-237	3.00E+01	3.05E+01	3.07E+01	3.09E+01	3.10E+01	3.10E+01	3.11E+01	3.11E+01	3.11E+01
u-234	3.74E+02	3.74E+02	3.74E+02	3.74E+02	3.74E+02	3.74E+02	3.74E+02	3.74E+02	3.74E+02
u-235	2.73E+04	2.73E+04	2.73E+04	2.73E+04	2.73E+04	2.73E+04	2.73E+04	2.73E+04	2.73E+04
u-236	1.14E+03	1.14E+03	1.14E+03	1.14E+03	1.14E+03	1.14E+03	1.14E+03	1.14E+03	1.14E+03
u-237	1.02E+00	5.23E-01	3.11E-01	1.24E-01	2.40E-02	1.29E-03	8.51E-06	1.29E-06	1.27E-06
u-238	9.64E+05	9.64E+05	9.64E+05	9.64E+05	9.64E+05	9.64E+05	9.64E+05	9.64E+05	9.64E+05
np-237	3.00E+01	3.05E+01	3.07E+01	3.09E+01	3.10E+01	3.10E+01	3.11E+01	3.11E+01	3.11E+01
np-239	2.27E+01	3.38E+00	7.65E-01	5.43E-02	4.93E-04	1.44E-07	2.90E-08	2.90E-08	2.90E-08
pu-238	1.43E+00	1.45E+00	1.46E+00	1.46E+00	1.46E+00	1.46E+00	1.47E+00	1.47E+00	1.47E+00
pu-239	2.10E+03	2.11E+03	2.12E+03	2.12E+03	2.12E+03	2.12E+03	2.12E+03	2.12E+03	2.12E+03
pu-240	1.86E+02	1.86E+02	1.86E+02	1.86E+02	1.86E+02	1.86E+02	1.86E+02	1.86E+02	1.86E+02
pu-241	4.26E+01	4.25E+01	4.25E+01	4.24E+01	4.24E+01	4.22E+01	4.19E+01	4.14E+01	4.06E+01
pu-242	1.59E+00	1.59E+00	1.59E+00	1.59E+00	1.59E+00	1.59E+00	1.59E+00	1.59E+00	1.59E+00
am-241	6.06E-01	6.43E-01	6.71E-01	7.22E-01	8.12E-01	9.72E-01	1.25E+00	1.75E+00	2.62E+00
am-243	3.36E-02	3.37E-02	3.37E-02	3.37E-02	3.37E-02	3.37E-02	3.37E-02	3.37E-02	3.37E-02
cm-242	3.13E-02	3.08E-02	3.02E-02	2.91E-02	2.71E-02	2.41E-02	1.94E-02	1.32E-02	6.71E-03
sr-90	9.95E+01	9.94E+01	9.94E+01	9.93E+01	9.92E+01	9.91E+01	9.87E+01	9.81E+01	9.71E+01
y-90	2.53E-02	2.52E-02	2.52E-02	2.52E-02	2.52E-02	2.51E-02	2.50E-02	2.49E-02	2.46E-02
ru-106	1.39E+01	1.37E+01	1.36E+01	1.34E+01	1.30E+01	1.23E+01	1.12E+01	9.46E+00	7.02E+00

Nuclide	Time (days)								
	0.00	6.50	11.55	20.54	36.52	64.95	115.50	205.39	365.24
ag-110m	6.13E-03	6.02E-03	5.93E-03	5.79E-03	5.54E-03	5.12E-03	4.45E-03	3.46E-03	2.22E-03
cs-134	2.82E+00	2.80E+00	2.79E+00	2.76E+00	2.72E+00	2.65E+00	2.53E+00	2.33E+00	2.01E+00
cs-137	1.77E+02	1.77E+02	1.77E+02	1.77E+02	1.77E+02	1.76E+02	1.76E+02	1.75E+02	1.73E+02
ba-137	2.37E+00	2.45E+00	2.50E+00	2.60E+00	2.78E+00	3.10E+00	3.66E+00	4.65E+00	6.40E+00
eu-152	6.77E-03	6.77E-03	6.76E-03	6.75E-03	6.74E-03	6.71E-03	6.66E-03	6.58E-03	6.44E-03
eu-154	5.17E-01	5.17E-01	5.16E-01	5.15E-01	5.13E-01	5.10E-01	5.04E-01	4.95E-01	4.77E-01
ce-144	1.00E+02	9.85E+01	9.73E+01	9.52E+01	9.16E+01	8.55E+01	7.56E+01	6.07E+01	4.12E+01
pr-144	4.23E-03	4.15E-03	4.10E-03	4.01E-03	3.86E-03	3.60E-03	3.18E-03	2.56E-03	1.73E-03

Table A.2: Build-up and decay of various nuclides over a period of 100 years.

Nuclide	Time (Years)								
	0	2	3	6	10	18	32	56	100
u-234	373.52	373.53	373.55	373.57	373.62	373.69	373.81	373.99	374.22
u-235	27329	27329	27330	27330	27330	27330	27331	27333	27335
u-236	1136.7	1136.7	1136.7	1136.8	1136.9	1137	1137.3	1137.7	1138.6
u-238	963830	963830	963830	963830	963830	963830	963830	963830	963830
np-237	30.03	31.056	31.068	31.102	31.198	31.456	32.097	33.494	36.128
np-239	22.709	2.9E-08	2.9E-08	2.9E-08	2.9E-08	2.89E-08	2.89E-08	2.88E-08	2.87E-08
pu-238	1.4324	1.4658	1.4516	1.4239	1.3756	1.2936	1.1598	0.95503	0.67615
pu-239	2095	2117.8	2117.7	2117.6	2117.3	2116.8	2116	2114.5	2111.8
pu-240	185.76	185.73	185.7	185.65	185.57	185.42	185.14	184.66	183.81

Nuclide	Time (Years)								
	0	2	3	6	10	18	32	56	100
pu-241	42.565	39.048	36.512	32.403	26.206	17.965	9.1809	2.7824	0.33299
pu-242	1.5861	1.5861	1.5861	1.5861	1.5861	1.5862	1.5862	1.5861	1.5861
am-241	0.60629	4.1171	6.6405	10.715	16.815	24.792	32.926	37.902	37.674
am-243	0.033562	0.03367	0.033666	0.033658	0.033644	0.03362	0.033576	0.033499	0.033361
y-89	68.35	82.014	82.015	82.015	82.015	82.015	82.015	82.015	82.015
sr-90	99.475	95.306	92.183	86.879	78.19	64.83	46.458	25.687	8.9554
cs-134	2.8166	1.5508	0.97457	0.42664	0.098198	0.007205	6.92E-05	1.79E-08	7.47E-15
cs-137	176.94	169.83	164.5	155.43	140.52	117.45	85.378	48.421	17.662
ba-137	2.3728	9.4768	14.808	23.878	38.789	61.86	93.932	130.89	161.65
eu-152	0.006773	0.006184	0.005761	0.005079	0.004059	0.002725	0.001342	0.00038	4.05E-05
eu-154	0.51745	0.44836	0.40104	0.32889	0.23113	0.12344	0.040464	0.005568	0.000164
ce-144	100.11	20.616	6.027	0.67655	0.013845	1.37E-05	6.26E-11	1.99E-20	2.56E-37
pr-144	0.004227	0.000868	0.000254	2.85E-05	5.83E-07	5.78E-10	2.64E-15	8.38E-25	1.08E-41
ru-106	13.872	4.1327	1.6104	0.30135	0.015301	7.64E-05	6.17E-09	3.25E-16	3.7E-29
ag-110m	0.006126	0.00101	0.000248	2.05E-05	2.43E-07	9.09E-11	7.34E-17	1.07E-27	5.81E-47
y-90	0.025281	0.024176	0.023383	0.022038	0.019834	0.016445	0.011785	0.006516	0.002272

Appendix B: Coordinates of Polyethylene Rods

Table B.1 presents the x-y coordinates of polyethylene rods that are within SNF casks.

Table B. 1: x-y Coordinates of polyethylene rods

Rod #	Angle (Degree)	Angle (radians)	x-coordinates (cm)	y-coordinates (cm)
1	0.00	0.0000	132.00	0.00
2	5.14	0.0898	131.47	11.83
3	10.29	0.1795	129.88	23.57
4	15.43	0.2693	127.24	35.12
5	20.57	0.3590	123.58	46.38
6	25.71	0.4488	118.93	57.27
7	30.86	0.5386	113.31	67.70
8	36.00	0.6283	106.79	77.59
9	41.14	0.7181	99.40	86.85
10	46.29	0.8078	91.22	95.41
11	51.43	0.8976	82.30	103.20
12	56.57	0.9874	72.72	110.16
13	61.71	1.0771	62.55	116.24
14	66.86	1.1669	51.88	121.38
15	72.00	1.2566	40.79	125.54
16	77.14	1.3464	29.37	128.69
17	82.29	1.4362	17.72	130.81
18	87.43	1.5259	5.92	131.87
19	92.57	1.6157	-5.92	131.87
20	97.72	1.7055	-17.72	130.81
21	102.86	1.7952	-29.37	128.69
22	108.00	1.8850	-40.79	125.54
23	113.14	1.9747	-51.88	121.38

Rod #	Angle (Degree)	Angle (radians)	x-coordinates (cm)	y-coordinates (cm)
24	118.29	2.0645	-62.55	116.24
25	123.43	2.1543	-72.72	110.16
26	128.57	2.2440	-82.30	103.20
27	133.72	2.3338	-91.22	95.41
28	138.86	2.4235	-99.41	86.85
29	144.00	2.5133	-106.79	77.59
30	149.14	2.6031	-113.32	67.70
31	154.29	2.6928	-118.93	57.27
32	159.43	2.7826	-123.58	46.38
33	164.57	2.8723	-127.24	35.11
34	169.72	2.9621	-129.88	23.57
35	174.86	3.0519	-131.47	11.83
36	180.00	3.1416	-132.00	0.00
37	185.14	3.2314	-131.47	-11.84
38	190.29	3.3211	-129.88	-23.57
39	195.43	3.4109	-127.24	-35.12
40	200.57	3.5007	-123.58	-46.39
41	205.72	3.5904	-118.93	-57.28
42	210.86	3.6802	-113.31	-67.71
43	216.00	3.7699	-106.79	-77.59
44	221.14	3.8597	-99.40	-86.85
45	226.29	3.9495	-91.22	-95.41
46	231.43	4.0392	-82.30	-103.20
47	236.57	4.1290	-72.71	-110.17
48	241.72	4.2187	-62.55	-116.24
49	246.86	4.3085	-51.87	-121.38
50	252.00	4.3983	-40.79	-125.54
51	257.15	4.4880	-29.37	-128.69

Rod #	Angle (Degree)	Angle (radians)	x-coordinates (cm)	y-coordinates (cm)
52	262.29	4.5778	-17.71	-130.81
53	267.43	4.6675	-5.92	-131.87
54	272.57	4.7573	5.93	-131.87
55	277.72	4.8471	17.72	-130.80
56	282.86	4.9368	29.38	-128.69
57	288.00	5.0266	40.80	-125.54
58	293.15	5.1164	51.88	-121.38
59	298.29	5.2061	62.56	-116.24
60	303.43	5.2959	72.72	-110.16
61	308.57	5.3856	82.31	-103.20
62	313.72	5.4754	91.22	-95.40
63	318.86	5.5652	99.41	-86.84
64	324.00	5.6549	106.79	-77.58
65	329.15	5.7447	113.32	-67.70
66	334.29	5.8344	118.93	-57.27
67	339.43	5.9242	123.59	-46.38
68	344.57	6.0140	127.24	-35.11
69	349.72	6.1037	129.88	-23.56
70	354.86	6.1935	131.47	-11.83

Appendix C: Coordinates of the CASTOR X/28 Casks

Appendix C provides the x-y coordinates of the casks, offering a detailed representation of their spatial arrangement as the separation between them is systematically increased.

Table C. 1: x-y coordinates of the SNF casks.

Cask #	Separation Distance (cm)	x (cm)	y (cm)
1	0	144.3	144.3
2		-144.3	144.3
3		-144.3	-144.3
4		144.3	-144.3
1	10	149.3	149.3
2		-149.3	149.3
3		-149.3	-149.3
4		149.3	-149.3
1	20	154.3	154.3
2		-154.3	154.3
3		-154.3	-154.3
4		154.3	-154.3
1	30	159.3	159.3
2		-159.3	159.3
3		-159.3	-159.3
4		159.3	-159.3
1	40	164.3	164.3
2		-164.3	164.3
3		-164.3	-164.3
4		164.3	-164.3
1	50	169.3	169.3
2		-169.3	169.3
3		-169.3	-169.3
4		169.3	-169.3
1	60	174.3	174.3
2		-174.3	174.3
3		-174.3	-174.3
4		174.3	-174.3
1	70	179.3	179.3
2		-179.3	179.3
3		-179.3	-179.3

Cask #	Separation Distance (cm)	x (cm)	y (cm)
4		179.3	-179.3
1	80	184.3	184.3
2		-184.3	184.3
3		-184.3	-184.3
4		184.3	-184.3
1	90	189.3	189.3
2		-189.3	189.3
3		-189.3	-189.3
4		189.3	-189.3
1	100	194.3	194.3
2		-194.3	194.3
3		-194.3	-194.3
4		194.3	-194.3
1	110	199.3	199.3
2		-199.3	199.3
3		-199.3	-199.3
4		199.3	-199.3
1	120	204.3	204.3
2		-204.3	204.3
3		-204.3	-204.3
4		204.3	-204.3
1	130	209.3	209.3
2		-209.3	209.3
3		-209.3	-209.3
4		209.3	-209.3
1	140	214.3	214.3
2		-214.3	214.3
3		-214.3	-214.3
4		214.3	-214.3
1	150	219.3	219.3
2		-219.3	219.3
3		-219.3	-219.3
4		219.3	-219.3
1	160	224.3	224.3
2		-224.3	224.3
3		-224.3	-224.3
4		224.3	-224.3
1	170	229.3	229.3
2		-229.3	229.3
3		-229.3	-229.3
4		229.3	-229.3

Cask #	Separation Distance (cm)	x (cm)	y (cm)
1	180	234.3	234.3
2		-234.3	234.3
3		-234.3	-234.3
4		234.3	-234.3
1	190	239.3	239.3
2		-239.3	239.3
3		-239.3	-239.3
4		239.3	-239.3
1	200	244.3	244.3
2		-244.3	244.3
3		-244.3	-244.3
4		244.3	-244.3

Appendix D: Data for k_{eff} as a Function of Area for Different Nuclide Groups

This section presents the results on the effect of different nuclide groups on k_{eff} at different areas.

Table D.1.: Results for changing k_{eff} for different nuclide groups.

Area (m^2)	k_{eff} (Fresh fuel)	±δ (Fresh fuel)	k_{eff} (Major actinides only)	±δ (Major actinides only)	k_{eff} (Actinides + principal fission products)	±δ (Actinides + principal fission products)	k_{eff} (Actinides + minor fission Products)	±δ (Actinides + minor fission Products)
33.316	0.86959	5.10E-05	0.86959	4.80E-05	0.84744	5.00E-05	0.86299	5.30E-05
34.480	0.86965	5.60E-05	0.86965	5.20E-05	0.84744	5.20E-05	0.86305	5.00E-05
35.665	0.86958	4.30E-05	0.86958	5.30E-05	0.84740	5.60E-05	0.86301	4.80E-05
36.869	0.86958	5.40E-05	0.86958	6.00E-05	0.84737	4.90E-05	0.86294	5.40E-05
38.094	0.86869	5.70E-05	0.86869	5.10E-05	0.84754	5.30E-05	0.86296	5.10E-05
39.338	0.86964	4.80E-05	0.86964	5.30E-05	0.84745	4.90E-05	0.86303	5.00E-05
40.602	0.86959	5.40E-05	0.86959	5.30E-05	0.84749	5.00E-05	0.86299	5.30E-05
41.887	0.86963	5.70E-05	0.86963	4.90E-05	0.84743	5.50E-05	0.86302	5.60E-05
43.191	0.86961	5.70E-05	0.86961	4.80E-05	0.84747	5.00E-05	0.86300	5.30E-05
44.516	0.86961	5.70E-05	0.86961	5.10E-05	0.84750	4.80E-05	0.86297	5.60E-05

Area (m^2)	k_{eff} (Fresh fuel)	±δ (Fresh fuel)	k_{eff} (Major actinides only)	±δ (Major actinides only)	k_{eff} (Actinides + principal fission products)	±δ (Actinides + principal fission products)	k_{eff} (Actinides + minor fission Products)	±δ (Actinides + minor fission Products)
45.860	0.86952	5.30E-05	0.86952	5.30E-05	0.84744	4.60E-05	0.86300	5.50E-05
47.224	0.86961	5.40E-05	0.86961	5.60E-05	0.84747	5.00E-05	0.86299	5.90E-05
48.609	0.86958	5.30E-05	0.86958	5.70E-05	0.84753	5.10E-05	0.86304	5.20E-05
50.013	0.86958	5.60E-05	0.86958	5.20E-05	0.84741	4.90E-05	0.86301	5.40E-05
51.438	0.86964	4.80E-05	0.86964	5.70E-05	0.84741	5.30E-05	0.86287	5.00E-05
52.882	0.86960	5.10E-05	0.86960	5.10E-05	0.84737	5.20E-05	0.86295	5.20E-05
54.346	0.86967	5.20E-05	0.86967	5.40E-05	0.84740	5.60E-05	0.86295	5.40E-05
55.831	0.86963	5.70E-05	0.86963	4.90E-05	0.84763	4.70E-05	0.86297	4.70E-05
57.335	0.86978	5.40E-05	0.86978	5.20E-05	0.84745	4.90E-05	0.86291	5.50E-05
58.860	0.86966	6.10E-05	0.86966	5.10E-05	0.84741	5.00E-05	0.86301	5.70E-05
60.404	0.86956	5.20E-05	0.86956	5.80E-05	0.84740	5.40E-05	0.86292	4.80E-05

Table D.2.: Reactivity savings as a function of k_{eff}.

Area (m^2)	Δk_{eff} = keff(fresh) - keff(major only)	Δk_{eff} = keff(fresh) - keff(actinides + Principal fission products)	Δk_{eff} = keff(fresh) - keff(actinides + minor fission products)
33.32	0.007184	0.029333	0.013780
34.48	0.007099	0.029318	0.013699
35.67	0.007125	0.029303	0.013696
36.87	0.007234	0.029445	0.013880
38.09	0.007095	0.029245	0.013828
39.34	0.007220	0.029414	0.013831
40.60	0.007184	0.029285	0.013780
41.89	0.007081	0.029281	0.013692
43.19	0.007158	0.029305	0.013770
44.52	0.007061	0.029174	0.013701
45.86	0.007248	0.029330	0.013771
47.22	0.007230	0.029373	0.013859
48.61	0.007176	0.029233	0.013716
50.01	0.007298	0.029464	0.013864
51.44	0.007129	0.029364	0.013895
52.88	0.007156	0.029385	0.013812
54.35	0.007144	0.029413	0.013866
55.83	0.007106	0.029105	0.013763
57.34	0.007011	0.029335	0.013880
58.86	0.007095	0.029348	0.013751
60.40	0.007094	0.029247	0.013729

Appendix E: Data for area saved when taking credit for burnup.

Table E.1: Calculation of Area Saved

ΔA	k_{eff} (fresh Fuel)	Δk_{eff} = k_{eff}(fresh) - k_{eff}(major only)	Δk_{eff} = k_{eff}(fresh) - k_{eff}(actinides + minor fission products)	Δk_{eff} = k_{eff}(fresh) - k_{eff}(actinides + Principal fission products)
0.000	0.87681	0.007184	0.013780	0.029333
1.164	0.87678	0.007099	0.013699	0.029318
2.349	0.87642	0.007125	0.013696	0.029303
3.553	0.87673	0.007234	0.013880	0.029445
4.778	0.8768	0.007095	0.013828	0.029245
6.022	0.87673	0.007220	0.013831	0.029414
7.286	0.8767	0.007184	0.013780	0.029285
8.571	0.87666	0.007081	0.013692	0.029281
9.875	0.87664	0.007158	0.013770	0.029305
11.2	0.87678	0.007061	0.013701	0.029174
12.544	0.87725	0.007248	0.013771	0.029330
13.908	0.87684	0.007230	0.013859	0.029373
15.293	0.87673	0.007176	0.013716	0.029233
16.697	0.87706	0.007298	0.013864	0.029464
18.122	0.87671	0.007129	0.013895	0.029364
19.566	0.87655	0.007156	0.013812	0.029385
21.03	0.87686	0.007144	0.013866	0.029413
22.515	0.87697	0.007106	0.013763	0.029105
24.019	0.87676	0.007011	0.013880	0.029335
25.544	0.8769	0.007095	0.013751	0.029348
27.088	0.87671	0.007094	0.013729	0.029247